UNIVERSITÀ DEGLI STUDI DI UDINE

Facoltà di Ingegneria
Dipartimento di Ingegneria Elettrica, Gestionale e Meccanica – DIEGM

Corso di Dottorato di Ricerca in Ingegneria Industriale e dell'Informazione
Ciclo XXVI

Tesi di Dottorato di Ricerca

INFRARED COMMUNICATION SYSTEMS FOR THE NAVIGATION IN INDOOR ENVIRONMENTS

Dottorando:
Dott. MARCO DE PIANTE

Tutor:
Prof. ANDREA TONELLO

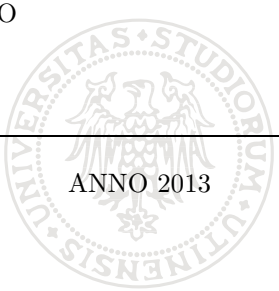

ANNO 2013

Contents

List of Tables

List of Figures

List of Acronyms

ADC Analog to Digital Converter

A-MTM Audio Multi Tone Modulation

AOA Angle Of Arrival

AP Access Point

AWGN Additive White Gaussian Noise

BER Bit Error Rate

BJT Bipolar Junction Transistor

BS Base Station

BSF Band Selection Filter

BT BlueTooth

CIE Commission Internationale de l'Eclairage

CNA Centralized Network Architecture

CRO Oncology Reference Center

CSMA-CD Carrier Sensing Multiple Access - Collision Detection

CU Control Unit

DAC Digital to Analog Converter

DC Direct Current

DEMOD DEMODulator

DSO Digital Storage Oscilloscope

FFT Fast Fourier Transform

FM Frequency Modulation

FPGA Field Programmable Gate Array

GPS Global Positioning System

IC Integrated Circuit

ID IDentifier

IIR Infinite Impulse Response

IR InfraRed

ISM Industrial Scientific and Medical

LED Light Emitting Diode

LNA Local Network Architecture

LoS Line of Sight

LRB Logical Routing Block

LUT Look Up Table

MOD MODulator

MOSFET Metal Oxide Substrate Field Effect Transistor

MS Mobile Station

MSB Most Significant Bit

MUL MULtiplier

OOK On Off Keying

P/S Parallel to Serial

PAM Pulse Amplitude Modulation

PCB Printed Circuit Board

PCM Pulse Coded Modulation

PDA Personal Device Assistant

PIM Pulse Interval Modulation

PPM Pulse Position Modulation

PWM Pulse Width Modulation

QR Quick Response

RF Radio Frequency

RGB Red Green Blue

ROM Read Only Memory

RSS Received Signal Strength

RTT Round Trip Time

SAW Surface Acoustic Wave

SNR Signal to Noise Ratio

SR Set - Reset

TDOA Time Difference Of Arrival

TFT Thin Film Transistor

TOA Time Of Arrival

TOF Time Of Flight

TS Training Sequence

UWB Ultra Wide Band

VHDL Very high speed integrated circuits Hardware Description Language

Abstract

The navigation systems are widely diffused in various fields of application. The most popular navigation system is well known as Global Positioning System (GPS): it is used essentially in an outdoor environment, due to the fact that the buildings introduce an extremely high attenuation to the satellite signals. In order to provide a navigation service inside the buildings, it is necessary to implement a communication system capable to retrieve the user's position and to deliver the navigation data in an appropriate format. This thesis describes the architecture of a navigation system for people that need to be guided through indoor environments, e.g., public buildings, hospitals, where orientation is very critical. The system has to provide both navigation and context aware information to people that may be in difficult emotive state as it happens to patients and visitors in a hospital. As it is widely explained in the whole thesis, the communication system uses an InfraRed (IR) optical link, thus a general overview to the IR light, and the modulations used in the optical communication systems is given. Moreover, one of the main topic of this thesis is to illustrate a complete study of the optimized architecture suitable to navigate an user inside a building.

The IR navigation system developed in this thesis has stemmed out from a first reverse engineering step where an existing IR analog solution suited to transmit only voice signals has been analyzed. A number of tests have been carried out to characterize the existing analog solution, the modulation used

(FM) and its main parameters. The need to have a new digital communication system is suggested by the possibility to improve the performance, developing a numerical transmission architecture: this allows to identify and, consequently, to locate an user. In this thesis a complete study on the feasibility of the digital architecture is proposed. All the technical details and justifications will be illustrated and discussed, including the study made upon the analog solution, keeping always in mind the need to maintain the compatibility with the analog solution. The thesis will also illustrate the development of the analog blocks that compose both transmission Front End and reception Front End. A particular attention will be paid to the Front End implemented on the receiver device, where the Received Signal Strength (RSS) value is needed. In fact, the user must point the receiver device to the transmitter illuminator as directly as possible (the : to do it correctly, a visual (or audible) indication of the RSS could be useful.

Since the receiver device must be pointed in direction of the illuminator, it should be useful to understand if the system's performance in an indoor environment could be corrupted by the reflections of the IR beams: these reflections are caused by the walls, windows or any other reflective surfaces. This effect, called *multipath* is taken into account: a generic analytical expression of the total received signal will be derived, and a simulation of the performance degeneration will be shown.

Finally, the implementation of a working prototype is presented, with the focus on the user interface.

The navigation system has been installed at the Oncology Reference Center (CRO) hospital in Aviano (Italy), in the framework of the EasyMob project. The EasyMob project will be introduced in this thesis, giving an overview about the entire set of technologies used to navigate an user into a confined space (e.g., colored visible light path guides and Thin Film Transistor (TFT) displays). Moreover a deep study on a number of IR navigation architectures is given, illustrating pros and cons of the infrastructure chosen and explained in the whole thesis.

Acknowledgements

Questi anni di dottorato sono stati parecchio strani. Ho incontrato persone davvero competenti, che mi hanno lasciato “in eredità” delle conoscenze e dei metodi che cercavo da tempo. Ho potuto fare esperienze professionali a cui pochi avrebbero potuto accedere. Molte volte ho incontrato scogli ardui, che mi hanno dato comunque modo di fare i conti con tutti i problemi che ne sono conseguiti, cercando di superarli, e di conseguenza crescere interiormente. Per fortuna posso dire di aver fatto del mio meglio in tutto, anche se ci sarà sempre chi sarà pronto a giudicare, a guardare dall'alto in basso il mio lavoro e il mio modo di approcciare alle cose. Senza certe persone, peró, non sarei stato in grado di sopportare il peso del percorso di dottorato. Vorrei dunque ringraziare mia mamma, che per fortuna c'è stata, c'è e ci sarà sempre, che ha sempre saputo mettermi sulla buona strada per tutto e in tutto, nonostante 10^{10} problemi; mia nonna che è comunque la parente più stretta a conoscenza della mia esistenza. Daniela, che dopo 28 anni è arrivata, che mi ha sostenuto in questo percorso, e che non dovrà più fare lo scherzo di allontanarsi. Ringrazio Samir perché, come ho sempre sostenuto, è il maestro di vita che ho da sempre cercato. Un ringraziamento particolare va a Massimo, amico sia dentro il laboratorio che fuori, e a tutti i miei colleghi, che mi hanno sopportato e che continueranno a farlo. Ringrazio ovviamente il mio tutor, prof. Andrea Tonello, che mi ha dato delle opportunità professionali molto più grandi di quanto mi aspettassi. Ringrazio il fraterno Stefano con cui condividiamo ben

più di semplici idee ed opinioni, ed è sempre un piacere farci quattro sane risate. Desidero ringraziare inoltre Cesco, che pur non essendo una persona di famiglia, si è sempre prodigato per il mio bene.

Grazie,

Marco

Chapter 1

Introduction

Since this thesis is focused on the InfraRed (IR) communication systems, it is useful to explain what this radiation is. The entire project will be introduced after the overview of the IR light and its fields of application.

1.1 A little bit of history: the discovery and early uses of infrared radiation

The IR light is a non - visible component of the electromagnetic spectrum. The visible spectrum, as it is well known, is a portion of the electromagnetic spectrum, as it is shown in the Fig.1.1.

The IR spectrum was discovered by the astronomer Frederick William Herschel. He was looking to the Sun with a red filter, and he noticed that the heat around the optical filter increased, even if the light didn't appear visible. After this observation, with the intent of discovering the source of the heat, he managed an experiment using a prism and a thermometer. He let pass a ray of sunlight through the prism: doing this, the light had been dispersed in the visible spectrum. He positioned the thermometer near the red portion of the visible spectrum, where apparently seems to be nothing visible. The thermometer indicated an increase of the heat and the IR radiation was discovered. After the discovery of the IR light, the importance of this radiation has been understood by the astronomers, and a great amount of studies of the

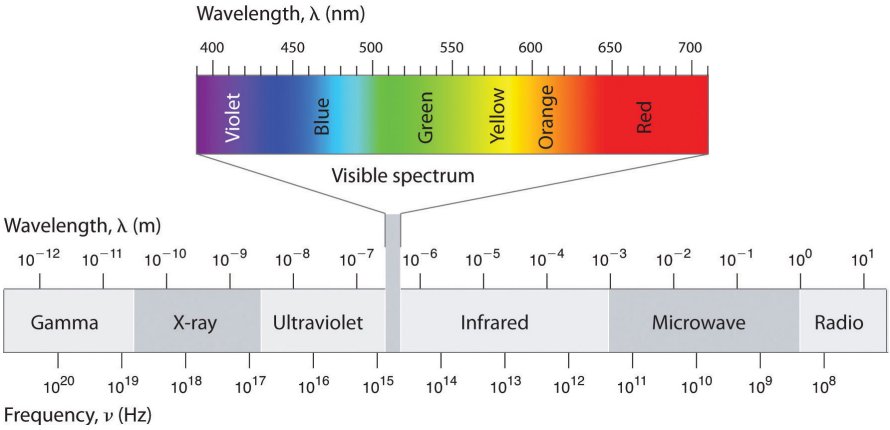

Figure 1.1: The division of the electromagnetic spectrum, with an expansion the visible portion.

deep space had been done in these two centuries.

The IR radiation is used also in the weather forecasts; in particular, a set of geostationary satellites capture the IR radiation that comes from the Earth, and predict the shape and the density of the clouds over a specified area. The physical phenomena behind this application is called *black body radiation*, discovered by W. Wien in 1896 and redefined with the introduction of the quantum physics by M. Planck in 1914 [1]. This theory explains the various colors emitted by an heated surface, and relates with a inverse proportionality the temperature of the surface with the wavelength emitted. Then, focusing on the the IR radiation, it has been discovered that a surface at a certain interval of temperature radiates in the IR spectrum. Since IR spectrum covers a large amount of spectrum, it is necessary to divide the IR spectrum in three bands. The division is not precise, and it vary in function of the application (astronomical, weather forecast, etc.). The Commission Internationale de l'Eclairage (CIE) divides the IR spectrum in function of the radiation wavelength (and consequently in function of the frequency):

- **Near Infrared, IR-A** : 700 nm - 1400 nm (215 THz - 430 THz)

- **Mid Infrared, IR-B** : 1400 nm - 3000 nm (100 THz - 215 THz)
- **Far Infrared, IR-C** : 3000 nm - 1 mm (300 GHz - 100 THz)

For the communication systems, the IR-A is widely used, and the main source of a IR-A radiation is an IR LED The developing of the IR LEDs has begun in 1961, when Bob Biard and Gary Pittman noticed that the Gallium Arsenide substrate emits in the IR-A. After this discovery, they received the patent for the IR LEDs [2]. In the following chapters a brief technical explanation about the theory of the LEDs is given.

The IR communication systems in the IR-A band embrace a lot of applications, including the remote controlling of a wide set of appliances, transferring data between electronic devices i.e., Personal Device Assistant (PDA) and laptops, and transmitting data through optical fibers, even with high data rates. Since the IR radiation is very similar to the visible light, the communications in an indoor environment could take benefits in terms of confinement: this means that the use of a IR device into a certain room will not be influenced by the signals of another device placed in the adjacent room. This fact carry with itself the consequence that the communication system will be largely affected by the reflections made by the walls or windows.

1.2 Introduction to the navigation architecture

In the following chapters, a deep study of a project that uses a IR communication system has been made. The project is developed for a particular use: the navigation of an user that approaches to a large building. Orientation in large buildings is a critical issue, especially for visually impaired people. Furthermore, in certain buildings, e.g., hospitals, people can be in a bad emotional state. The deployment of an indoor navigation system is of great interest in such scenarios.

There are many localization techniques, using a various types of technologies. An introduction of them is clarified in [3], where an overview of the localization methods is given. Particularly, three different ways to determine the position of an user can be used:

- *Time-based Methods*, where, in a general approach, the distance between two nodes is calculated using the transmission time delay t_d:

$$d = t_d v \tag{1.1}$$

with V the speed of the transmitted data. There are three ways for calculating the distance:

  - Time Of Arrival (TOA): where the distance is retrieved using the rule in Eq.1.1;
  - Time Difference Of Arrival (TDOA): where the distance is retrieved sending two signals with different speeds:

$$\frac{d}{v_1} - \frac{d}{v_2} = t_1 - t_2 \tag{1.2}$$

The time difference identify the distance, knowing the two speeds v_1, v_2.

  - Round Trip Time (RTT): where the distance is retrieved taking into account the hardware time delay of the receiver node. This implies that the TOA method is used, with the addition of the hardware taken time t_{hw}. Particularly:

$$d = \frac{(t_d - t_{hw})v}{2} \tag{1.3}$$

It should be noted that in this case, the synchronization between transmitter and receiver is not required.

- *Angle Of Arrival (AOA)* In [4], the position of an user is retrieved from knowing the AOA of the transmitted wave. This can be achieved by using an antenna array, where the incident plane wave hits each antenna with a different Time Of Flight (TOF) (and consequently a different phase). This implies that a triangulation algorithm must be implemented, as in [6]. Basically, the algorithm will retrieve the user's position calculating

the point of intersection of at least two directions calculated with the received AOA.

- *RSS* With this method, the strength of the received signal from a number of transmitters is computed. After, the distance of the transmitter is calculated taking into the account the received power, using the Friis rule.

With the exception of the AOA method, a trilateration algorithm is needed to calculate the user's position. Basically, at least three distances are needed to retrieve the transmitter position in a two dimensional space.

One of the most important implementation of a TOA positioning method can be found in the Ultra Wide Band (UWB) transmission modulation. In [5], a complete study of the pulse detection is given, with the extension to the dense multipath environments. The UWB is widely used mainly because a very narrow time pulses are transmitted, and the multipath effects are consequently resolved. In other hand, in [8] and [9], the 802.11 transmission infrastructure is used for the position calculation of an user connected to a WiFi net. Also in this case, trilateration algorithms must be used, since the RSS is taken into the account. The main strength of these solutions is the implementation of the algorithm in an existent infrastructure, and no other devices installation is required.

In this thesis, an IR architecture for the user localization is studied. As it is explained in [7], the IR solution can be useful for the localization in an indoor environment, mainly because the light beam is confined into a room. This means that the first localization of an user can be done instantaneously. With a certain number of IR transmitters inside a room, the localization become finer. The IR technology allows to implement simple modulators and demodulators, and it is suitable for the digital domain, since the mostly used modulations are impulsive. Moreover, the high directivity of the optical devices allows to implement a cheap and simple IR-LED array with a specific radiation pattern: the Radio Frequency (RF) technologies requires a specific study upon the antenna arrays.

In the following, a general overview on the IR communications is given, with focusing on the modulations generally used in an IR link, and describing the main electrical components used to realize the communication system. After, a deep focus on the EasyMob [11] project has been given.

In order to introduce the project, a research of a similar projects has been made: there are several examples of navigation systems in the literature. In [12], a GPS-based positioning system gives precise position information that are elaborated by a talking map. This approach, however, cannot be implemented in an indoor environment due to the lack of coverage of the satellite system into buildings. Other approaches particularly suited for blind people are based on beacons [13], [14]. These systems generally use beacons placed in suitable locations that are triggered or queried by the blind travelers. Suitable speech and / or sound messages are then delivered to the users. Typically, these solutions employ IR technology that is particularly suited to give precise position information due to its very high directionality.

In [15], an architecture called *Topaz* has been shown. This kind of architecture uses Bluetooth technology to locate tags (via trilateration) in indoor environment. Furthermore, in order to provide a room level accuracy, it exploits the IR technology. In fact, since the IR signals can't penetrate through the walls, coverage is offered at room level. The EasyMob system, is a fully integrated solution that comprises a system management software application, a network infrastructure and a number of technologies to deliver information and to allow the navigation of people. For what the navigation system is concerned, an ad-hoc hand held device comprises a joint radio and IR interface. The radio interface uses short range Bluetooth technology (which exploits the 2.4 GHz Industrial Scientific and Medical (ISM) RF band and does not exhibit co-existence problems with the other radio devices that are present into a hospital). Bluetooth is used only to provide the navigation instructions and not to provide navigation information as in [15]. The IR interface instead is a custom and novel solution developed in this project. It is used to accurately detect the position. The entire project has been presented into a [16], at the ESTEL Conference 2012.

1.3 Related Publications

The main results of the work presented in this thesis have been the subject of publications.

Conferences

[C-1] M. De Piante, D. Inserra, A. M. Tonello, "People Navigation System in Confined Spaces," *Proc. of IEEE AESS European Conference on Satellite Telecommunications* 2012, Rome, September 2012.

Journals

[J-1] M. De Piante, A. M. Tonello, "Digital Implementation for a Indoor Positioning System using Infrared Optical Link", *to be submitted*

Other contributions

[O-1] POR FESR 2007-2013, Project EasyMob, Deliverable A1.2.1, "Studio sull'impiego della tecnologia IR all'interno di ambienti confinati" Jun., 2013.

[O-2] POR FESR 2007-2013, Project EasyMob, Deliverable A2.1.2 - A2.1.3, "Sviluppo di prototipi di apparati di trasmissione e ricezione IR" Jun., 2013.

Chapter 2

Overview on the IR Transmission Systems

In this chapter, an overview of the modulation techniques is given. These modulations are fully referenced in the literature, and here the main goal is to show the differences between them. In the optical links, the transmitter is composed by a number of IR LEDs, that are corresponding with an antenna in the RF links (the receiver antenna in RF links is substituted by the photodiodes, or phototransistors in an IR link). The IR LEDs are driven generally by a current amplifier, that is commonly implemented with a net of Metal Oxide Substrate Field Effect Transistor (MOSFET) or Bipolar Junction Transistor (BJT) connected in a current mirror configuration. The amplifier is driven directly by the modulator chosen for the application. In this way, it is useful to see an overview of the impulsive modulations commonly used in the IR communication links. Before, a simple explanation of how the main electronic components (such as LED and photodiodes) works is given: this is useful to understand why the impulsive modulations are widely used in the optical communication systems.

2.1 IR LEDs: a simple explanation of the physics behind them

As a matter of fact, the IR LED is a semiconductor - based light emitter. The semiconductor is generally doped forming a p-n junction, that must have a direct band gap between the valence energy band and the conduction energy

band [10]. When a current is given from a power generator to the diode (e.g., the p - n junction), the electrons present at the conduction energy band recombine themselves with a hole in the valence energy band. This recombination causes a photon emission, and, particularly, the energy of the photon is the same of the energy gap between the conduction and valence energy bands. Using the Einstein's formula, where the energy gap E_{gap} is directly referred to the chemical characteristics of the used semiconductor,

$$E_{gap} = h\nu \Rightarrow \nu = \frac{E_{gap}}{h}$$

it is possible to know the required energy gap for the desired frequency of the radiated photons. With this knowledge, it is possible to have a precise radiated frequency by a IR LED. Particularly, the IR LEDs that will be used in the whole experimentation LED, have the following emitting characteristics:

- Code : OP290 by OPTEK
- Substrate: AlGaAs (Gallium Aluminum Arsenide);
- λ: 890 nm

Now, it is good to explain what happens when a LED is connected to a power supply: it is the base of how a IR LED transmits the pulse that comes from the modulator. The IR LED could be into two separate states:

- The LED is turned ON: the current that drives the device is the nominal forwarding current. In an ideal p - n junction, the current is related to the voltage with the relationship:

$$I_D = I_S \left(e^{\frac{V_D}{n V_{th}}} - 1 \right) \tag{2.1}$$

  where I_S is the saturation current of the junction, V_D is the voltage of the junction (taken positive from the anode to the cathode of the diode), n is the ideality factor for the junction, and V_{th} is the thermal voltage.

- The LED is turned OFF: the current that flows through the anode to the cathode of the diode is zero, and no photons are emitted.

This implies that the Direct Current (DC) electrical power consumption is $P_{el} = V_D I_D$. The power efficiency is defined as:

$$\eta_{\text{power}} = \frac{P}{V_D I_D} \tag{2.2}$$

where $P = N_{ph}\frac{h}{\nu}$, and N_{ph} is *the total amount of photons emitted into the free space per second.* In an ideal case, each electron recombined into the substrate must be converted into a photon. This is not true, and some photons may never be emitted. This cause a loss of efficiency, with an increasing of the electrical power to obtain the desired light power.

2.2 Photodiodes: the receiver elements

The corresponding element for the receiver antenna in RF links, is the photodiode. It is composed by a package that is transparent to the wavelengths transmitted. Inside the package, it is present a p - n junction used in the opposite way than the diode function. In this case, a photon, with a certain energy E_{ph}, collides on the surface of the junction. This event gives the E_{ph} energy to the substrate, that responds permitting to an electron to jump from the valence energy band to the conductive energy band: the main macro effect is the increasing of the device's conductance. The photodiodes can be connected in a circuit in different ways, but the photoconductive mode is the most useful mode. In this case, the photodiode is connected in reverse biasing, and this fact causes the increase of the depletion region inside the p - n junction: the capacitance of the device will decrease and the response will became faster. The photocurrent will be linearly proportional to the total amount of photons that collide on the substrate.

2.3 Transmission methods

Since the diodes are biased with a certain amount of current, it is easy to understand that an amplitude - based modulation (such as Pulse Amplitude Modulation (PAM)) is hard to implement with an IR link, mainly because the light power transmitted by an IR LED is a non - linear function of the voltage applied. This is the main reason why the impulsive modulations are preferred. In this section, a general overview on the three most used impulsive modulations has been done. The most important reference for this matter is [17], where a deep study of the most used modulations has been done, with a general approach to the noise sources in the IR communications.

2.3.1 OOK modulation

OOK modulation is the simplest way for transmitting a general bit stream. In fact when the transmitter (i.e., the IR LED) is turned on, the transmitted bit is set to "1", and when the IR LED is turned off, the transmitted bit is set to "0". A simplified modulation scheme is shown in Fig.2.1 The $b(kT)$ signal

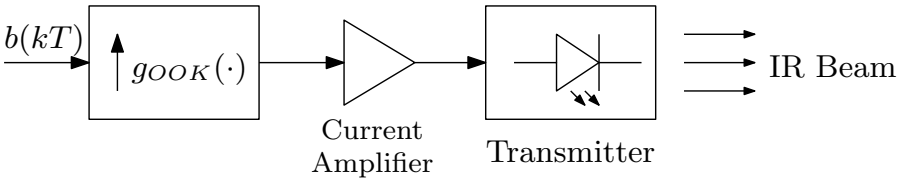

Figure 2.1: A simplified block scheme for the OOK modulator.

is the bitstream, with a bitrate equal to $1/T$, and $g_{OOK}(\cdot)$ is the impulse response of the interpolator filter:

$$g_{OOK}(t) = \text{rect}\left(\frac{t - T/2}{T}\right) \tag{2.3}$$

The interpolator filter is used to drive the current amplifier in a continuous time domain, and consequently the IR LEDs.

2.3.2 PPM modulation

PPM is a modulation technique differs from the OOK modulation mainly because it allows to send a symbol that identify a group of bits. Particularly, calling T_b the bit period, T_{sy} a symbol duration, and T_c the period of a single pulse chip, with PPM is possible to transmit a set of N bits in a T_{sy} seconds, with a logic explained graphically in Fig.2.2, where a 16-PPM modulation signals have been depicted. As it is shown, a single symbol is divided by M

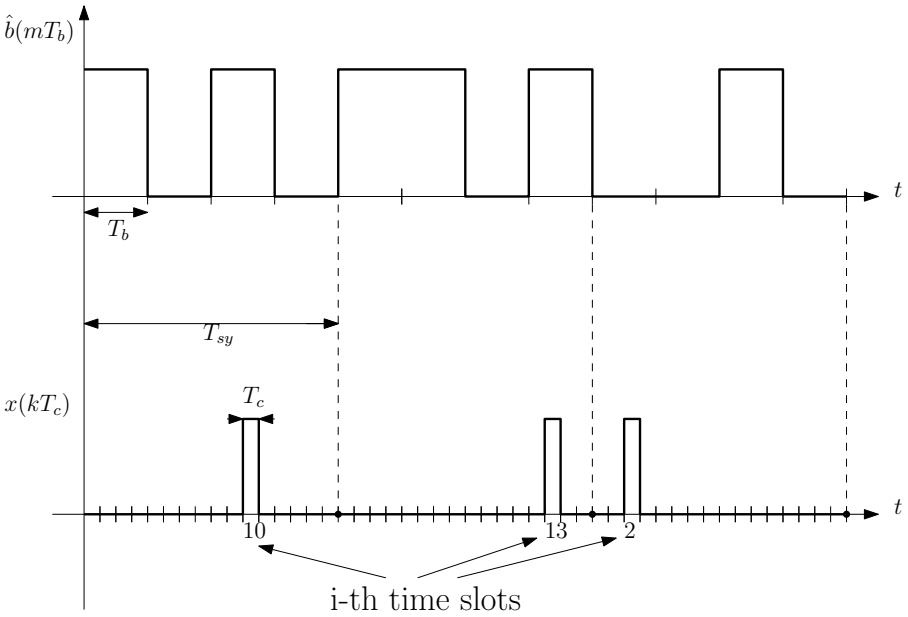

Figure 2.2: Unmodulated bitstream and the correspondent PPM symbols.

time slots, where:

$$M = 2^N \tag{2.4}$$

Each time slot is representative of the decimal value indicated by the N bits. When a bitword is ready to be sent, the pulse chip will be placed into the correspondent time slot of the symbol. After, the symbol can be sent to the IR LEDs and finally transmitted. The simplified block scheme for a PPM

modulator is shown in Fig.2.3. The bitstream $b(kT_b)$ has a bit period equal to T_b seconds: this implies that the interpolation filter will have a impulse response given by:

$$g_b(t) = \text{rect}\left(\frac{t - \frac{T_b}{2}}{T_b}\right) \tag{2.5}$$

The Buffer Parallel to Serial (P/S) block is used to store the set of N bits that will be encoded into a PPM symbol. The Buffer P/S block works synchronously to a clock with a period equal to T_b seconds. This clock (named T_b) drives also a counter block, that is used to set the "READY" control signal high when T_b clock has made N cycles. This assure that the Binary to Symbol (Bin to Sym) block creates a PPM symbol: its output is composed by M wires, that carry the M chips of the PPM symbol. After, a P/S block is required to transform the M signals into a PPM symbol. The P/S block must be driven by a clock with a period equal to the chip period T_c. Then, a PPM symbol will have a duration of $L_{PPM} = MT_c$ seconds, and, comparing the time durations in Fig.2.2, the PPM symbol duration must be NT_b seconds. As it is explained in the IV section of [17], PPM reduces the required optical power compared with OOK modulation. Obviously, reducing the duration of the pulses, the bandwidth increases. AS it is shown in Fig.2.3, the transmitter must be equipped with a Training Sequence (TS) Look Up Table (LUT): in this registry is stored a known sequence of chips, that must be transmitted to synchronize the receiver before the data symbols. In this way, the training chip sequence is transmitted, the receiver recovers the used clock at the transmitter, and it gets synchronized with the exact begin of the symbol stream.

2.3.3 PIM modulation

PIM is another impulsive transmission method, useful for sending symbols that identify a group of bits. But, while for the PPM the pulse location inside a symbol encodes the data, for the PIM the pulse indicates only the beginning of a length of empty time slots, and the number of them indicates the decimal value of the bitword. In order to understand the encoding procedure, Fig.2.4 shows the unmodulated bitstream $b(mT_b)$ and the transmitted signal $x(kT_c)$.

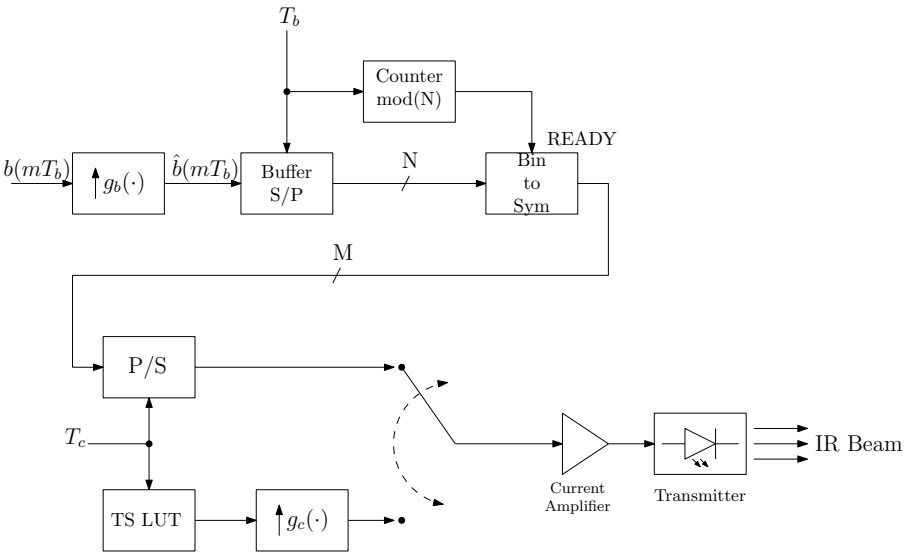

Figure 2.3: Simplified block diagram for a PPM transmission system.

As it is clear to understand looking at the Fig.2.4, a specific symbol duration doesn't exist in the PIM transmission. This implies that the transmitted bit-stream must be stored in a buffer larger than the N bits as it is explained in the PPM technique. In fact, a long sequence of zeros gives a short symbol duration. Since the average value of time duration of a PIM symbol is $(M-1)/2$, the PIM bitrate increases if compared with the PPM transmission system. For the complete study of the PIM transmission technique, including the performance, the main reference is [18].

2.3.4 A-MTM modulation

In this thesis, the developed communication architecture uses an FM modulation to transmit the IDentifier (ID) data. The modulated message will be formed by a certain number of tones, equally spaced in frequency. Each tone will identify a single bit to transmit. The A-MTM modulation will be deeply studied in the following chapters, and here only an overview is given.

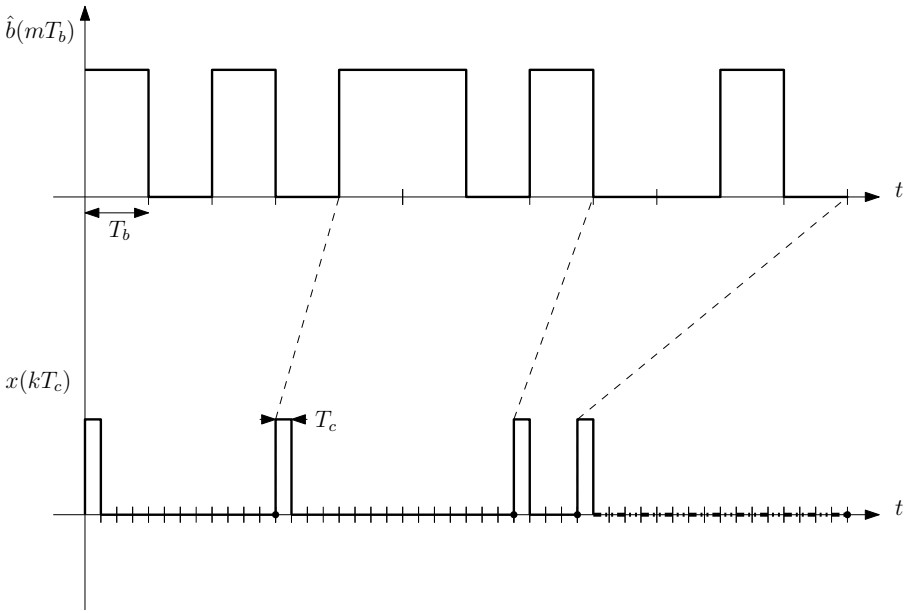

Figure 2.4: Unmodulated bitstream and the correspondent PIM symbols.

In Fig.2.5 it is possible to see the received modulated signal. The FM signal carry with itself a composition of audio tones, equally spaced in frequency. A FM demodulator and a filter bank will check the presence of a tone at a specified frequency. Finally a decision element will compare each filter bank

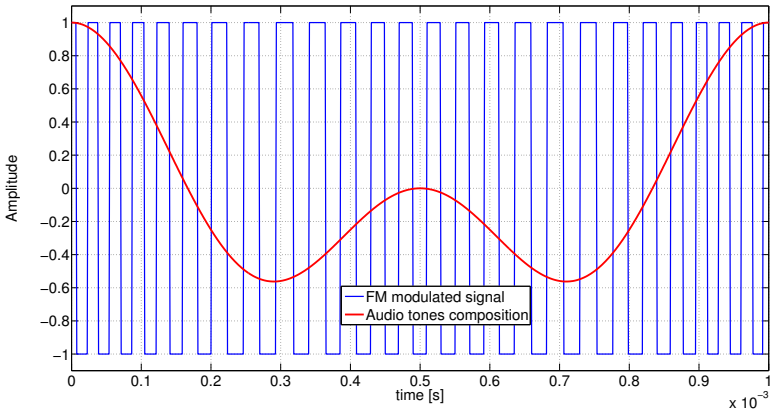

Figure 2.5: Modultaed A-MTM symbol and the transmitted tone composition

output signal with a threshold, giving the information about the presence of a tone. Implicitly with the comparison, the decoded bit word is retrieved.

Chapter 3

Overview of the EasyMob project

The EasyMob system is novel and fully integrated solution, that comprises a system management software application, a network infrastructure and a number of technologies to deliver information and to allow the navigation of people. This system has been developed within the framework of the homonym project, that aims at developing novel solutions and carry out a real deployment at the Oncology Reference Center (CRO) in Aviano, Italy. For what the navigation system is concerned, an ad-hoc hand held device comprises a joint radio and IR interface. The RF interface uses a BT communication system, that is used only to provide the navigation instructions and not to provide navigation information.

3.1 The EasyMob System

In the EasyMob system, different technologies have been considered since service has to be offered to a broad variety of persons with different needs, abilities, and physical/physiological status. These technologies can be divided into two categories: the first one includes colored visible light path guides (implemented by using Red Green Blue (RGB) LEDs) that provide immediate information about paths, Thin Film Transistor (TFT) displays that give context aware information, and Quick Response (QR) codes to identify users and their associated routes. The latter technology set comprises wireless navigation

devices, in particular mobile phones and ad-hoc hand held devices equipped with both IR and BT interfaces.

The visible light path guide uses a number of light points installed on every possible route. In this way the user has just to follow the color displayed by the light points that identify the correct route to reach its destination. The light points must be programmable in order to assure the path reconfigurability. Moreover, the light points should have a simple shape, e.g., an arrow or similar, that allow users to easily find the correct way.

TFT screens can be placed in some strategical points, i.e., where the probability to choose a wrong route is high. These displays can offer more detailed information about the destination and the route. Other context aware information can be also displayed.

Another considered technology is represented by the QR codes. The printed QR code is assigned to a given user. Then, along the route, a QR reader, with a display, enables to show the entire path to get with the instructions to reach the destination.

The EasyMob system also considers the use of mobile phones equipped with BT interface, as it will be explained in the following.

Finally, hand held device can also be distributed to users at reception points. In this thesis a complete study is focused on both the hand held device device and the navigation infrastructure. The hand held device is referred to Mobile Station (MS) in the following.

3.2 IR - based Navigation Architectures

A generic navigation system is composed by two main logical blocks: positioning infrastructure and navigation unit. The positioning infrastructure is implemented in order to give the position information. In this project, it is realized by placing a certain number of IR beacons (or illuminators) at known position. The navigation unit instead is the central core of the navigation system that elaborates the position information and decides which is the right route. In general, it will also be capable to recalculate the entire route if the user takes a wrong path. Several approaches can be used to implement a nav-

igation system depending on the navigation unit placement. Obviously, this will influence the system complexity.

There are three possible solutions that have been studied:

- the navigation unit is implemented into the mobile device;
- the navigation information is delivered by a central processing unit. This solution relies on the availability of a bidirectional IR link;
- the IR link (unidirectional) is used for positioning, and a BT link serves as the communication channel between the centralized navigation unit and the users.

In order to implement these three solutions, three different architectures must be developed, i.e., both the navigation unit and the positioning infrastructure have to provide different features. Nonetheless, the IR link is common to all architectures. Its main blocks are depicted in Fig.3.1. The IR Transmitter

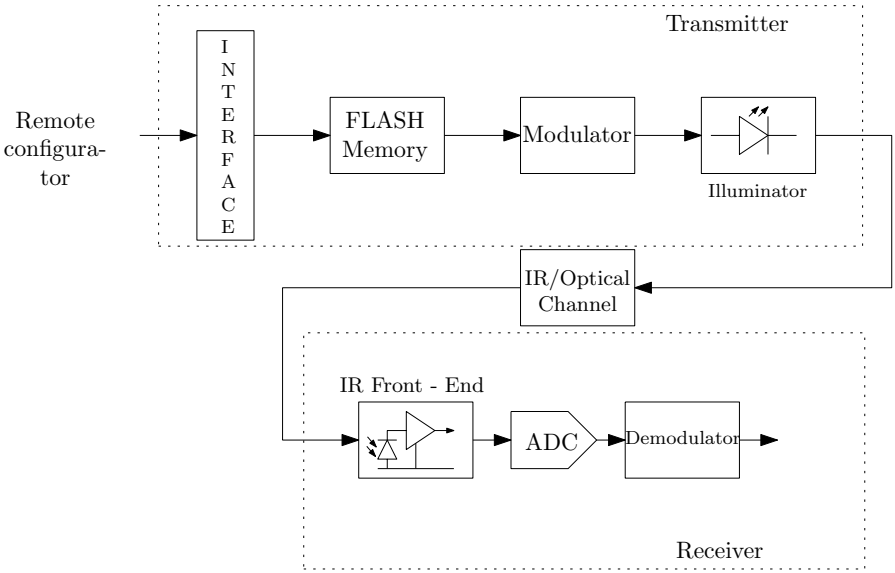

Figure 3.1: IR communication system block diagram.

is composed by an Interface block, used to program a FLASH Memory with data samples. Modulated data samples drive the Illuminator block, composed by a variable number of IR LEDs. This number depends on the light power required in order to achieve a certain space coverage. Moreover, the number of IR LEDs depends on the requested beam angle which is a function of the system accuracy.

The first block of the IR receiver is an analog IR front end, where IR photodiodes are connected to an amplifier. This optical transducer is connected, through an Analog to Digital Converter (ADC), to a demodulator.

Now, the three navigation architectures are discussed.

3.2.1 IR unidirectional link

For this architecture, that is referred to as Local Network Architecture (LNA), it is possible to make a parallelism with the GPS system, since navigation is locally, i.e., it is implemented in the hand held device. Fig. 3.2 shows a general environment where the LNA is implemented: the IR link shown is referred to the linked Base Station (BS) by the MS, but all the other BSs are transmitting.

As it is shown in Fig. 3.2, the MS is the IR receiver of the user, and the BSs are the IR transmitters. All the BSs are connected through Ethernet links to a central server, that can be used only in case of an ID reconfiguration.

In this architecture, the IR transmitter sends only its programmed ID, that is unique in the network. The receiver decodes the ID data and gives navigation instructions to the user.

Since the navigation unit is implemented into the MS device, its complexity is high. Furthermore, the entire user's route must be stored in the MS. An example of a possible hardware implementation of the IR receiver is depicted in Fig. 3.3.

The FLASH Memory stores the complete list of BS's IDs that the user may encounter in its route, and the Read Only Memory (ROM) block contains all the vocal messages used for the navigation. The Logical Routing Block (LRB) computes the logical steps listed in the following.

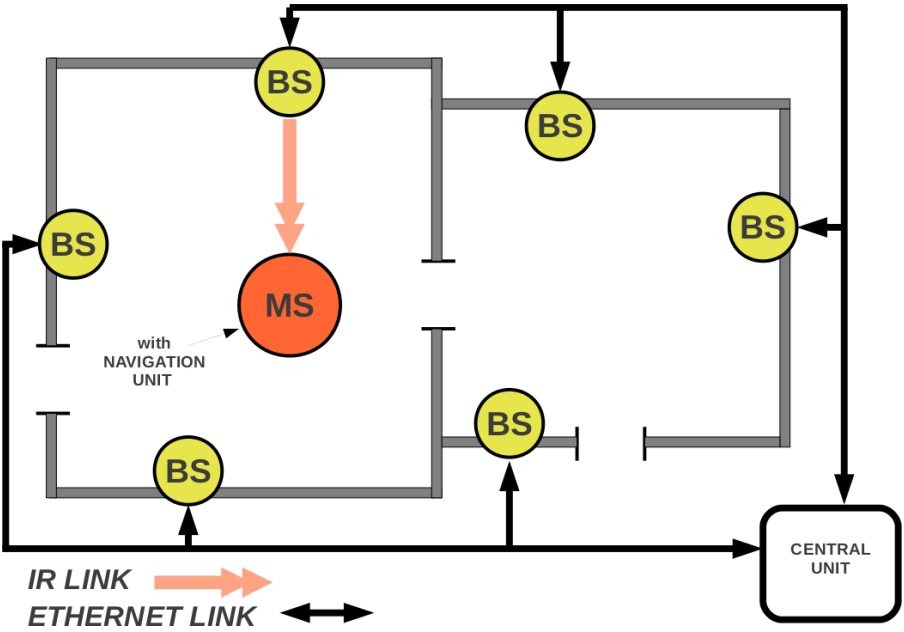

Figure 3.2: LNA general environment.

1. The recognized ID is compared with all IDs stored in the FLASH Memory;
2. if the decoded ID exists in the memory, the LRB will receive the index of the next message to play; otherwise it will receive the index of a "wrong route" message;
3. the LRB sends a query to the ROM memory with the message index;
4. the LRB sends to the Digital to Analog Converter (DAC) the vocal samples from the ROM.

Another key point of this architecture is the reduced BSs complexity. In fact, the BS comprises only a memory that stores the ID, an IR transmitter and an Ethernet network interface for the connection to the Control Unit (CU) (which is used only in case of an ID reconfiguration).

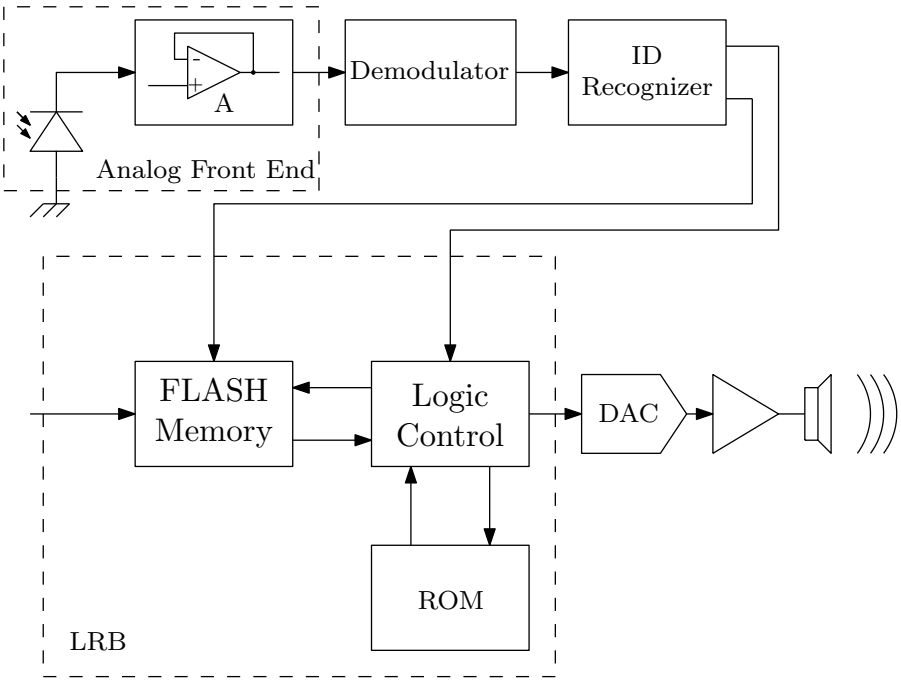

Figure 3.3: IR Receiver for the unidirectional link architecture.

3.2.2 IR bidirectional link

This architecture, that is referred to as Centralized Network Architecture (CNA), uses the optical IR channel in two directions. The MS and all the BSs incorporate an IR transmitter and an IR receiver. Fig. 3.4 shows a general environment where the CNA is implemented.

Every MS device is firstly programmed with a static ID, unique for all the mobile devices.

In this architecture, and differently to the LNA, the MS transmits its own ID, MS_{ID}, to a specific BS through the IR link, and the BS communicates with the Central Unit through Ethernet cabled network, providing both the BS_{ID} and the MS_{ID}. In this way, the position (given by the BS_{ID}) is provided to the navigation unit implemented into the CU. Obviously, the destination and

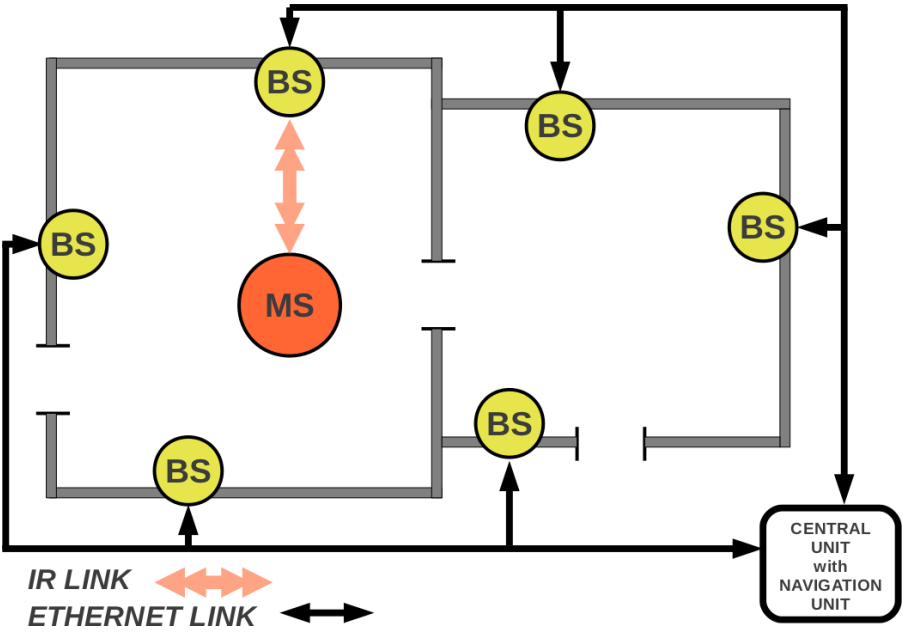

Figure 3.4: Centralized Network Architecture (CNA).

the entire route of each user are stored in the CU where all the destinations are indexed, and the database is refreshed every time that a new user approaches the system. Once the navigation unit has computed the correct route, it transmits this information to the linked BS that forwards it to the MS. Fig. 3.5 explains the navigation algorithm implemented into the CU.

It should be noted that this algorithm is similar to the one implemented by the LRB in the LNA, but in that case it is implemented into the MS. The bidirectional link allows to simplify the hardware complexity at the receiver, because the navigation unit algorithm resides in the CU. With respect to the LNA, in this case the navigation unit is common to all the users, and a multiple access technique has to be implemented. There are two levels of media access: the first is the CU access, that is regulated by the Ethernet protocol (in particular Carrier Sensing Multiple Access - Collision Detection (CSMA-CD)). The second level of access is at the BSs. Nevertheless, the probability that two

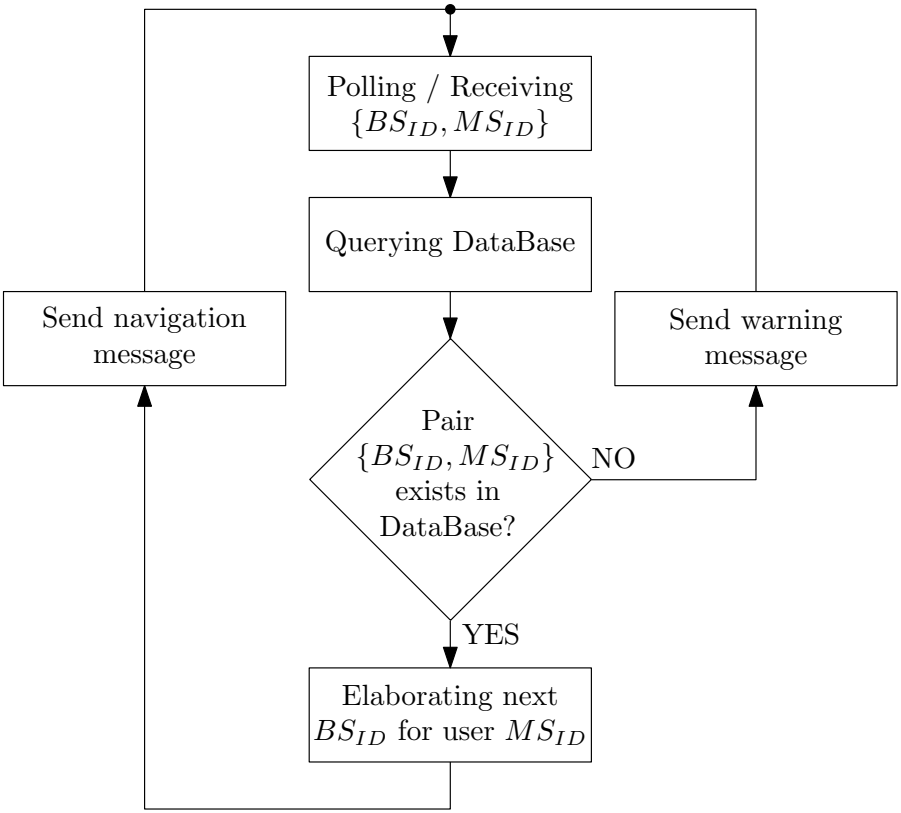

Figure 3.5: Navigation algorithm for the CNA.

or more users transmit at the same time their MS_{ID} is very low. In fact, the analog front end of a BS cannot have a wide angular aperture since it provides the correct navigation information only when the user is in a position where this information is useful. A more probable event is that the BS transmits the navigation data to two (or more) users. For this reason, the MS must be capable of recognizing and demodulating only its own navigation message. This can be simply implemented with an ID comparator used to identify the correct message.

The use of a CU increases latency and delays. Moreover, CNA is more sen-

sible to the CU faults, and the main requirements are the software robustness and system stability.

3.2.3 BT - IR link

This architecture is similar to the one discussed in the previous section. However, at the physical layer, two wireless technologies are used, i.e., BT and IR. Particularly, the IR link is unidirectional from the BS to the MSs, and BT is used in bidirectional mode. In order to implement this BT CNA, the positioning infrastructure requires additive components, i.e., the BT Access Point (AP)s, that are placed in several points in the building. The main idea (Fig.3.6) is to use the IR unidirectionally, to send the BS_{ID} to the MS device, in order to transfer the position information, from the BS to the MS. Then, the BT interface is triggered and it transmits to a BT AP the $\{BS_{ID}, MS_{ID}\}$ pair. Similarly to the CNA, this information reaches the CU that computes the route and sends the navigation information to the MS through the BT link.

Thus, in the BT CNA case, the MS device not only includes an IR receiver, but also a BT transceiver used to transfer and to retrieve the correct navigation information to and from the CU. The main steps for the navigation are briefly reported in the following.

1. The user approaches the system with an MS device;

2. through the IR link, the user receives the BS_{ID} that implicitly includes the position;

3. the pair $\{BS_{ID}, MS_{ID}\}$ is sent to the CU via a BT uplink channel;

4. the CU runs the algorithm of Fig. 3.5 and sends navigation information to the BT AP where the navigation query has been sent;

5. the BT AP delivers navigation information to the linked MS device, and the user will listen the correct navigation step.

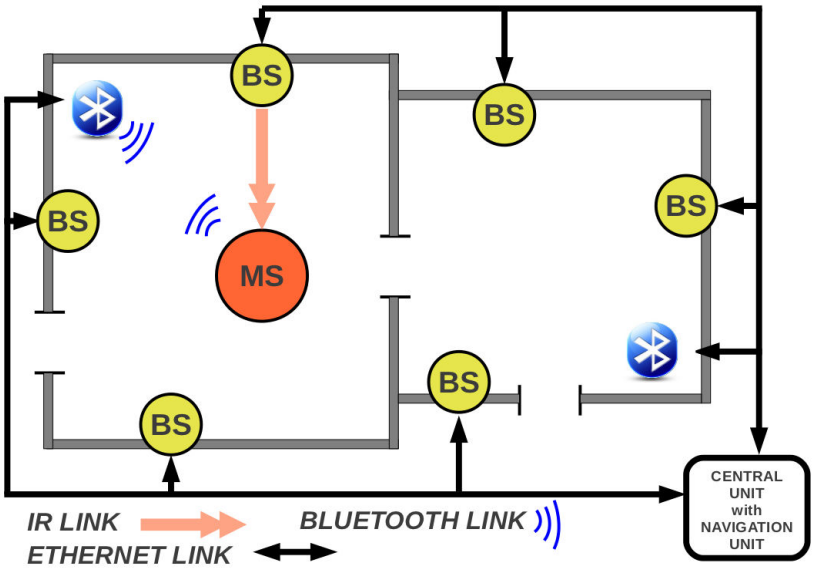

Figure 3.6: BT CNA.

The number of BT APs is lower than the number of IR BSs: in fact BSs are used only to give the correct user position in points where the orientation is difficult, while the BT AP handles many links, and it is capable to manage all users present in the same area. It should be noted that the complexity of the MS device increases, in order to interface IR and BT technologies. Particularly, the IR demodulator must be equipped with a ID recognizer interfaced with the BT baseband elaboration block, in order to send through the BT link the received BS_{ID}. Obviously, costs will increase for this MS hardware architecture, but latency and delays to retrieve the navigation information are limited, mainly for the possibility to send an entire navigation instruction (for example coded as a WAV file) with a higher bit rate than the IR link. Moreover, the power consumption does not increase significantly, since the BT transceiver switches on only when a BS_{ID} is received.

Finally, since BT is largely diffused in smart phones, the BT AP infrastructure can in principle also be used for trilateration.

3.3 Selection of the Architecture

In the previous section, three main architectures have been discussed, and in the following the discussion of the pros and cons for each one has been done. It should be noted that every single architecture previously shown is capable to navigate an user in an indoor confined environment. However, for the EasyMob project, a choice must be done in order to give a concrete and definitive project architecture. In Tab. 3.1, the three architectures are grouped, and for each architecture pros and cons are shown.

For what the LNA concerns, the major limitation of this architecture is the complexity of the MS. In fact, the MS is a hand held device, so it has to be handy and its size has to be limited. It should not require a high power consumption, and, preferably, it has to be inexpensive. Hence, the LNA was considered unsuitable for the EasyMob project.

In the CNA, both the MS and BS are equipped with the IR transmitter and IR receiver. In the BT CNA instead, the MS has the only IR receiver, and the BS has the only IR transmitter. Moreover, the MS requires a BT transceiver, and some BT APs have to be installed. However, the presence of a BT transceiver does not increase significantly the power consumption, since it is not always switched on. Anyhow, it increases the link bit rate, facilitating the transmission of more data, for example a high quality audio message, and reducing the latencies.

For these reasons, the BT CNA is preferable, and it has been chosen as the navigation architecture of the EasyMob project.

Table 3.1: Top level architectures' Comparison

Architecture	Pros	Cons
LNA	• Simple BS transmitter; • Active Central Unit not necessary; • BS_{ID} can be set without a network cabling and left in this state as long as new reconfiguration is needed;	• High MS hardware complexity;
CNA	• Navigation logic resides in the Active Control Unit: MS device does not need the Navigation Logic;	• Requires an Active Central Unit; • Every BS must be cabled and connected to the Central Unit; • BSs and MSs must implement both IR front - ends • Latency and delays in message delivering become important;
BT-CNA	• Simple IR transmitter; • IR BS_{ID} can be programmed like in LNA; • Latency and delays are reduced using BT AP; • Navigation service can be delivered even through BT trilateration with smart phones;	• MS hardware complexity grows up; • Requires an Active Central Unit;

Chapter 4

Analog Architecture

In this chapter, a deep study of an existing first solution for navigating an user is given. This solution uses an electronic system that works in a continuous time domain: this means that the modulator is composed by a certain number of analog components. Paying attention to the electrical scheme of the transmitter and the receiver for the analog architecture, and exploring the signals with a measurement campaign, it has been possible to retrieve the most important parameters about the modulation used for delivering contextual information. Particularly it has been discovered that the entire system uses a FM, and in the following the analysis that have permitted to discover the modulation type is given.

The measurement of the modulated signal is shown in Fig.4.1.

As it is clear to see, the modulator shifts the instantaneous frequency in function of the message amplitude. This suggest to study the entire modulator system taking into the account the set of analog phase modulations.

In the following sections, a study of the main modulator's components is given, in order to understand how the architecture modulates and demodulates the messages. It must be noted that the architecture is able to demodulate only vocal messages, and for the goals of this thesis, the study of the main blocks must be done, in order to develop a digital architecture suitable for demodulating both numerical or vocal messages.

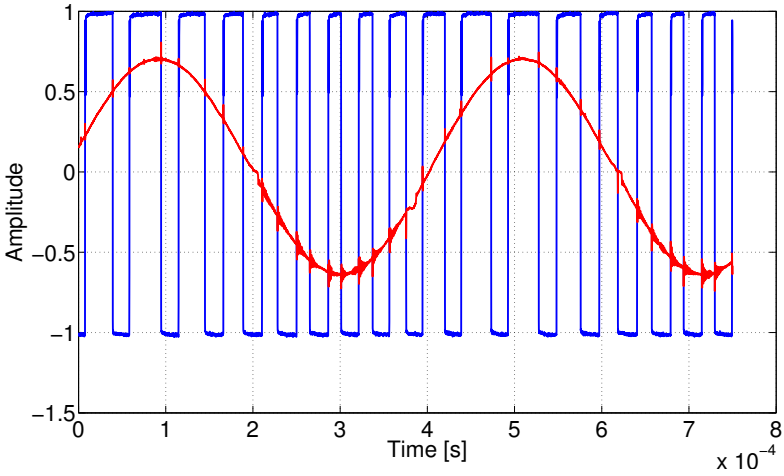

Figure 4.1: Measured signal at the output of the analog modulator.

4.1 Analog transmitter

The transmitter contains a digital memory, where Pulse Coded Modulation (PCM) audio samples have been stored. The audio samples are 16 bit depth, with a sampling frequency of 16 kHz. The transmitter block scheme is shown in Fig.4.2.

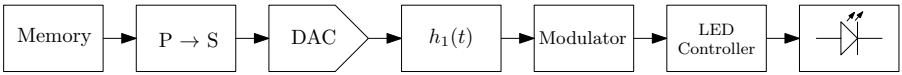

Figure 4.2: Transmitter block scheme.

As it is should be noted, the DAC output is connected to a filter with an impulsive response $h_1(t)$. This filter is a *multiple feedback* lowpass filter. Analyzing the filter electric scheme (Fig.4.3), it is possible to obtain the $h_1(t)$ bandwidth.

Using the electric components labels of Fig.4.3, the Laplace transfer func-

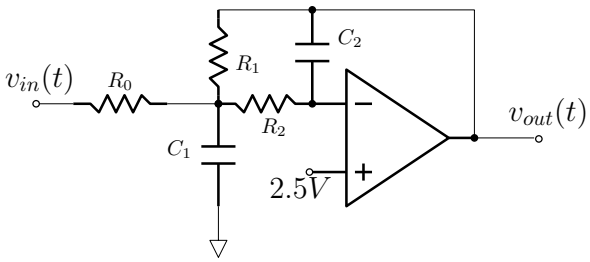

$C_1 = 10\,nF$

$C_2 = 2.2\,nF$

$R_0 = 6.8\,k\Omega$

$R_1 = 5.6\,k\Omega$

$R_2 = 10\,k\Omega$

Figure 4.3: Multiple feedback lowpass filter electric scheme.

tion $H_1(s)$ is:

$$H_1(s) = -\frac{1}{R_0 R_1 C_1 C_2} \frac{1}{s^2 + \frac{1}{C_1}\left(\frac{1}{R_0} + \frac{1}{R_1} + \frac{1}{R_2}\right) s + \frac{1}{R_1 R_2 C_1 C_2}} \tag{4.1}$$

The absolute value of $H_1(s)$ transfer function is obtained with the help of `bode()` Matlab function. In Fig.4.4 the dB magnitude of $H_1(s)$ has been shown.

The $h_1(t)$ bandwidth is $\varepsilon_{h_1(t)} \in [-4.3; 4.3]$kHz.

Going on with the study of the transmitter, the modulator is composed by a simple NE555, an Integrated Circuit (IC) largely used as oscillator. In the following a complete study of this modulator has been given, describing the electrical signals that are present in the components. Fig.4.5 explains how the NE555 could be connected in order to modulate a band limited signal present at the `cv` pin [19]. Pay attention to the acronyms: in the datasheet [19] the modulation is called PPM, but it is completely different to the Pulse Position

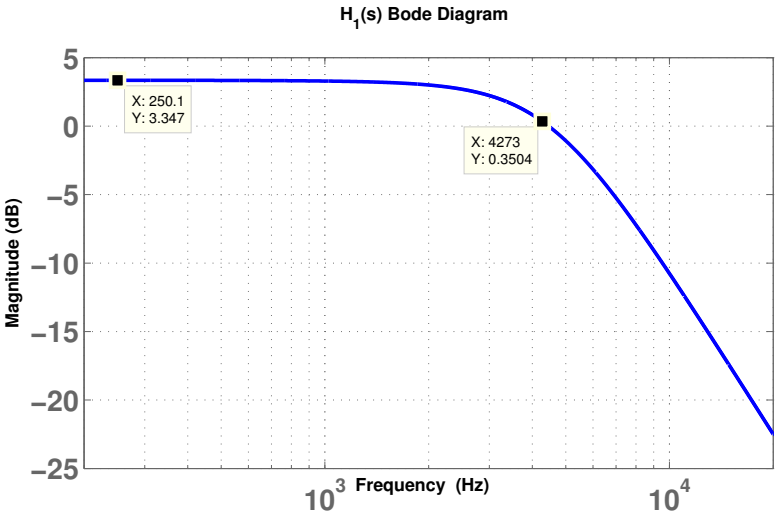

Figure 4.4: Magnitude of $H_1(s)$

Modulation (PPM) seen in this thesis. In the following, a deep study of the modulator is given, demonstrating that the NE555 IC is used for modulating a signal with an argument modulation.

In order to understand how it is possible to modulate a message, a look inside the NE555 IC is needed. Fig.4.6 shows the equivalent electric circuit of the IC, taking care to the connections with the external components. Preliminary, the components create a square wave oscillator which, in case of $v_in(t) = 0 \forall t$, gives a 50% duty cycle square wave at the `out` pin. Let $v_{in}(t) = 0$ be $\forall t$. The logical working steps are explained in the following:

- $v_c(t) = 0, \Rightarrow$ OpAmp1 has an high output, then the output Set - Reset (SR) flip-flop is in a low output state, and the modulator output is high;

  $\Rightarrow$ The Q Transistor is turned off, then the capacitor C will increase its charge, because it is connected between the ground and V_{cc} through the series connection of R_a and R_b resistors;

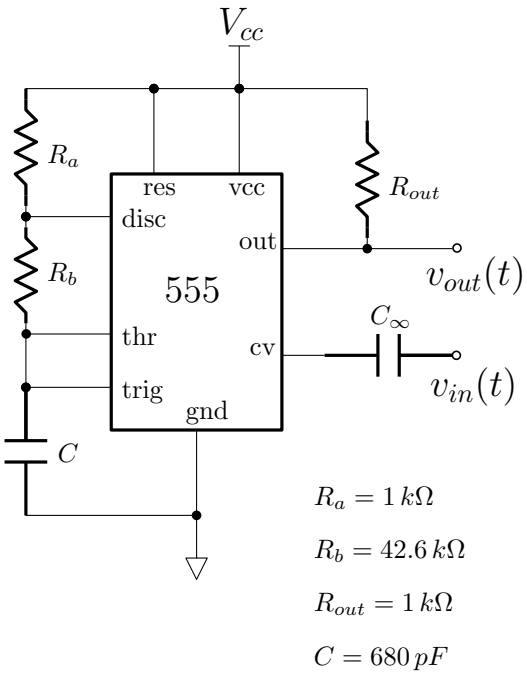

Figure 4.5: Modulator's electrical scheme.

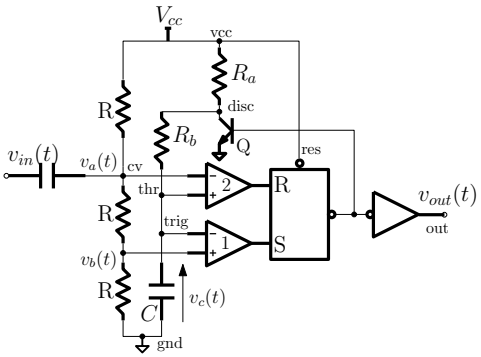

Figure 4.6: Inside the modulator: the electrical scheme of the inner blocks.

- In the capacitor charging period when $v_b(t) < v_c(t) < v_a(t)$, the SR flip-flop has both Set and Reset inputs at low level, then it maintains the high output state due to the memory effect;
- When $v_c(t) = v_a(t) = \frac{2}{3}V_{cc}$, the OpAmp2 resets the SR flip-flop and the modulator output goes at the low level, $\Rightarrow v_{out}(t) = 0$:
  - Q transistor turns on, then the capacitor C begins to discharge with the exponential law on the R_b resistor;
  - Until $v_c(t) > v_b(t)$, the modulator output will remain at low level;

4.1.1 Capacitor charging

When the modulator turns on, the capacitor is completely discharged. This cause an entire charge cycle from 0 to V_{cc} volt. After this first transient, the capacitor voltage $v_c(t)$ will be limited inside the set of values given:

$$v_c(t) \in \left[\frac{1}{3}V_{cc}, \frac{2}{3}V_{cc}\right]$$

For the capacitor charging phase, it is possible to derive the temporal law for the $v_c(t)$. Particularly:

$$i_c(t) = \frac{V_{cc} - v_c(t)}{R_a + R_b} = C\frac{dv_c(t)}{dt} \tag{4.2}$$

Resolving this differential equation referred to the capacitor current, it is possible to find the expression of the capacitor voltage, that depends to the time and current $v_c(t) = v_c(t, i_c(t))$:

$$v_c(t) = v_{c,0} + \frac{1}{C}\int_{-\infty}^{t} i_c(u)\,du \tag{4.3}$$

Calling $R_{tot} = R_a + R_b$, it is possible to make the substitution of Eq.4.3 in the Eq.4.2, obtaining:

$$i_c(t) = \frac{V_{cc} - \left(v_{c,0} + \frac{1}{c}\int_{-\infty}^{t} i_c(u)\,du\right)}{R_{tot}} \tag{4.4}$$

$$\Rightarrow R_{tot} i_c(t) = V_{cc} - \left(v_{c,0} + \frac{1}{C}\int_{-\infty}^{t} i_c(u)\,du\right) \tag{4.5}$$

Differentiating in both sides of the equation respect to the t time variable, a first order differential equation is derived, referred to the current $i_c(t)$:

$$R_{tot}\frac{di_c(t)}{dt} = -\frac{1}{C}i_c(t) \Rightarrow R_{tot}C\frac{di_c(t)}{dt} + i_c(t) = 0 \tag{4.6}$$

Substituting $R_{tot}C = \tau_c$, and, resolving the linear equation associated to Eq.4.6

$$\tau_c s + 1 = 0 \Rightarrow s = -\frac{1}{\tau_c} \tag{4.7}$$

it is possible to calculate the current expression referred to a charging phase for a capacitor, and it will be:

$$i_c(t) = i_{c,0}e^{-\frac{t}{\tau_c}}; \quad i_{c,0} = \frac{V_{cc} - v_{c,0}(t)}{R_{tot}} \tag{4.8}$$

Finally, the temporal expression for the capacitor charge is calculated substituting the charging current into the Eq.4.3:

$$v_c(t) = v_{c,0} + \frac{1}{C} i_{c,0} \int_{-\infty}^{t} e^{-\frac{u}{\tau_c}}\, du \tag{4.9}$$

$$= v_{c,0} + \frac{1}{C} \frac{V_{cc} - v_{c,0}}{R_{tot}} \int_{0}^{t} e^{-\frac{u}{\tau_c}}\, du \tag{4.10}$$

$$= v_{c,0} + \frac{V_{cc} - v_{c,0}}{R_{tot} C} (-\tau_c) \left[e^{-\frac{t}{\tau_c}} - 1 \right] \tag{4.11}$$

$$= v_{c,0} + (V_{cc} - v_{c,0}) \left[1 - e^{-\frac{t}{\tau_c}} \right] \tag{4.12}$$

$$= v_{c,0} + V_{cc} \left[1 - e^{-\frac{t}{\tau_c}} \right] - v_{c,0} \left[1 - e^{-\frac{t}{\tau_c}} \right] \tag{4.13}$$

$$= v_{c,0} e^{-\frac{t}{\tau_c}} + V_{cc} \left[1 - e^{-\frac{t}{\tau_c}} \right] \tag{4.14}$$

$$= V_{cc} - (V_{cc} - v_{c,0}) e^{-\frac{t}{\tau_c}} \tag{4.15}$$

After the first transitory, the capacitor charge phase will begin from $v_{c,0} = \frac{1}{3} V_{cc}$ voltage, and then the analytical law that expresses the charge voltage in function of the temporal variable will be:

$$v_c(t) = V_{cc} \left(1 - \frac{2}{3} e^{-\frac{t}{\tau_c}} \right) \tag{4.16}$$

4.1.2 Capacitor discharge

As it is already shown before, when the capacitor voltage becomes $v_c(t) = \frac{2}{3} V_{cc}$, the SR flip-flop inside NE555 IC will be reset, then its output will take an high level voltage, thus the Q transistor will work in saturation state (see Fig.4.6 for the components labels). The capacitor will begin to discharge, with a current flow through the resistor R_b. Due to the Kirchhoff's law for the voltage, the sum of the capacitor voltage and the resistor voltage must be zero, then:

$$v_c(t) + R_b i_c(t) = 0 \Rightarrow v_c(t) + R_b C \frac{dv_c(t)}{dt} = 0 \tag{4.17}$$

The solution of this differential equation is well known and it is:

$$v_c(t) = v_{c,0} e^{-\frac{t}{\tau_s}}; \quad \tau_s = R_b C \tag{4.18}$$

Due to the fact that the initial discharge phase sees the capacitor voltage always $v_{c,0} = \frac{2}{3} V_{cc}$, the temporal expression for the capacitor voltage during the discharge phase will be:

$$v_c(t) = \frac{2}{3} V_{cc} e^{-\frac{t}{\tau_s}} \tag{4.19}$$

4.1.3 Oscillation frequency

Referring to Fig.4.7, it is possible to calculate the oscillation frequency of the modulator (always in case of $v_{in}(t) = 0$). This parameter is simple to calculate, after the derivation of the capacitor charge - discharge temporal voltage law;

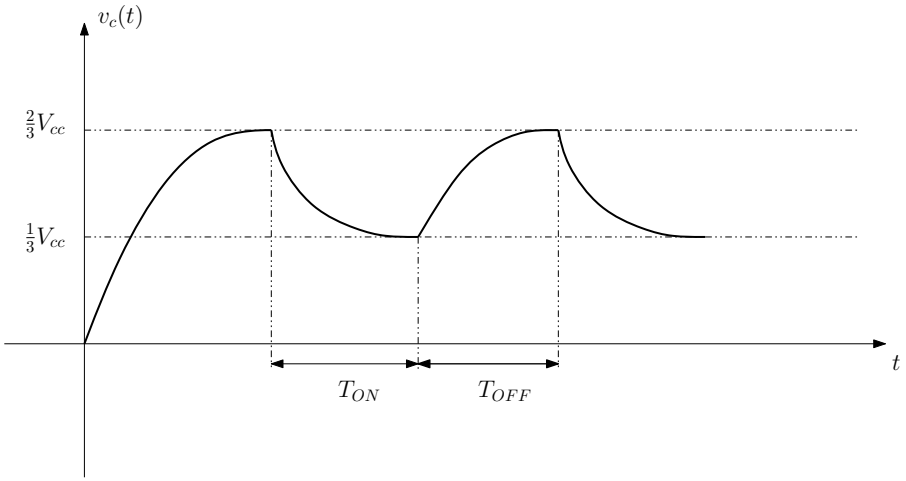

Figure 4.7: Time variations of the capacitor voltage.

For the derivation of T_{ON}, it is possible to use the Eq.4.15, and forcing the final voltage to the maximum capacitor voltage achievable in a period, e.g.,

$v_c(T_{ON}) = \frac{2}{3}V_{cc}$.

$$v_c(t) = \frac{2}{3}V_{cc} = V_{cc}\left(1 - \frac{2}{3}e^{-\frac{t}{\tau_c}}\right) \Rightarrow \frac{1}{3} = \frac{2}{3}e^{-\frac{t}{\tau_c}} \tag{4.20}$$

Extracting the natural logarithm at both sides of the equation, the time interval for an high level voltage at the output of the modulator is calculated:

$$\log\left(\frac{1}{3}\cdot\frac{3}{2}\right) = -\frac{t}{\tau_c} \Rightarrow -\tau_c \log\left(\frac{1}{2}\right) \approx 0.69\tau_c = t \tag{4.21}$$

Under the hypothesis that the begin of the time domain is referred to the begin of the charge phase, the t variable already calculated represents the time interval taken by the capacitor to modify its voltage from $\frac{1}{3}V_{cc}$ to $\frac{2}{3}V_{cc}$, thus:

$$T_{ON} = 0.69\tau_c \tag{4.22}$$

In the same way (but considering the discharge phase with the adequate voltage levels), the analytical expression of the time interval that represents the low level voltage at the output of the modulator is:

$$\frac{1}{3}V_{cc} = \frac{2}{3}V_{cc}e^{-\frac{t}{\tau_s}} \Rightarrow t = 0.69\tau_s \tag{4.23}$$

Then:

$$T_{OFF} = 0.69\tau_s \tag{4.24}$$

The oscillation frequency will be the union of T_{ON} and T_{OFF}:

$$f_{osc} = \frac{1}{0.69(R_a + 2R_b)C} \tag{4.25}$$

With the resistance and capacitance values of Fig.4.5, the frequency oscillation of the modulator, with $v_{in}(t) = 0$ is 25 kHz.

4.1.4 Input signal not equal to zero

Let see a more important case: when $v_{in}(t) \neq 0$. This is the case when the modulator receives a message. It is useful to see that the voltage at the points labeled with A and B in Fig.4.6 will be:

$$V_A(t) = \frac{2}{3}V_{cc} + v_{in}(t) \tag{4.26}$$

$$V_B(t) = \frac{1}{3}V_{cc} + \frac{v_{in}(t)}{2} = \frac{V_A(t)}{2} \tag{4.27}$$

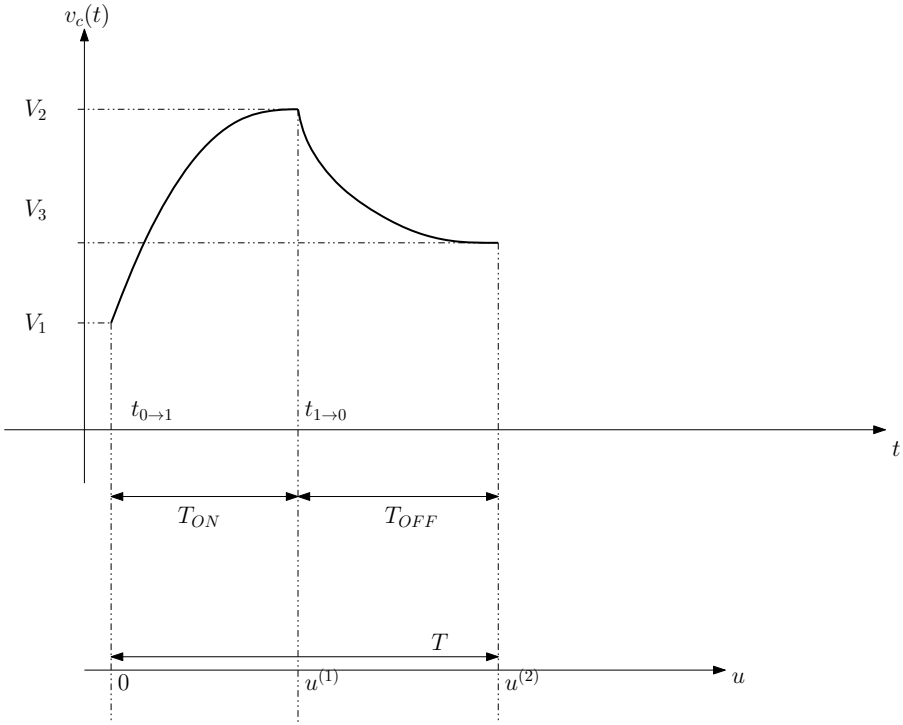

Figure 4.8: Capacitor voltage for $v_{in}(t) \neq 0$.

These two voltage values will move the thresholds used by OpAmp1 and

OpAmp2 for commutating their output levels. Particularly, referring to the Fig.4.8, it is possible to define a new temporal variable u:

$$V_1(t) = \frac{1}{3}V_{cc} + \frac{v_{in}(t_{0\to1})}{2} \to V_1(u) = \frac{1}{3}V_{cc} + \frac{v_{in}(0)}{2} \tag{4.28}$$

$$V_2(t) = \frac{2}{3}V_{cc} + v_{in}(t_{1\to0}) \to V_2(u) = \frac{2}{3}V_{cc} + v_{in}(u^{(1)}) \tag{4.29}$$

A remapped time domain has been chosen, particularly:

$$u = t - t_{0\to1}; \tag{4.30}$$

$$u^{(1)} = t_{1\to0} - t_{0\to1}; \tag{4.31}$$

$$T = [T_{ON} \cup T_{OFF}] = [0, u^{(2)}] - t_{0\to1} \tag{4.32}$$

Using the u time domain, the temporal capacitor charge law will become:

$$\begin{cases} v_c(u) = V_{cc} - [V_{cc} - v_c(0)]e^{-\frac{u}{\tau_c}}; \\ \tau_c = (R_a + R_b)C; \end{cases} \tag{4.33}$$

where:

$$v_c(0) = V_1(u) = \frac{1}{3}V_{cc} + \frac{v_{in}(t_{0\to1} \in t \equiv 0 \in u)}{2} \tag{4.34}$$

The capacitor voltage with the u time domain then will be:

$$v_c(u) = V_{cc} - \left(V_{cc} - \frac{1}{3}V_{cc} - v_{in}(0)\right)e^{-\frac{u}{\tau_c}} \tag{4.35}$$

$$= V_{cc} - \left(\frac{2}{3}V_{cc} - v_{in}(0)\right)e^{-\frac{u}{\tau_c}} \tag{4.36}$$

$$= V_{cc}\left(1 - \frac{2}{3}e^{-\frac{u}{\tau_c}}\right) + v_{in}(0)e^{-\frac{u}{\tau_c}} \tag{4.37}$$

Referring to the Fig.4.8, it should be noticed that the discharge phase is ex-

tended from $u = 0$ to $u = u^{(1)}$, and then $v_c(u^{(1)})$ will be

$$v_c(u^{(1)}) = \frac{2}{3}V_{cc} + v_{in}(u^{(1)}) \tag{4.38}$$

by definition.
Forcing the value of $u^{(1)}$ in the Eq.4.37 and matching it to Eq.4.38, the result will be:

$$v_c(u^{(1)}) = \frac{2}{3}V_{cc} + v_{in}(u^{(1)}) = V_{cc}\left(1 - \frac{2}{3}e^{-\frac{u^{(1)}}{\tau_c}}\right) + v_{in}(0)e^{-\frac{u^{(1)}}{\tau_c}} \tag{4.39}$$

$$= V_{cc} - \frac{2}{3}V_{cc}e^{-\frac{u^{(1)}}{\tau_c}} + v_{in}(0)e^{-\frac{u^{(1)}}{\tau_c}} \tag{4.40}$$

Thus:

$$\frac{1}{3}V_{cc} - v_{in}(u^{(1)}) = \left(\frac{2}{3}V_{cc} + v_{in}(0)\right)e^{-\frac{u^{(1)}}{\tau_c}}$$

and the value of $u^{(1)}$:

$$u^{(1)} = -\tau_c \log\left(\frac{\frac{1}{3}V_{cc} - v_{in}(u^{(1)})}{\frac{2}{3}V_{cc} + v_{in}(0)}\right) \tag{4.41}$$

The same analytical steps can be applied to the capacitor discharge phase: in order to find the time instant when the capacitor voltage will reach the minimum amplitude level, it is possible to match Eq.4.42 with Eq.4.43:

$$v_c(u^{(2)}) = \frac{1}{3}V_{cc} + \frac{v_{in}(u^{(2)})}{2} \tag{4.42}$$

$$v_c(u^{(2)}) = v_c(u^{(1)})e^{-\frac{u^{(2)}}{\tau_s}} \tag{4.43}$$

Obtaining:

$$e^{-\frac{u^{(2)}}{\tau_s}} = \frac{\frac{1}{3}V_{cc} + \frac{v_{in}(u^{(2)})}{2}}{v_c(u^{(1)})} \tag{4.44}$$

Applying the natural logarithm, and substituting the $v_c(u^{(1)})$ value, the $u^{(2)}$

expression could be derived:

$$u^{(2)} = -\tau_s \log\left(\frac{\frac{1}{3}V_{cc} + \frac{v_{in}(u^{(2)})}{2}}{V_{cc} - \left(\frac{2}{3}V_{cc} + v_{in}(0)\right)}\right) \tag{4.45}$$

Taking advices by these analytical steps, it should be noted that the input signal at the modulator at time $u = 0$ gives its influence to the n-th time instant $u^{(n)}$. It is clear to understand that the waveform's periods at the output of the modulator depend also on the initial value of the input signal, according with the measurement campaign, and the signal investigation: in fact a FM modulated signal has been discovered at the output of the modulator.

Therefore, it is possible to give a simpler analytical form for the voltage signal that drives the IR LEDs:

$$x_{TX}(t) = \frac{1}{2} + \frac{1}{2}\text{sign}\left\{\cos\left(2\pi f_c t + 2\pi k \int_0^t x(u)\,du\right)\right\} \tag{4.46}$$

Fig.4.9 gives the proof that the modulated signal is actually a FM signal. The result has been retrieved demodulating with a Matlab script the output signal from modulator of Fig.4.1. The obtained waveform is congruent with the message transmitted.

4.2 Analog receiver

Another confirmation about the used modulation is given by studying the receiver architecture. The receiver device is composed by a certain number of simple components, used mainly in FM broadcast radio demodulators. Studying the electric scheme, it is possible to describe the existing receiver using a block diagram, as it is depicted in Fig.4.10. where $h_d(t)$ is a lowpass filter with a bandwidth $\varepsilon_{h_d(t)} \in [-4; 4]$ kHz.

In this section, the main topic is the demodulation methodology: it is entirely done by using a specific IC named MC3361CD (and its main internal structure is shown in Fig.4.14). This IC execute the FM demodulation with a spectrum centered around the 455 kHz frequency; the optical received signal by the photodiode is amplified and filtered, and it has a spectrum centered

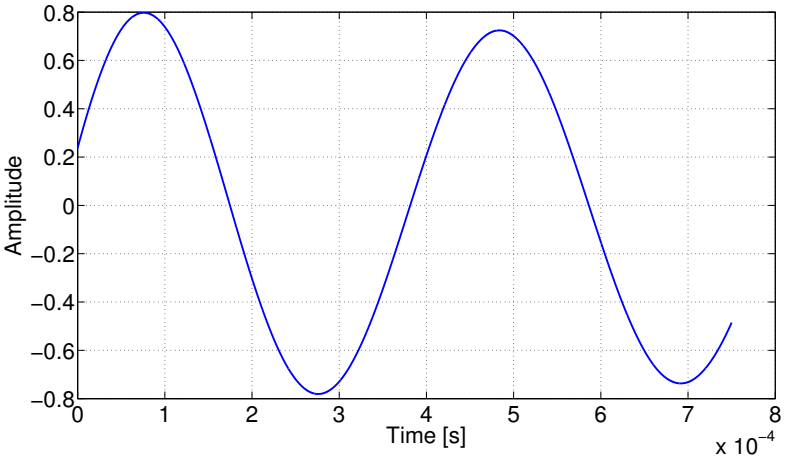

Figure 4.9: Numerically demodulated FM transmitted signal.

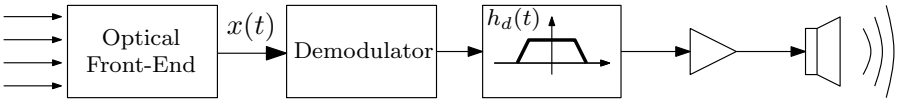

Figure 4.10: Receiver block scheme.

around the carrier frequency f_c that follows the Carson's rule:

$$B_{FM} = 2(B_s + \Delta F) = 2(B_s + k) \tag{4.47}$$

Using the Fourier expansion series, it is possible to demonstrate that the spectral extension for a squared FM signal (Eq.4.46) occupy the odd spectral repetitions as it is explained in Eq.4.48:

$$B_{FM,n} = 2n(B_s + k) \tag{4.48}$$

The graphical representation of the FM squared spectrum (the signal labeled with $x(t)$ in Fig.4.10) is displayed in Fig.4.11.

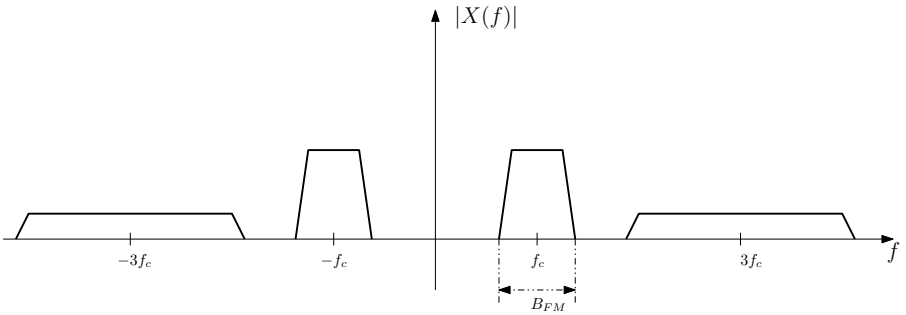

Figure 4.11: Spectrum of a squared FM signal.

Isolating the fundamental contribution of the entire FM spectrum (the spectrum centered around f_c), it should be noted that $x(t)$ is connected to the mixer present inside the MC3361CD IC: the demodulated signal is multiplied by a tone generated locally:

$$v_{lo}(t) = \cos(2\pi f_{lo} t) \tag{4.49}$$

Calling $m(t)$ the modulated message, and $x(t)$ the received signal, the expression for the output signal from the mixer is:

$$y(t) = x(t)v_{lo}(t) = \text{sign}\left\{\cos\left(2\pi f_c t + 2\pi k \int_0^t m(u)\,du\right)\right\}\cos(2\pi f_{lo} t) \tag{4.50}$$

where the mean value of $x(t)$ is deleted. This operation has been performed in order to shift the received signal spectrum around the 455 kHz frequency (and the reason will be explained in the following). To do this, the tone frequency of the local oscillator must be $f_{lo} = 480$ kHz, thus the spectrum of the received signal will be shifted around the requested frequency (see Fig.4.12).

The next demodulator block is a Surface Acoustic Wave (SAW) passband filter (fig.4.13) centered around 455 kHz: this is a standard frequency value, used in the FM radio demodulators, and this is the reason why the local oscil-

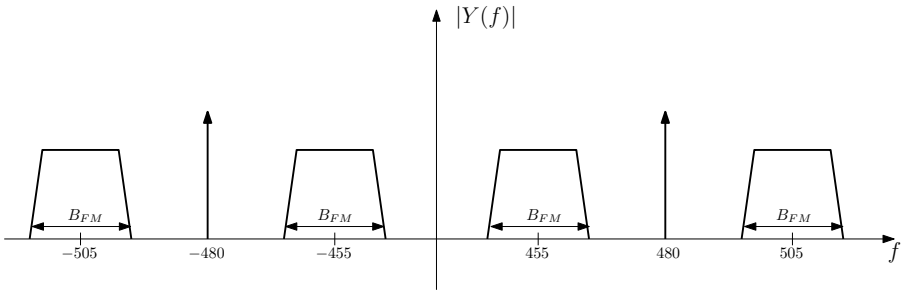

Figure 4.12: $y(t)$ spectrum

lator connected to the mixer shifts the received signal around this frequency.

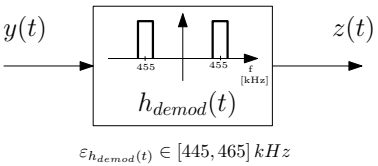

Figure 4.13: SAW filter.

Since this SAW filter has an high selectivity (achievable via a resonator structure), the signal $z(t)$ is a FM sinusoidal modulated signal centered around the 455 kHz frequency, that is the frequency that is accepted by the MC3361CD IC. The demodulator is composed by a quadrature discriminator, and a low-pass filter to isolate the audio spectrum.

Finally, the demodulated message is amplified and sent to a loudspeaker.

It should be clear that only a vocal message could be played, and only a contextual information could be sent in order to give any kind of help to an user. For this reason, a digital architecture is needed, in order to improve the flexibility of the system, and allowing to implement a numerical transmission for sending numerical data. This is useful when a complete navigation architecture must be implemented. The deviation and the carrier frequency have been obtained with an Digital Storage Oscilloscope (DSO), and the analysis

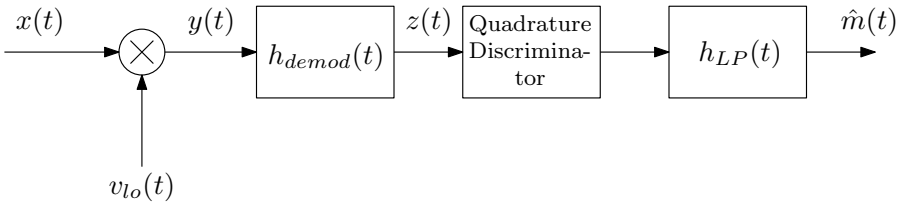

Figure 4.14: MC3361CD block scheme.

has been made using Matlab scripts. In the following the parameters of the modulation are expressed, with the labels used in the whole thesis.

- Carrier frequency: $f_c = 25$ kHz;
- Deviation $k = 7260$ $[(Vs)^{-1}]$;

Chapter 5

Digital architecture

As it is proposed in [21], a development and an implementation of the digitalized architecture is presented and realized, describing all the constitutive digital blocks and the analytical steps used. This architecture must preserve the entire set of parameters seen in the study of the analog architecture, in order to have the complete compatibility. This allows to use the already available analog platform studied in the previous chapter, with the digital one studied here. This assures that a digital transmitter could be used with an analog receiver, and vice versa. The whole digital architecture is realized describing each block with VHDL language, and implementing it on a FPGA.

5.1 Digital transmitter

In order to realize a digital fully compatible transmitter, a discretization of the analytical model is needed. Using the analytical form seen for the analog transmitter, the schematic approach is shown in Fig.5.1.

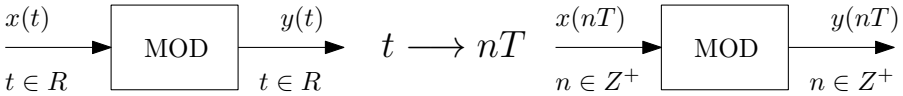

Figure 5.1: Transmitter digitalization.

Mathematically:

$$y(t) = \frac{1}{2} + \frac{1}{2}\text{sign}\left\{\cos\left(2\pi f_c t + 2\pi k \int_0^t x(u)\,du\right)\right\} \tag{5.1}$$

Since all of the digital components use a discrete time domani, it is useful to apply the rule of Fig.5.1, and the mathematic expression becomes:

$$y(nT) = \frac{1}{2} + \frac{1}{2}\text{sign}\left\{\cos\left(2\pi f_c nT + 2\pi k \sum_{i=0}^{n} x(iT)\right)\right\} \tag{5.2}$$

With this discrete analytical model, it is possible to draw the block diagram of the transmitter, with all the operations needed. Fig.5.2 shows the conceptual approach to the development.

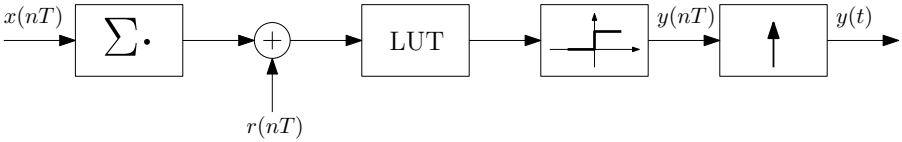

Figure 5.2: Block scheme for the digital modulator.

The signals used are

- $x(nT)$: input signal to the modulator, with a sample period of T seconds;
- $r(nT)$: time ramp signal

$$r(nT) = 2\pi f_c T n; \quad n \in [0, ..., 1/T] \tag{5.3}$$

- $y(nT)$: discrete time modulated signal;
- Look Up Table (LUT) used to contain the cosine function samples;

The effective schematic block useful to be implemented is shown in Fig.5.3

The signal at the input of LUT block is the cosine argument. The waveform at the output of LUT block is squared and finally interpolated. This operation

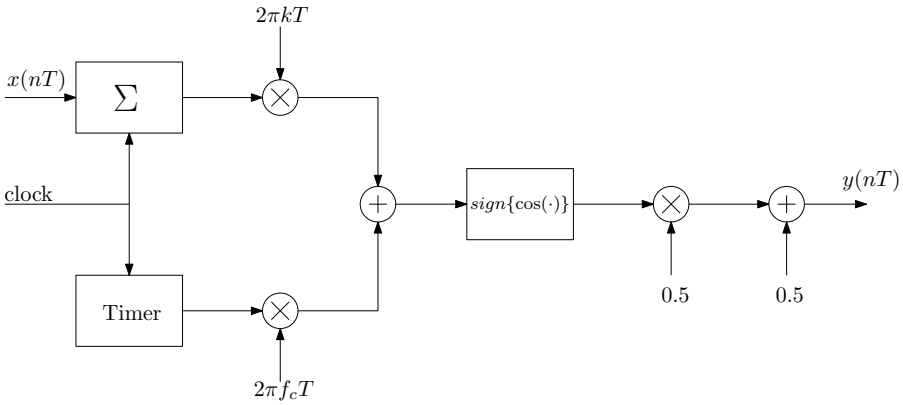

Figure 5.3: Block scheme for the implementation of the modulator.

is performed in order to give a continuous time domain signal to the IR LED illuminators.

As it is explained, the sign of cosine function is requested. To do this, it is possible to save resources on the FPGA platform simply unifying the LUT and squaring blocks. Moreover, taking care to the digital saving resources, the two multipliers present at the output of the discrete integrator and at the output of the Timer block, can be absorbed or moved in a strategical points of the scheme.

The first part of the resource saving steps concerns the possibility to have the sign of the cosine function (Fig.5.4(a)) without the use of a LUT block. In fact, the modulated signal is:

$$y(nT) = \cos\left(2\pi f_c nT + 2\pi kT \sum_{i=0}^{n} x(iT)\right); \quad \sum_{i=0}^{n} x(iT) = X(nT) \tag{5.4}$$

$$= \cos\left[2\pi\left(f_c nT + kTX(nT)\right)\right] \tag{5.5}$$

$$= \cos(2\pi\alpha(nT)); \qquad \alpha(nT) = f_c nT + kTX(nT) \tag{5.6}$$

The parameter named $\alpha(nT) \in [0, 1[$, then the graphic shown in Fig.5.4(a)

could be modified, taking as argument $\alpha(nT)$ (fig.5.4(b)). Thus:

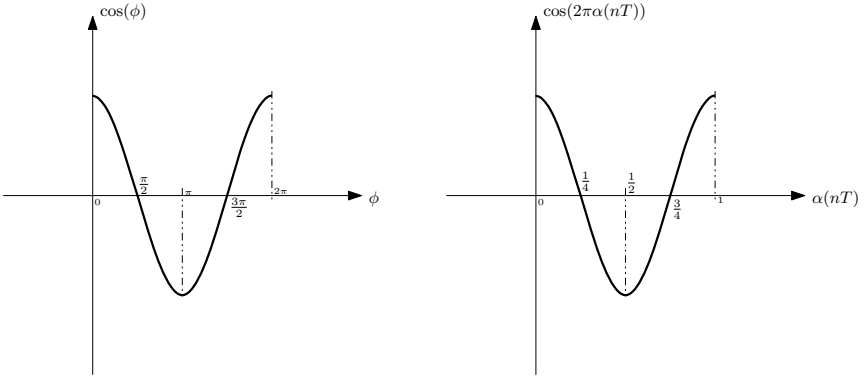

(a) Cosine function

(b) Cosine function in the $\alpha(nT)$ domain

Figure 5.4: $\cos(\phi)$ and $\cos(2\pi\alpha(nT))$ functions

$$\begin{cases} y(nT) & = 1 \Rightarrow \alpha(nT) \in \left[0; \frac{1}{4}\right[\cup \left]\frac{3}{4}; 1\right] \\ y(nT) & = 0 \Rightarrow \alpha(nT) \in \left[\frac{1}{4}; \frac{3}{4}\right] \end{cases} \tag{5.7}$$

The cosine squaring operation is simple and its cost is terms of digital resources over the FPGA is lower than the LUT implementation. In fact, the operation is reduced to a comparison between the values indicates in Eq.5.7 and the value of $\alpha(nT)$. Since cosine function is even, the absolute value of $\alpha(nT)$ can be compared, due to the fact that the argument can be negative. The optimized block scheme becomes as it is depicted in Fig.5.5.

Referring to Fig.5.5, the M2 Multiplier can be united with the block Timer implicitly. In fact the output of the Timer block counts multiple values of f_cT. It is useful to choose a certain value for the parameters used in the modulator (such as the sampling frequency), in order to optimize the used digital resources. Choosing a sampling frequency of 800 kHz, and knowing the carrier frequency $f_c = 25$ kHz, the product $f_cT = 0.03125 = 2^{-5}$. The Timer block will be composed by a sequential adder that, at every clock cycle, adds 2^-5 to the previous value stored at its output. Moreover, in order to reduce

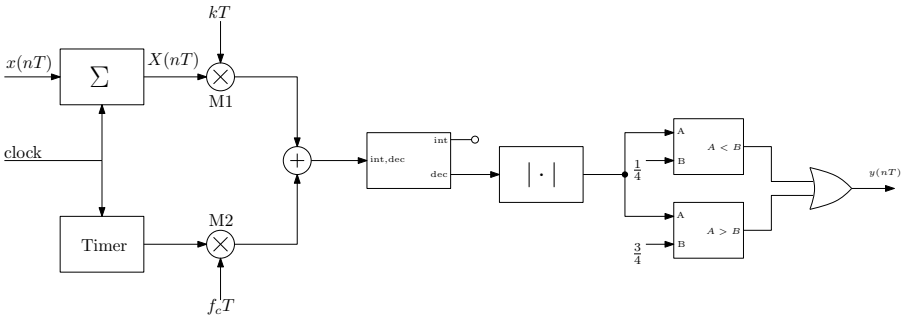

Figure 5.5: Optimized modulator block scheme, using the comparison of the $\alpha(nT)$ value.

the dimension of the buses inside the FPGA, the M1 Multiplier can be moved before the cumulative sum, at the input of the modulator. This allows to avoid the overflow sum when the input signal presents a large number of samples with an amplitude near to the maximum value. Moreover this allows to use a reduced dimension for the buses used inside the modulator. Particularly, the data are codified with 16 bits as it is shown in Fig.5.6.

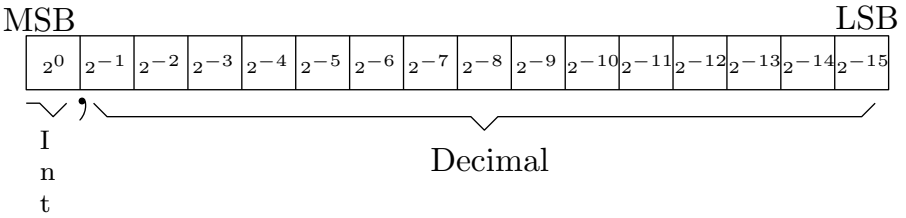

Figure 5.6: Bit word for the modulator.

The Most Significant Bit (MSB) is also used as sign bit, and then with this particular configuration, the representable values will be $[-1, 1 - 2^{-15}]$. Due to the fact that the Σ block computes the cumulative sum:

$$X(nT) = x(nT) + X((n-1)T) \tag{5.8}$$

the signal $X(nT)$, under the hypothesis that $x(nT) \in [-1, 1]$, could represent a value with the integer part greater than 1. With the strategical move of M1, the maximum values at the input of the Σ block will be in the set $[-0.009075, 0.009075[$. It is important to take care only about the decimal part of the cumulative sum: this means that it is not important to do any extension to the default bit word dimension. The final block scheme is presented in Fig.5.7, and the hardware implementation will follow it.

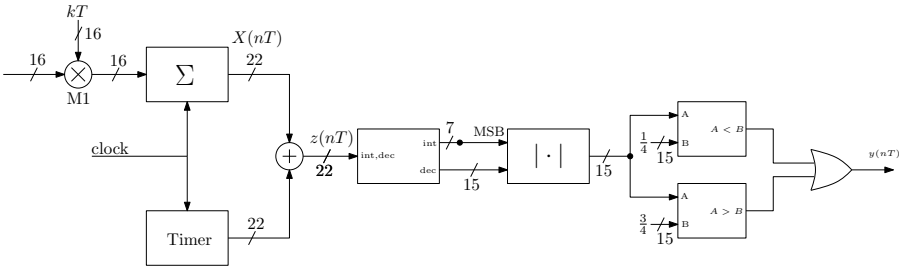

Figure 5.7: Final VHDL Modulator block scheme.

5.1.1 Overview on the digital implementation

Cumulative sum

With the reference of Fig.5.8, the signal at the output is similar to the Eq.5.8:

$$y(nT) = x(nT) + y((n-1)T) \tag{5.9}$$

Timer

As it is explained before, the output of the Timer block must be a multiple value of $f_c T = 2^{-5}$. For a bit word that have a dimension of 16 bits, the structure of Timer block is shown in Fig.5.9.

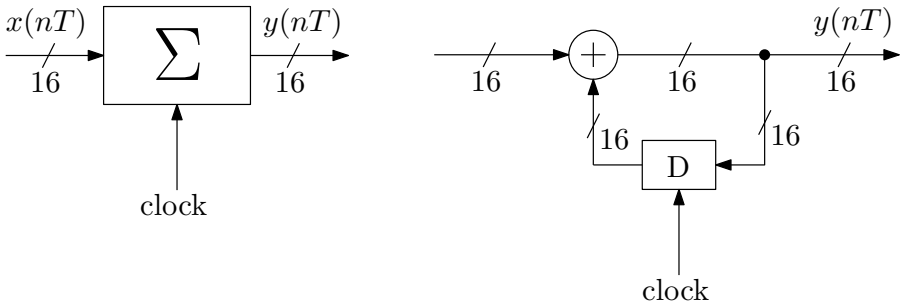

Figure 5.8: Cumulative sum block scheme.

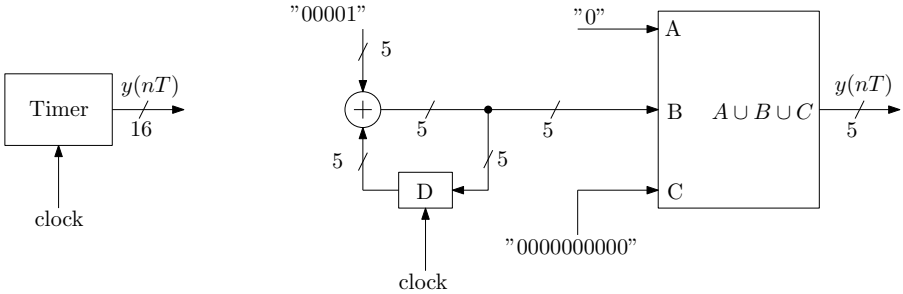

Figure 5.9: Timer block scheme.

Squaring block

The squaring block takes the entire bit word that represent $\alpha(nT)$ and calculates the absolute value. This operation can be performed easily processing the MSB of the input word, executing the XOR logic operation bitwise with the MSB. After, a comparison with the values expressed in system of Eqs.5.7 has been done. The detailed scheme is shown in Fig.5.10.

Optical transmission front - end

The optical transmission front - end is composed by a number of IR LEDs and a current amplifier, that assure a sufficient amount of current to the LEDs.

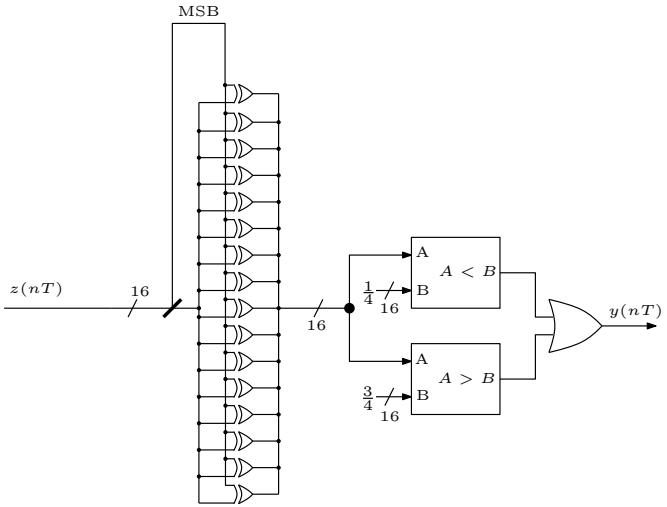

Figure 5.10: Squaring block scheme.

The total number of IR LEDs is in function of the requested optical power. For instance, low power is preferred in smaller rooms, in order to avoid the reflections made by the walls: in fact a strong reflected beam may hit the receiver, even if the user has not oriented the receiver to the transmitter. This may causes a misunderstanding when the user tries to follow the received navigation data.

5.2 Digital receiver

The first step to digitalize the demodulator block is to decide which kind of architecture could be used. In [22] are shown two demodulator's type, based on trigonometrical algorythms: in this section a simpler demodulator is used for reasons that will be clear in the following of this section. Fig.5.12 shows the demodulator's block diagram chosen, where:

- $v(nT)$: received signal from optical front-end;

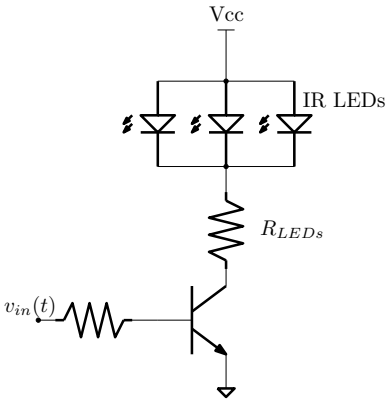

Figure 5.11: Electric scheme for the transmitter optical front - end.

- $h(nT)$: impulsive response of a bandpass filter with:

$$H(f) \in [-B, -\varepsilon] \cup [\varepsilon, B] \tag{5.10}$$

  where B is the maximum frequency that is contained in a vocal message, and ε is a very small value of frequency close to 0;

- $y(nT)$: demodulated vocal message;

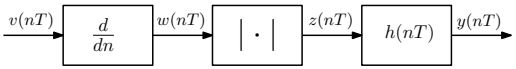

Figure 5.12: Digitalized FM demodulator.

First of all, it is useful to give a correct expression of signal $v(nT)$ which is

$$v(nT) = \text{sign}\left\{\cos(\alpha(nT))\right\} \tag{5.11}$$

Since a differentiation will be done, a frequency representation must be used to derive the entire set of signals. This assures to obtain an analytical function of the differentiated signal $v(nT)$. Using Fourier expansion series, it is possible

to calculate signals $w(nT)$ and $z(nT)$ in an easy way. Signal $v(nT)$ can be modeled as an even function, and Fourier series referred to $v(nT)$ will be:

$$v(nT) \sim \sum_{k=1}^{+\infty} \frac{4}{k\pi} \sin\left(k\frac{\pi}{2}\right) \cos(k\alpha(nT)) \tag{5.12}$$

where mean value and all the sine coefficients are zero. With this expression, is easy to derive the analytical form of $w(nT)$ and $z(nT)$.

$$w(nT) = \frac{d}{dn} v(nT) \tag{5.13}$$

$$= [4f_cT + 4K_{FM}T\,x(nT)] \sum_{k=1}^{+\infty} \times \tag{5.14}$$

$$\times \left[\cos\left(k\alpha(nT) + \frac{k\pi}{2}\right) - \cos\left(k\alpha(nT) - \frac{k\pi}{2}\right)\right]$$

and the analytical steps to retrieve this result are:

$$w(nT) = \frac{d}{dn} v(nT) \tag{5.15}$$

$$= \frac{d}{dn} \sum_{k=1}^{+\infty} \frac{4}{k\pi} \sin\left(k\frac{\pi}{2}\right) \cos(k\alpha(nT)) \tag{5.16}$$

$$= \sum_{k=1}^{+\infty} \frac{4}{k\pi} \sin\left(k\frac{\pi}{2}\right) \frac{d}{dn} \cos(k\alpha(nT)) \tag{5.17}$$

$$= \sum_{k=1}^{+\infty} \frac{4}{k\pi} \frac{d\alpha(nT)}{dn} k \sin\left(k\frac{\pi}{2}\right) (-\sin(\alpha(nT)k)) \tag{5.18}$$

Using the identity

$$\sin(\alpha)\sin(\beta) = \frac{1}{2}\left[\cos(\alpha - \beta) - \cos(\alpha + \beta)\right]$$

and

$$\frac{d\alpha(nT)}{dn} = \alpha'(nT) = 2\pi f_cT + 2\pi K_{FM}T\,x(nT)$$

derivation can be continued to the result seen before:

$$w(nT) = \frac{2\alpha'(nT)}{\pi} \sum_{k=1}^{+\infty} \left[\cos\left(k\alpha(nT) + \frac{k\pi}{2} \right) - \cos\left(k\alpha(nT) - \frac{k\pi}{2} \right) \right] \quad (5.19)$$

$$= [4f_c T + 4K_{FM} T\, x(nT)] \times$$

$$\times \sum_{k=1}^{+\infty} \left[\cos\left(k\alpha(nT) + \frac{k\pi}{2} \right) - \cos\left(k\alpha(nT) - \frac{k\pi}{2} \right) \right] \quad (5.20)$$

Since the time domain is discrete, the sum will be trunked, according with the Shannon's theorem. Particularly, the upper limit of the sum will be given using the Carson's rule. The maximum frequency occupied by an FM system is:

$$f_{MAX,FM} = B + k_{FM} \quad (5.21)$$

where B is the occupied band of the modulating signal. According with the expression of $w(nT)$, the maximum value of the sum index k will be given by:

$$(B + k_{FM})k \leq \frac{1}{2T} \Rightarrow k \leq \frac{1}{2T(B + k_{FM})} \quad (5.22)$$

Thus, calling:

$$\chi = \frac{1}{2T(B + k_{FM})} \quad (5.23)$$

the final form for $w(nT)$ signal is:

$$w(nT) = [4f_c T + 4K_{FM} T\, x(nT)] \times$$

$$\times \sum_{k=1}^{\chi} \left[\cos\left(k\alpha(nT) + \frac{k\pi}{2} \right) - \cos\left(k\alpha(nT) - \frac{k\pi}{2} \right) \right] \quad (5.24)$$

For the derivation of $z(nT)$ it is useful to call

$$w_o(nT) = \sum_{k=1}^{\chi} \left[\cos\left(k\alpha(nT) + \frac{k\pi}{2} \right) - \cos\left(k\alpha(nT) - \frac{k\pi}{2} \right) \right] \tag{5.25}$$

thus:

$$w(nT) = [4f_cT + 4K_{FM}Tx(nT)]w_o(nT); \tag{5.26}$$

Now, applying absolute value operation, $z(nT)$ becomes:

$$z(nT) = |4f_cT + 4K_{FM}T\,x(nT)|\,|w_o(nT)| \tag{5.27}$$

But f_c is always greater than K_{FM}, and sent message has limited amplitude value $|x(nT)| \leq 1$, then absolute value of the first part of $z(nT)$ is equal to its argument, because it is always positive:

$$z(nT) = (4f_cT + 4K_{FM}T\,x(nT))\,|w_o(nT)| \tag{5.28}$$

Keeping always in mind block diagram displayed in Fig.5.12, the output signal $y(nT)$ is the result of convolution operation between $z(nT)$ and a bandpass filter with impulse response $h(nT)$. But a digital filter with a bandpass described in Eq.5.10 is hard to implement: the solution described in the following allows to use a very simple lowpass IIR filter instead a FIR filter with an high coefficients number, saving resources on digital platform. Let $g(nT)$ be the impulse response of a digital lowpass IIR filter with $\varepsilon_{g(nT)} \in [-B, B]$:

$$y(nT) = z * g(nT) = 4f_cT + 4K_{FM}T\,x(nT) \tag{5.29}$$

This result is achievable remembering the expression of $|w_o(nT)|$, that represents a sequence of Dirac deltas. Hypothesizing the signal $x(nT) = 0$, $\forall n \in \mathbb{Z}$, the upper limit of the sum of eq.5.23 becomes:

$$\Gamma = \frac{1}{2f_cT} \tag{5.30}$$

Thus:

$$|w_o(nT)| = \left| \sum_{k=1}^{\Gamma} \left[\cos\left(\omega_c k n T + \frac{k\pi}{2}\right) - \cos\left(\omega_c k n T - \frac{k\pi}{2}\right) \right] \right| \tag{5.31}$$

$$= \frac{1}{2f_c T} \sum_{k=1}^{N_\delta} \delta\left(nT - \frac{k}{2f_c}\right) 1(nT) \tag{5.32}$$

where N_δ is the number of impulses during a period of N samples of $|w_o(nT)|$. This number is given by the number of zero crossings of the cosine functions in Eq.5.24, when $k = 1$. This result is the differential of the squared version of a cosine function. Since the zero crossings have a periodicity of $\frac{1}{2f_c}$, it is easy to calculate N_δ:

$$N_\delta \frac{1}{2f_c} = NT \Rightarrow N_\delta = 2f_c NT \tag{5.33}$$

The spectral components of this representation of $|w_o(nT)|$ can be calculated using the Fast Fourier Transform (FFT) over the N points, where N is the number of samples per period of $w_o(nT)$:

$$W_o\left(\frac{m}{NT}\right) = \frac{1}{2f_c NT} \sum_{n=0}^{N-1} \sum_{k=1}^{N_\delta} \delta\left(nT - \frac{k}{2f_c}\right) 1(nT) e^{-i2\pi \frac{nm}{N}} \tag{5.34}$$

We are interested about the $m = 0$ contribution, in order to calculate the $|w_o(nT)|$ harmonic value at zero frequency. This helps to calculate the contributions that survive after a filtering operation (done by $g(nT)$ lowpass filter).

$$W_o(0) = \frac{1}{2f_c NT} \sum_{n=0}^{N-1} \sum_{k=1}^{N_\delta} \delta\left(nT - \frac{k}{2f_c}\right) 1(nT) \tag{5.35}$$

Eq.5.35 can be resolved firstly using the sampling property of the delta function. In fact, eq.5.35 is equal to the sum of N_δ deltas during a period composed by N samples. The result is simply:

$$W_o(0) = 1 \tag{5.36}$$

Moreover, the spectrum is composed by Dirac deltas at multiple frequencies of $\frac{1}{2f_c}$ with an amplitude equal to 2: this is clear to see, thinking about the Fourier transformation of Eq.5.24. According with Eq.5.28, the convolution with the spectrum of $\frac{2\alpha'(nT)}{\pi}$ by the spectrum of $|w_o(nT)|$ shifts the spectrum of $|w_o(nT)|$ around the spectrum of $\frac{2\alpha'(nT)}{\pi}$, giving the possibility to retrieve the audio spectrum. Now it is easy to extract received message $\hat{x}(nT)$ which is:

$$\hat{x}(nT) = \frac{y(nT) - 4f_cT}{4K_{FM}T} \tag{5.37}$$

The complete demodulator's block diagram is shown in Fig.5.13, where $h(nT)$ is the equivalent impulse response of the dashed block that includes lowpass filter $g(nT)$,

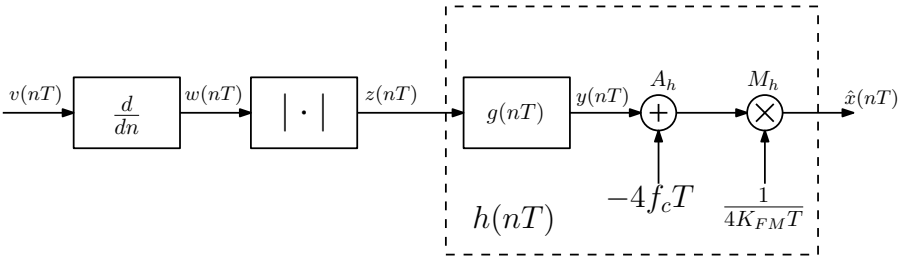

Figure 5.13: Digitalized FM demodulator using IIR lowpass filter.

5.2.1 Overviwen on the digital implementation

Digital IIR Filter

As it is explained before, $g(nT)$ is a digital lowpass IIR filter, and its coefficients have been calculated with Matlab tool `fdatool`. Particularly $g(nT)$ is a Chebychev IIR fourth order lowpass filter with 0.1 dB passband ondulation; Structure of $g(nT)$ is shown in Fig.5.14.

where

- Dx : Delay component that copies input data on the output every falling or rise edge system clock;

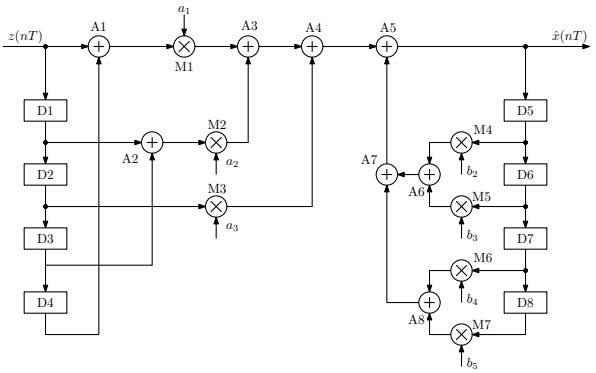

Figure 5.14: IIR fourth order lowpass filter structure.

- Mx : Multiplier;
- Ax : Adder;
- $z(nT)$: input signal;
- $\hat{x}(nT)$: output signal;

Coefficients that appear in the structure are referred to the numerator and denominator coefficients of $\mathcal{Z}\{g(nT)\}$. Using signal names as in Fig.5.14, zeta transformation of transfer function is:

$$G(z) = \frac{\hat{X}(z)}{Z(z)} = \frac{\sum_{i=0}^{N_g-1} a_{i+1} z^{-i}}{1 + \sum_{i=1}^{N_g-1} b_{i+1} z^{-i}} \tag{5.38}$$

where N_g is the order of the filter.

It is possible saving M1 filter multiplier, with a little modification of architecture shown Fig.5.13. Particularly, a_1 coefficient can be united with multiplier coefficient relative to M_h. This is allowed by the linearity rule, that it can also used to move adder A_h before $g(nT)$. Fig.5.15 shows the final block scheme for FM demodulator, and $g'(nT)$ is the same filter $g(nT)$ without M1 multiplier inside itself.

To implement it in a correct way, it is useful to simulate the numerical

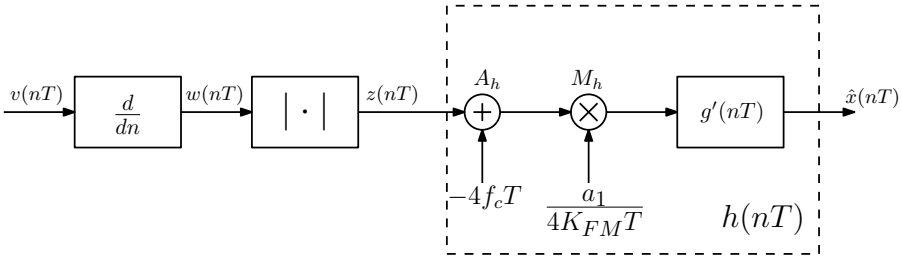

Figure 5.15: Final architecture for FM demodulator.

amplitude of the inner signals of the filter. Using a Matlab script, the working amplitude range is completely covered by using a bit word with a 25 bit dimension, divided in 19 bits used for the decimal part representation, and 6 bits for the integer part, taking care to use the MSB as sign of the value.

Differential block

This block is a simple recursive subtraction, and the implementation is depicted in Fig.5.16

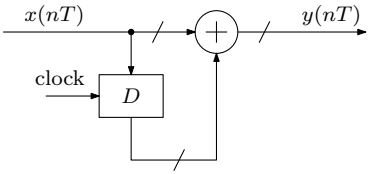

Figure 5.16: Differential block.

The output relationship is defined as:

$$y(nT) = x(nT) - x((n-1)T) \tag{5.39}$$

Absolute value block

This block is similar to the one seen for the modulator. It uses the MSB of the signal to execute the bitwise XOR logic operation with itself. Fig.5.17 shows

the physical implementation.

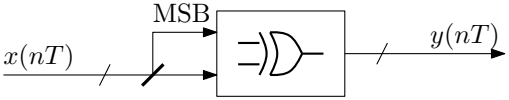

Figure 5.17: Absolute value block.

Chapter 6

Digital encoding and decoding architecture

As is explained in the introduction, this simple IR link has been used for vocal messages transmission, but, in order to implement an architecture that allows user's localization, numerical data transmission is needed. Taking care of fact that the compatibility must be preserved, it is not possible to change the global modulation type. This means that the FM link must be used to transmit both vocal and numerical data. For this reason, the blocks cascade composed by FM MODulator (MOD), IR channel, and FM DEMODulator (DEMOD) can be assumed as an equivalent channel. Maximum frequency allowed in this equivalent channel is given mainly by the cutoff frequency of $g'(nT)$ lowpass demodulator filter. Fig.6.1 shows the basic idea used to transmit numerical data with an FM optical link.

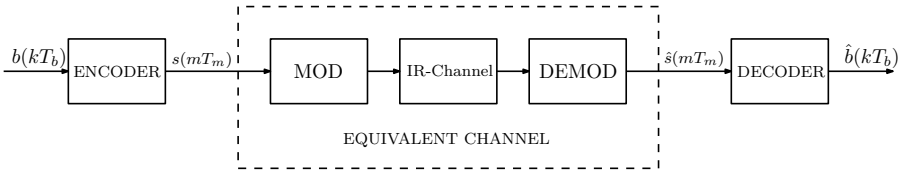

Figure 6.1: Equivalent IR channel and numerical modulation system.

The two external blocks connected to the Equivalent Channel, implement the numerical modulation. The input of the Encoder block $b(kT_b)$ is a M bit

parallel word, with a word period equal to T_b seconds. The signal $s(mT_m)$ at the output of the Encoder block is the signal which drives the MOD block. Its sample period is T_m seconds, according with the architecture for the digitalized FM modulator.

In order to transmit the digital data, an A-MTM has been implemented and in the following we will give a brief description of this kind of modulation. A-MTM uses a set of M tones, where each tone will be transmitted if the correspondent bit of the $b(kT_b)$ bit vector is set on '1' logical value. If the bit is set to '0' logical value, the correspondent tone will not transmitted. It is a matter of fact that it is possible to send M bits with M tones. Fig.6.2 shows the positive part of the total frequency spectrum, with the M = 4 tones used to codify four bits. In the figure, the bit sequence codified results '1101'.

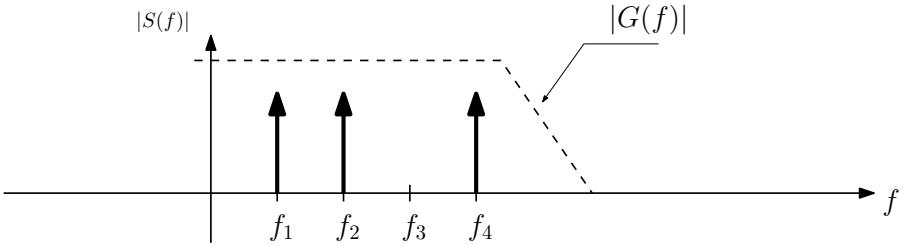

Figure 6.2: A-MTM used spectrum.

The total amount of the available spectrum depends to the $|G(f)|$ frequency response of the lowpass filter used to demodulate the FM signal. It should be noted that an entire A-MTM symbol is composed by a number of samples that allows to codify the minimum frequency period. It is convenient to express the analytical expression for the signal $s(mT_m)$, in order to derive the block scheme for the Encoder. It should be noted that the amplitude of each tone must be calculated due to the condition:

$$|s(mT_m)| \leq 1 \forall m \in \mathbb{Z} \tag{6.1}$$

Then, calling $\bar{b}$ the bit vector $b(kT_b)$, and $\bar{f} = [f_1 \dots f_M]$ the frequency vector that groups the M tones, we can write:

$$s(mT_m) = \sum_{l=1}^{M} \frac{b_l}{\sum_{i=1}^{M} b_i} \cos(2\pi f_l m T_m) \tag{6.2}$$

where b_i and b_l are the components of $\bar{b}$, and f_l is the components of $\bar{f}$.

6.1 A-MTM Encoder

Eq.6.2 shows that the signal $s(mT_m)$ is composed by M tones multiplied by the inverse of the sum of each $\bar{b}$ component. This allows to be sure to verify the condition 6.1, and this is the first step to design the block scheme for the Encoder block. The second part of the Encoder block is to generate the cosine samples. This could be done with M LUTs that contain $N_{s,i}$ samples of the cosine waveform for each f_l frequency. In order to understand how many samples are needed, a simple calculation could be done: the lowest frequency f_1 is calculated as:

$$f_1 = \frac{1}{N_{s,1} T_s} \Rightarrow N_{s,1} = \frac{1}{f_1 T_s} \tag{6.3}$$

All the M LUTs will contain the same number of samples, in order to simplify the implementation: in fact, with a fixed dimension LUTs, only one "LUT Counter" block is required. If f_1 is the fundamental frequency, each LUT will contain a number of periods equal to L, where L is the number of the channel that is driven by its correspondent LUT.

The multiplication coefficients are stored in a specific MULtiplier (MUL) Look Up Table (LUT): this choice has been taken to avoid the implementation of a divider block on the hardware platform, that uses much more resources ([23]) than the proposed solution. The index bus for the MUL LUT is represented by the sum of each component of the $\bar{b}$ vector, and it will be composed by $\log_2 \dim \bar{b}$ bits. Following Eq.6.2, it is easy to see that the AND gate connected to the output of each LUT permits to implement the multiplication of the cosine samples by the logical value of the correspondent bit b_l.

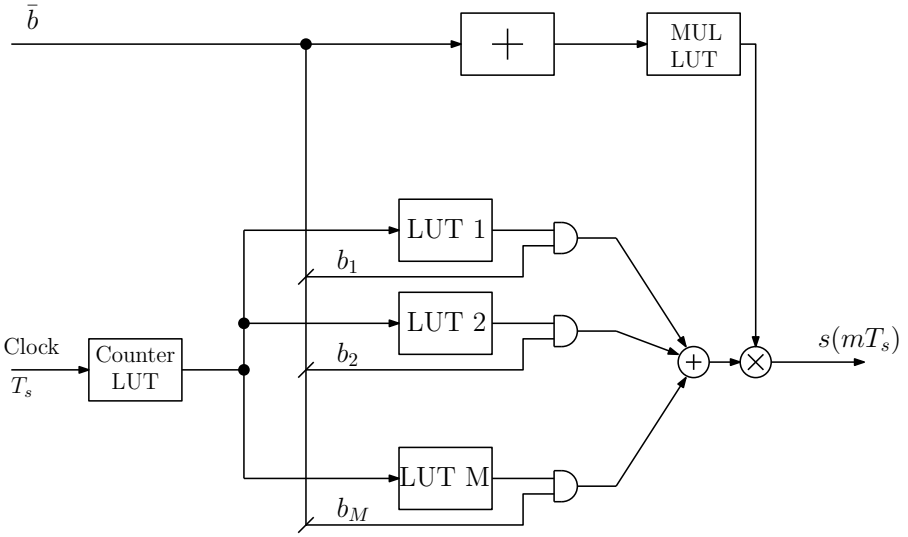

Figure 6.3: A-MTM Encoder schematic blocks.

6.2 A-MTM Decoder.

For the A-MTM decoder a simple correlation receiver [24] is used to rebuild the transmitted symbol. Fig.6.4 shows the correlator receiver using the discrete time domain. The main idea is to use the scalar product to determine the existence of a single A-MTM tone. $\hat{s}(mT_m)$ is the demodulated signal from the FM Demodulator (see Fig.6.1). This signal will be multiplied by the set of orthogonal functions $\bar{\phi} = [\phi_1 \dots \phi_M]$ defined as in the following:

$$\phi_i = \cos(2\pi f_i m T_m); \quad f_i \in \bar{f} \tag{6.4}$$

The discrete integration of the product $\hat{s}(mT_m)\phi_i$ gives the discrete time scalar product and, consequently, the energy of the product between these two signals. Using the continuous time for the analytical derivation the scalar product will become:

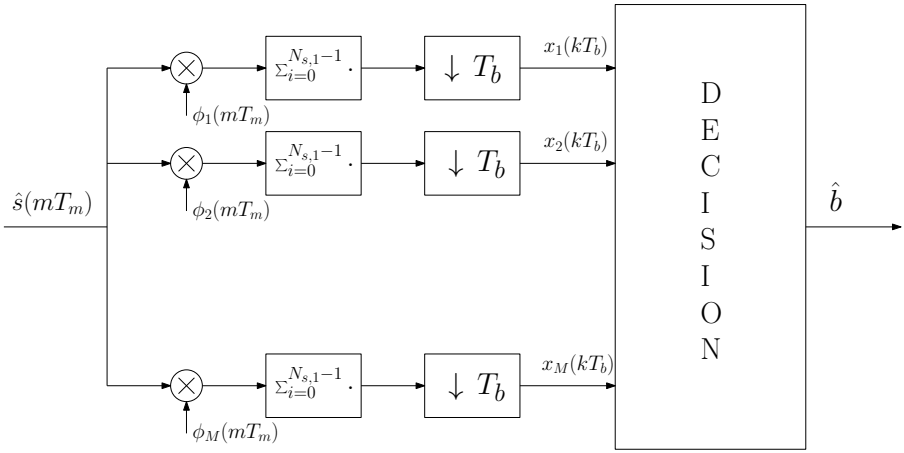

Figure 6.4: Schematic blocks for the correlator receiver used for the A-MTM Decoder

$$\left\langle \tilde{s}, \tilde{\phi_i} \right\rangle = \int_0^{T_b} \tilde{s}(t)\tilde{\phi_i}(t)\, dt \tag{6.5}$$

where $\tilde{s}(t)$ and $\tilde{\phi_i}(t)$ are the continuous time versions of the signals $\hat{s}(mT_m)$ and $\phi(mT_m)$. For the general case, the components of $s(t)$ have amplitudes that depend to the number of the bits set at '1' logical value. In particular, the amplitude of each tone in the transmitted A-MTM symbol can be expressed as $A_k = \frac{1}{\sum_{i=1}^{M} b_i(kT_b)}$. Considering the $j-th$ bit of the transmitted bit word, Eq.6.5 will give the cumulative sum $\varepsilon_j(T_b)$:

$$\varepsilon_j(T_b) = \left\langle \tilde{s}_j, \tilde{\phi_i} \right\rangle = \int_0^{T_b} A_k \cos(2\pi j f_1 t)\cos(2\pi i f_1 t)\, dt \tag{6.6}$$

$$= \frac{A_k}{2}\int_0^{T_b} \cos(2\pi(j+i)f_1 t) + \cos(2\pi(j-i)f_1 t)\, dt \tag{6.7}$$

then

$$\left\langle \tilde{s}_j, \tilde{\phi}_i \right\rangle = \begin{cases} 0 & \text{if } i \neq j; \\ \frac{A_k T_b}{2} & \text{if } i = j; \end{cases} \tag{6.8}$$

In the discrete time domain, the scalar product is expressed as:

$$\langle \hat{s}_j, \phi_i \rangle = \frac{A_k}{2} \sum_{m=0}^{N_{s,1}-1} \cos(2\pi(i+j) f_1 m T_m) + \cos(2\pi(i-j) f_1 m T_m) \tag{6.9}$$

thus

$$\langle \hat{s}_j, \phi_i \rangle = \begin{cases} 0 & \text{if } i \neq j; \\ \frac{A_k N_{s,1}}{2} & \text{if } i = j; \end{cases} \tag{6.10}$$

Then, the scalar product is sampled with a sampling block with a T_b seconds period, exactly the same period of an A-MTM symbol, and a Decision element computes the amplitude of signal $x_i(kT_b)$ and creates the decoded bit vector $\hat{b}$. This correlator receiver needs to have a synchronization with the received signal, in order to compute the scalar product of Eq.6.9 without adding any phase between the two signals $\hat{s}(mT_m)$ and $\phi(mT_m)$. Particularly, quadrature phase difference has to be avoided: in fact, in that case the two signals will be orthogonal and the scalar product will return a null value. This effect can be avoided using a quadrature correlator bank, that computes the two vector components:

$$\varepsilon_j^{(I)} = \langle \hat{s}_j, \phi_i \rangle ; \tag{6.11}$$

$$\varepsilon_j^{(I)} = \left\langle \hat{s}_j, \tilde{\phi}_i \right\rangle ; \quad \tilde{\phi}_i = \sin(2\pi f_i t) \tag{6.12}$$

The proposed A-MTM Decoder schematic blocks are shown in Fig.6.5. It should be noted that the architecture of Fig.6.4 uses M multipliers, and, for the implementation, M LUTs with cosine samples. This is not an optimized architecture for the hardware utilization. A simple modification could be done using the Pulse Width Modulation (PWM) to modulate every $\phi_i(mT_m)$ signal.

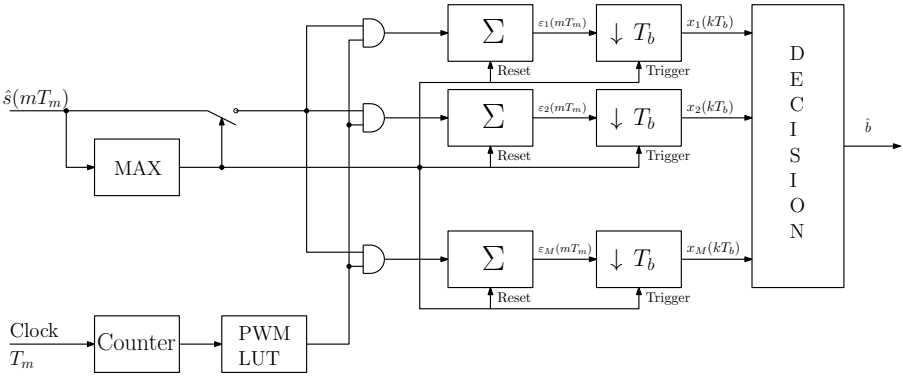

Figure 6.5: Schematic blocks for the A-MTM Decoder.

For the main aspects of PWM see cite [25], that is a survey on this kind of modulation, that is mostly used in power electronics. Briefly, an overview is given in the following.

6.2.1 A brief Pulse Width Modulation (PWM) introduction

The PWM is an impulsive modulation: in Fig.6.6 are explained the signals (in a continuous time domain) useful for the PWM. The message $m(t)$ will be added to the ramp signal $r(t)$. The expressions of the two mentioned signals can be easily derived as:

$$m(t) = \sin(2\pi f_m t) \tag{6.13}$$

where f_m is the frequency of the tone.

The ramp signal is calculated with the Fourier expansion:

$$r(t) = \frac{2}{\pi} \sum_{k=1}^{+\infty} \frac{1}{k} \sin\left(\frac{2\pi k}{T_{PWM}} t + \pi\right) \tag{6.14}$$

The output $x_{PWM}(t)$ of a PWM modulator, with a message $m(t)$ and a

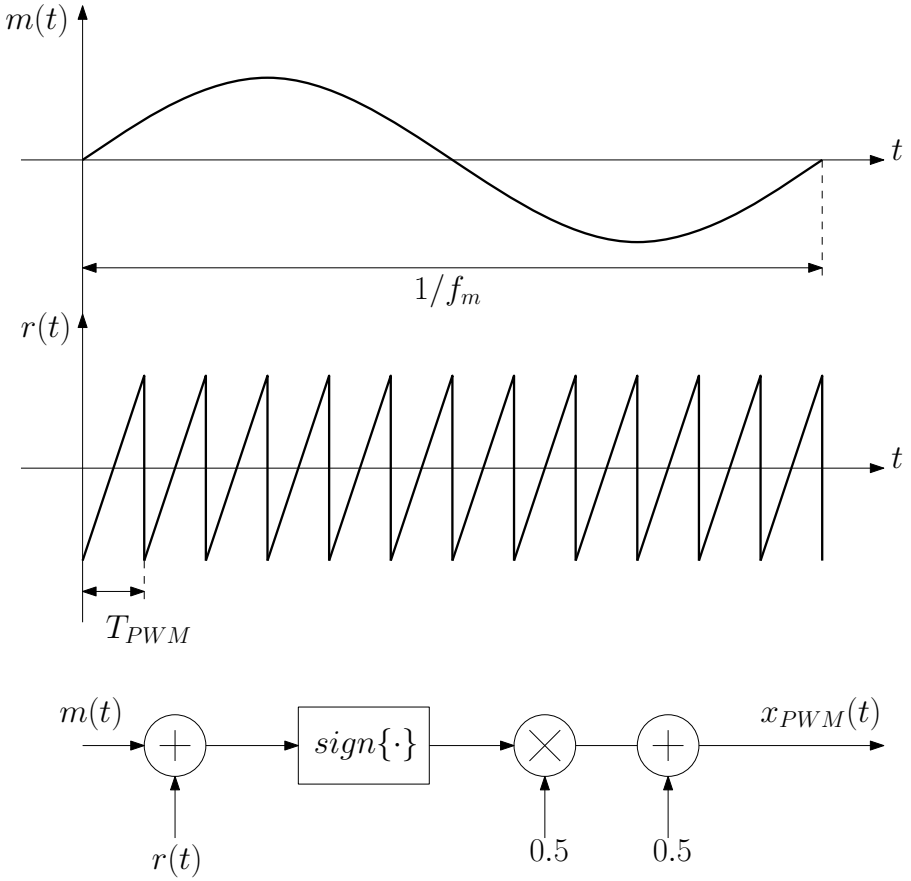

Figure 6.6: Signals in the PWM technique.

ramp signal $r(t)$ can be derived from the schematic in Fig.6.6:

$$x_{PWM}(t) = \frac{1}{2} + \frac{1}{2}\text{sign}\left\{m(t) + r(t)\right\} \tag{6.15}$$

$$= \frac{1}{2} + \frac{1}{2}\text{sign}\left\{\sin(2\pi f_m t) + \frac{2}{\pi}\sum_{k=1}^{+\infty}\frac{1}{k}\sin\left(\frac{2\pi k}{T_{PWM}}t + \pi\right)\right\} \tag{6.16}$$

$x_{PWM}(t)$ represents the modulated signal, and its spectrum is derived numerically. Fig.6.7 shows the spectrum $X_{PWM}(f)$, with a message composed by a single tone at frequency $f_m = 1$ kHz.

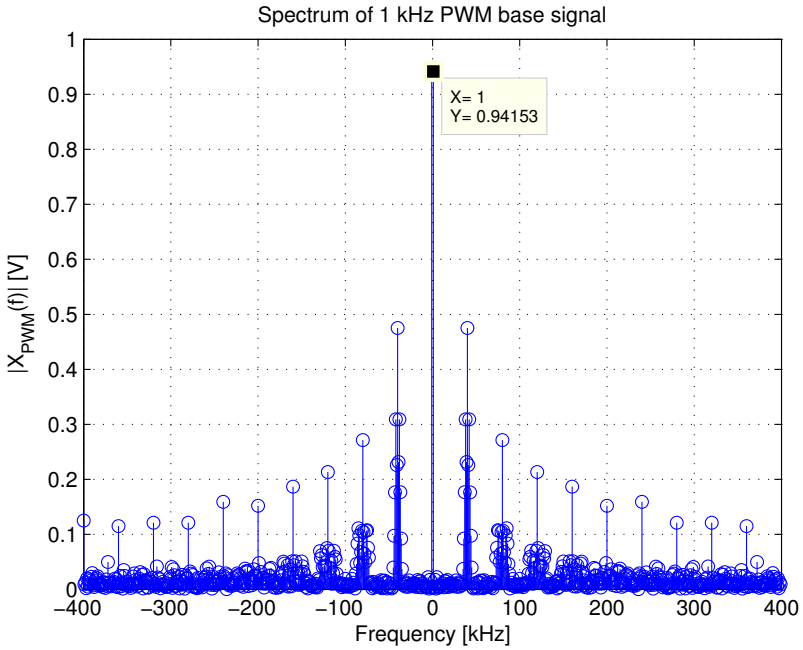

Figure 6.7: Spectrum of a 1 kHz PWM base signal.

In order to preserve logical resources on the FPGA platform, each $\phi_i(mT_m)$ can be represented by its PWM version $x_{PWM,i}(mT_m)$. Since a PWM output signal can assume only two values (logical high or logical low), a LUT that

contains the $x_{PWM,i}(mT_m)$ signals, will occupy only a 1-bit dimensional signal for each signal. Referring to the Fig.6.5, the output of PWM LUT is then composed by M bits, and each represent the correspondent PWM signal for $\phi(m_T m)$: this means that the usage of multipliers can be avoided using a simple AND gate. Since a quadrature correlator bank would use double logic resources on the digital platform, the Decoder synchronization is executed by the MAXimum value (MAX) block: it is used to find the peak of $\hat{s}(mT_m)$. In fact, when different cosine signals, equally spaced in frequency, are added each other, the result is a signal with a peak that corresponds to the begin of each cosine function. For this reason, the MAX block implements a threshold comparator, that decides if the peak occours during the acquisition. This block also resets the discrete time integrators "Σ" and triggers the sampling blocks "$\downarrow T_b$". At the end, every single signal $x_i(kT_b)$ is sent to a Decision element, and decoded bit vector $\hat{b}$ is created.

6.2.2 A-MTM system simulations

The entire A-MTM system has been simulated using a Matlab script. Fig.6.8 shows the trend of the signals $\varepsilon_i(mT_m)$ declared in Fig.6.5. This graphic shows the values assumed by $\varepsilon_i(mT_m)$ during the computation of the scalar product. For the simulation, M = 8 tones has been used, and the byte "10010101" has been transmitted. It is possible to see that the signals $\varepsilon_1(mT_m)$, $\varepsilon_4(mT_m)$, $\varepsilon_6(mT_m)$ and $\varepsilon_8(mT_m)$, at the end of $N_{s,1}$ samples, are not equal to zero. The Decision element will compose $\hat{b}$ comparing the signals $x_i(kT_b)$ and the result will be '10010101'. The Decision element is a simple comparison with a threshold and the result of cumulative sum for each correlator. In this first simulation, the threshold is decided taking into account the minimum value that a single tone can assume: as it is explained before, the minimum value of a tone is equal to the inverse of the number of the tones in the A-MTM constellation. Moreover, the multiplication operation by the demodulated tones and the $x_{PWM,i}(mT_m)$ signal bases , reduces the amplitude of the cumulative sum. In fact, the amplitude of the $X_{PWM}(f)$ first harmonic contribution is shown in Fig.6.7. Hypothesizing to transmit a single tone at 1 kHz, the fre-

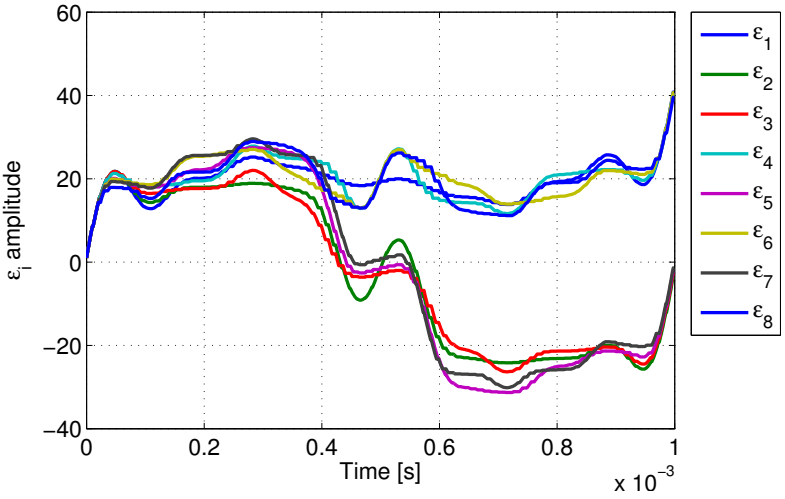

Figure 6.8: Simulation of the trend of the signals ε_i.

quency convolution between the spectrum of the received tone $\hat{s}(mT_m)$ and the spectrum of the $x_{PWM,i}(mT_m)$ is:

$$\hat{Y_i}(f) = \hat{S} * X_{PWM,i}(f) \tag{6.17}$$

According with the value pointed out on Fig.6.7, the final value of the $\varepsilon_i(mT_m)$ signals will be multiplied by a value of 0.9415.

6.3 Performance in presence of thermal noise

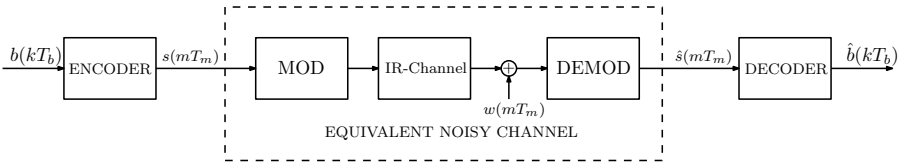

Figure 6.9: Equivalent IR channel and numerical modulation system, with the addiction of thermal noise at the receiver.

In this section a performance analysis of the entire system is done, taking into the account the thermal noise at the receiver. In Fig.6.9, the simulated communication system is shown, where the signal $w(mT_m)$ represents the thermal noise at the receiver. $w(mT_m)$ can be modeled as an Additive White Gaussian Noise (AWGN), with a zero - mean and a constant spectral density:

$$w(mT_m) \sim \mathcal{N}\left(0, \frac{E[x^2]}{\text{SNR}}\right) \tag{6.18}$$

where $E[x^2]$ is the statistical power of the received signal, assuming it with a zero - mean. The simulations will show the Bit Error Rate (BER) at the receiver, with an increasing Signal to Noise Ratio (SNR). In order to mitigate the effect of the noise, it should be useful to acquire a certain number of periods of the received signal. After this acquisition, an average operation is done between each acquired period. This operation increases the performance of the communication system, but the overall data rate will decrease by a factor of N_a: in fact, calling N_a the number of acquisitions, it is necessary to provide N_a periods of the same bit word to decode it. In order to analyze the system performance, a complete simulation has been done, with a different number of acquisitions per period. In Fig.6.10 the simulation results are shown. It is clear to see that as N_a increases, consequently the BER for a given SNR decreases.

These simulations are performed using a threshold decision for each ε_i value, as it is explained in the previous section of this chapter. The threshold is chosen looking at the ε_i trends in Fig.6.8, in absence of the additive noise. With the simulations performed here, it is easy to choose the correct threshold that guarantees a certain BER value. In the Fig.6.11 and Fig.6.12 are displayed the trends of ε_i in function of the SNR, with a different number of averages N_a. In particular, in Fig.6.11 are plotted the ε_i final values (obtained at the end of the integration operations made by the correlator bank) for each number of ones N_o in the transmitted bit word, in function of the SNR.

In order to get the optimal threshold, it is useful to simulate also the trends

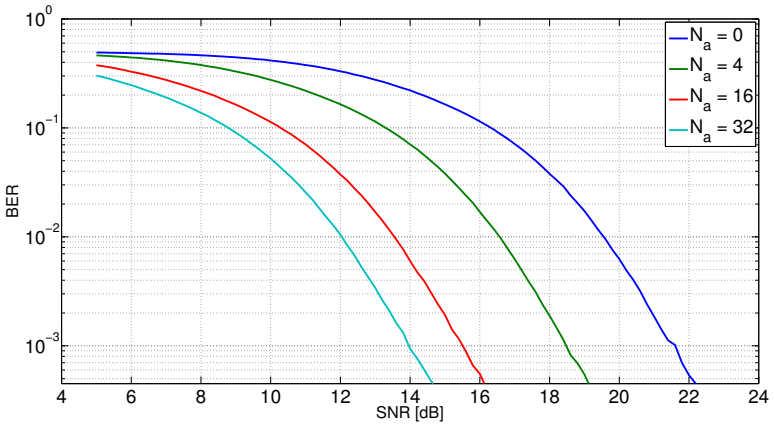

Figure 6.10: Performance simulation results with the noise impairment.

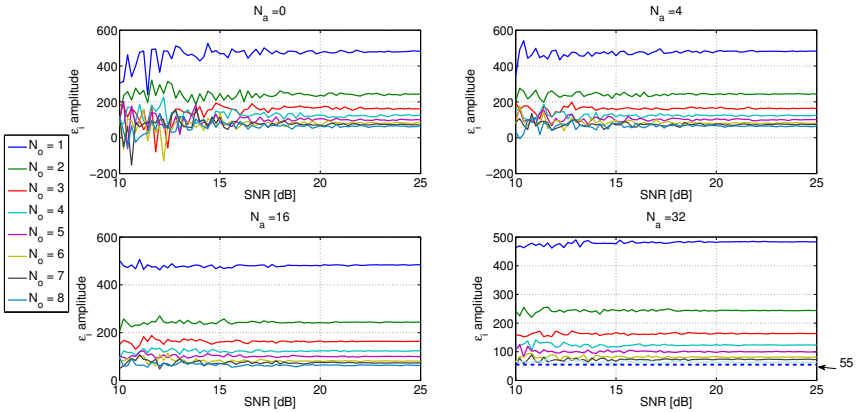

Figure 6.11: ε_i values for each number of ones in the transmitted bit word.

of a ε_i that tends to the zero value. In Fig.6.12, the simulations give the final value of a $varepsilon_i$ signal that represent a bit equal to zero. Also in this case, the simulations have been done for all the possible numbers of zeros N_z in a bit word.

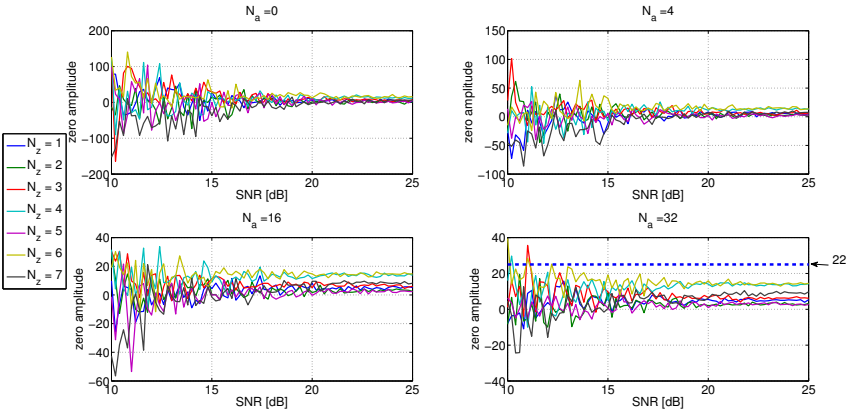

Figure 6.12: ε_i of a zero value in presence of noise.

With the simulation results, the decoder system will be set to acquire $N_a = 32$ periods of the received signal, and the decision threshold will be set at the mean value calculated using the upper and lower bounds drawn in Figs.6.11-6.12; thus the threshold will be set at 38. This assure that the maximum achievable theoretical BER is 0.025, as it is suggested by the curve in Fig.6.10.

Chapter 7

Receiver optical Front End

As it is explained in the previous chapters, the main element at the receiver block of an IR communication system is the optical front end. It is used to receive the IR beams, and it is the equivalent of the antenna in a radio communication system. As it is shown in the introduction of this thesis, the sensor used is called photodiode, and a selection of a device has been done, due to the IR wavelength emitted by the IR LEDs used in the project. In literature, a number of IR front end types are presented, for example in [26]: in this case, a operational amplifier architecture has been used. In the following, an alternative amplifier architecture is presented with the entire electrical scheme. The output signal is the received and amplified IR signal. This signal also includes with itself the amplitude of the received optical IR light: this means that acquiring the amplitude with an ADC, an indication of the Received Signal Strength (RSS) is given.

7.1 Overview of the front end architecture

For the first understanding of the operation of the front end, it is useful to give an overview using the block scheme depicted in Fig.7.1.

The first block is a current amplifier, used to increase the IR received signal. This is implemented using a BJT *cascode* amplifier configuration. A background light compensation is also implemented, erasing the non - mod-

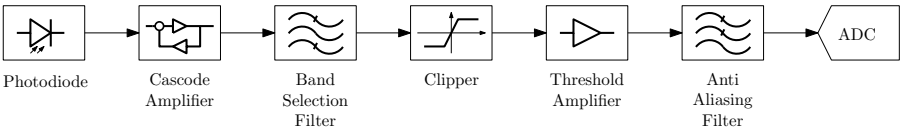

Figure 7.1: Schematic blocks of the Front End.

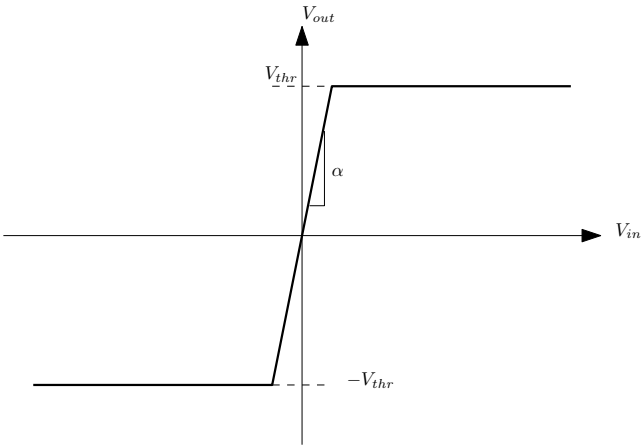

Figure 7.2: Output to input characteristic for the Clipper block.

ulated IR received light. A Band Selection Filter (BSF) is inserted after the cascode amplifier, for selecting the band of interest, where the modulated signal is present: this band pass filter must have a quality factor that let passes the entire Carson's band. The Clipper block has a output to input voltage characteristic depicted in Fig.7.2. This block is characterized by an high voltage gain (that is the slope α shown in Fig.7.2), with a fixed threshold voltage V_{thr}: the input signal is amplified by a factor equal to α, and limited to the V_{thr}. This block is necessary because of the amplitude envelope introduced by the BSF frequency response: in fact, with a lumped elements filter, it is impossible to achieve an high Q band pass filter in a small portion of the spectrum. This means that the signal at the edges of the Carson's band will have a relative low amplitude compared with the BSF center frequency. The clipper erases the amplitude modulation effects, maintaining the RSS information. The Threshold Amplifier block is used to set the maximum amplitude of the received signal. This allows to send to the ADC block a signal with an amplitude equal to the dynamic range of the converter. The low pass Anti Aliasing Filter must be placed before the ADC block, and the bandwidth must be half of the sampling frequency used for acquiring the analog signal.

7.2 Deep study of the architecture

In Fig.7.3 the electronic scheme of the front end is presented.

Let see the implementation of the blocks of Fig.7.1. The cascode amplifier is composed by T_1 and T_2 BJTs. Particularly, T_1 is connected in common base configuration, and T_2 is connected in common emitter configuration. In [27], the configurations are presented and studied. Hypothesizing T_1 equivalent to T_2, the cascode configuration has a current gain equal to the current gain of the BJT β_0 and a relative high voltage gain:

1. $A_v = \frac{v_{out}}{v_{in}} = -\frac{\beta_0 R_c}{r_{be,2}}$;
2. $A_i = \frac{i_{out}}{i_{in}} = \beta_0$;
3. $r_{in} = r_{be,2}$;

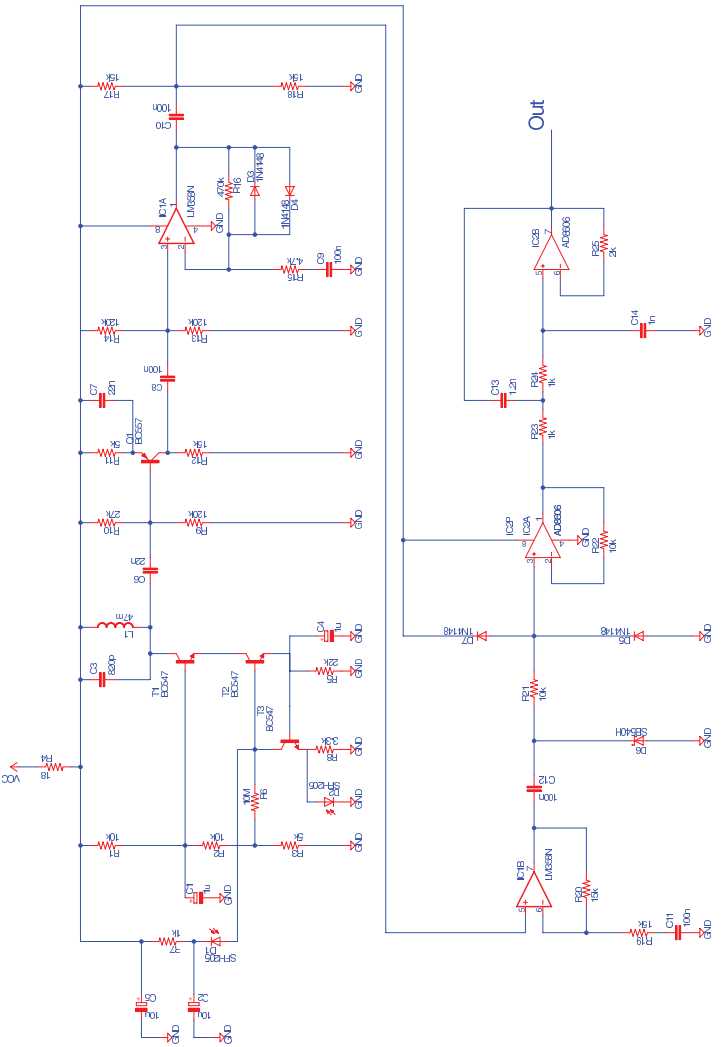

Figure 7.3: Electric schematic for the optical front end.

In the front end, the collector resistor is substituted by a LC filter, that composes the BSF, and R_1, R_2 and R_3 are used for biasing the two T_1 and T_2 BJTs. It should be noted that C_1 capacitor has a great capacitance in order to create a short circuit to the ground for the small signals. Referring to the small signal circuit for the cascode configuration, the output voltage is calculated assuming an high value of the Early effect resistance, then it is possible to ignore it, simplifying the small signals circuit. Since the photodiode D_1 is the IR receiver biased in a reverse configuration, the current generated by the photons i_{ph} will be injected directly to the base of T_2 (due to the presence of the decoupling capacitors C_2 and C_5). Assuming the BJT's current gain flat in function of the frequency (or, in this case, the pulsation ω), the small signals circuit for the cascode gives:

$$\beta_0 i_{be,2}(i\omega) = (\beta_0 + 1) i_{be,1}(i\omega) = (\beta_0 + 1) i_{ph}(i\omega) \tag{7.1}$$

then

$$v_{out}(i\omega) = -\beta_0 Z_{BSF}(i\omega) i_{ph}(i\omega) \tag{7.2}$$

The Z_{BSF} represents the impedance of a parallel LC filter, that has a frequency form given by:

$$Z_{BSF}(i\omega) = \frac{i\omega L}{1 - \omega^2 LC} \tag{7.3}$$

It is clear to see that this complex function has a pole in $\omega = 1/\sqrt{LC}$, and consequently the $v_{out}(i\omega)$ should assume an infinite value. This means that a great transimpedance gain is obtained when a tuned LC filter is set to the carrier frequency, as it is explained in Eq.7.2. Physically, this is not possible to achieve, and the reason is the simplified small signal circuit used for studying the cascode amplifier. It should be noted that a high resistance (10 megaohms) is placed between the bias net and the T_2 base pin: this is a good compromise to avoid the flowing of i_{ph} from D_1 to the bias net and the possibility to bias the T_2 BJT and D_1. In fact, the input resistance of the cascode amplifier is at least four orders of magnitude lower than the R_6 resistor: this allows to let

flow the i_{ph} through the T_2 base - emitter junction.

Keeping always in mind the electrical scheme depicted in Fig.7.3, the T_3 BJT and the D_2 photodiode are used as a feedback control, for the compensation of the ambient background light. Particularly, D_2 is connected in a photovoltaic mode with a zero bias polarization, on R_8. The photovoltaic voltage depends on the incident light on D_2, and when a background light strikes D_2, the voltage on R_8 increases. It should be noted that the C_4 capacitor turns off the T_3 BJT for the high frequencies, thus the photocurrent referred to the FM modulated received signal flows only in the T_2 base emitter junction. Studying the circuit only for the bias values, the feedback action can be explained in a few steps. Calling V_B the voltage on the collector pin of T_3 BJT, it is possible to write:

$$V_B = V_{R_5} + V_{be,2} \tag{7.4}$$

where V_{R_5} is the voltage on R_5 resistor.

The voltage across the base - emitter junction for the T_2 BJT remains set to its ON constant value, thus $V_{be,2} = k_2$. It is also true that:

$$V_B = V_{cc} - (V_{R_1} + V_{D_1}) \tag{7.5}$$

Since the D_1 photodiode is connected in a reverse bias mode, it reduces its voltage when a quantum of energy of the background light E_{BL} strikes the semiconductor. Then Eq.7.4 and Eq.7.5 can be put into a system, giving:

$$\begin{cases} V_B = V_{R_5} + V_{be,2} = V_{R_5} + k_2 \\ V_B = V_{cc} - (V_{R_1} + V_{D_1}) \end{cases} \tag{7.6}$$

Then:

$$V_{R_5} + k_2 = V_{cc} - (V_{R_1} + V_{D_1}) \tag{7.7}$$

Calling $k = V_{cc} - k_2$, $k > 0$, then the rule occurs:

$$k = V_{R_5} + (V_{R_1} + V_{D_1}) \tag{7.8}$$

But the voltage given by $V_{R_1} + V_{D_1}$ decreases when E_{BL} increases, thus V_{R_5} must increase in order to verify the Eq.7.8. It is also clear that:

$$V_{be,3} = V_{R_5} - V_{D_2} \tag{7.9}$$

The voltage on D_2 photodiode increases when E_{BL} increases, and consequently $V_{be,3}$ increases. This makes T_3 more conductive, and a larger amount of the constant photocurrent that is generated by D_1 will flow through T_3 BJT.

The T_4 BJT is connected in a common emitter configuration, and the voltage gain is approximative to:

$$A_{v,4} = \frac{v_{out,4}}{v_{in,4}} = -\frac{\beta_0}{r_{eb,4}} R_{12} \tag{7.10}$$

The IC1A operational amplifier is used as a clipper, as it is explained with respect to Fig.7.2. Assuming a square characteristic for theD_3 and D_4 silicon diodes (with a threshold voltage V_γ) and hypothesizing that the voltage signal amplitude of the IC1A has a very low amplitude, this non inverting amplifier has a voltage gain given by:

$$A_{v,IC4A} = \left(1 + \frac{R_{16}}{R_{15}}\right) \tag{7.11}$$

This value is the slope (indicated with α) in Fig.7.2. Calculating the voltage in the feedback loop, it is possible to find the characteristics of this clipper: because of the virtual short circuit between the two input pins of the operational amplifier, the $V_{R_{16}}$ is:

$$V_{R_{16}} = V_{out,IC1A} - V_{in,IC4A} = V_{in,IC4A} \frac{R_{16}}{R_{15}} \tag{7.12}$$

Since there are two diodes in opposite polarity, When $|V_{R_{16}}| > V_\gamma$, the voltage of the feedback loop is set to a constant value of V_γ volts. Supposing

a positive amplitude value for the input signal, i.e.:

$$v_{in,IC1A} > V_\gamma \frac{R_{15}}{R_{16}} \tag{7.13}$$

then the output voltage amplitude from the clipper will be:

$$v_{out,IC1A} = V_\gamma + v_{in,IC1A} \tag{7.14}$$

The input voltage is negligible with respect of V_γ, thus the clipper has a threshold voltage $V_{thr} = V_\gamma$. The IC1B non inverting amplifier is the second operational amplifier of the LM358 package, and it is used to amplify the voltage amplitude from the clipper, into the dynamic range of the ADC acquiring block. Since the operational amplifiers will be supplied by the V_{cc} voltage, the supply voltage of the ADC must be $V_{cc}/2$, in order to use the whole set of amplitude voltage available from the operational amplifiers (in fact the ADC dynamic range uses a maximum upper bound equal to the supply voltage). The IC1B has a voltage gain equal to 2, and this because the threshold of the D_3 and D_4 diodes is about $V_{cc}/4$. The C_{12} capacitor deletes the mean value of IC1B output voltage, and the D_6 Schottky diode assures that the signal at the input of IC2A will be only positive. IC2A is a voltage buffer and IC2B, with the R_{23}, R_{24}, R_{25} resistors and C_{13} and C_{14} capacitors, forms a Sallen Key low pass filter, used here as an anti aliasing filter. The frequency response of the filter is well known [27], and here only the final Laplace transfer function is given:

$$H(s) = \frac{1}{C_{13}C_{14}R_{23}R_{24}s^2 + C_{14}(R_{23} + R_{24})s + 1} \tag{7.15}$$

Chapter 8

Multipath effects

Since this system is designed for an indoor environment, it is necessary a robusteness study: in an indoor environment a great amount of light reflectors can be found. In order to understand the effects of the multipath, a review of the existent literature has been done, and, after, the application for the system is studied. For the complete understanding of the effects, a review of the analytical processes seen in [29], [30] is given. This allows to understand and to manage the models for the EasyMob system.

8.1 Multipath environment

Since the topic of the system is the navigation of an user in an indoor environment, a generic model for the analysis is needed. Particularly, since the devices will be installed in the rooms of a building, Fig.8.1 shows the application field of the multipath model. This room is edged by white walls and three windows. Depending to the directivity of the optoelectronics, it is clear to understand that a decreasing number of beams will hit the receiver with a increasing directivity of the IR transmitter, and IR optical receiver. Referring again to the Fig.8.1 a total number of three rays hit the receiver. These three rays are in accord with the Snell law for a plane wave on a reflection surface:

$$\Theta_{i,TX} = \Theta_{i,RX} \tag{8.1}$$

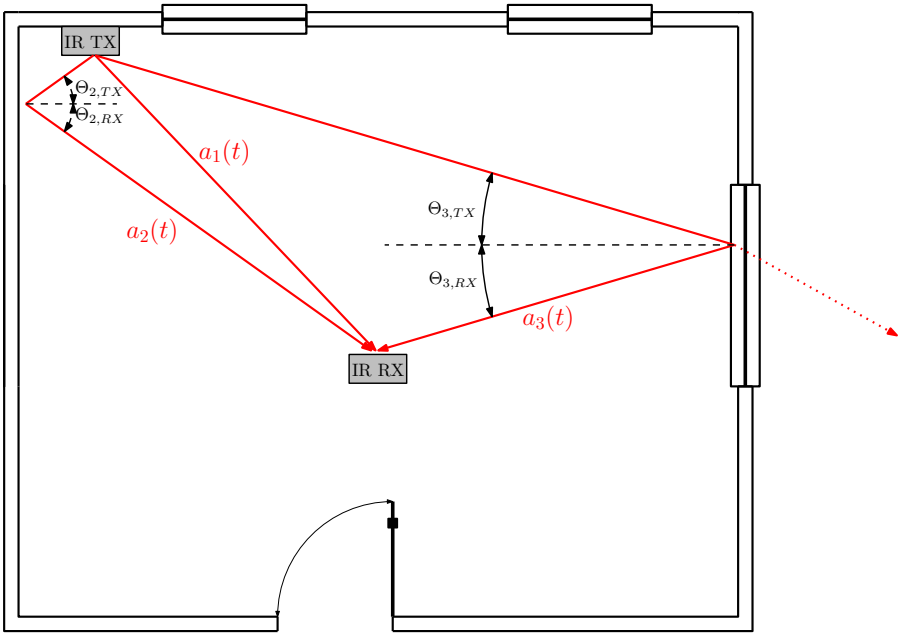

Figure 8.1: IR communication system environment with a multipath effect.

where Θ_i is the angle of the incident plane wave referred to the perpendicular at the point of incidence: the reflected plane wave will have the same angle of the incident one.

Each beam, labeled $a_h(t)$, represents the received signal reflected by the the h-th scatterer (that could be a wall, the glass of a window, or whatever it is possible to fix on the wall), with $h \in [2, N_p]$, where N_p is the number of taps of the IR optical channel. The direct beam a_1 is the received IR signal from the Line of Sight (LoS).

8.1.1 General approach

Using the previous physical environment, it is possible to understand the effects of the reflections using a continuous time domain for the FM transmitted

signal. This is expressed as:

$$x_{TX}(t) = A_{TX} \cos\left(2\pi f_c t + 2\pi k_{FM} \int_0^t m(u)\, du\right) \tag{8.2}$$

where

- f_c : Carrier frequency for the transmitted signal;
- k_{FM} : Frequency modulation index;
- $m(t)$: Transmitted message;

In the [29], [30], the derivation of the interference of two - taps channel and a $N_p \neq 2$ taps channel have been done, and in the following a simplified derivation is shown. The reflected h-th beam is always a FM signal, with an amplitude gain less than 1. This means that each reflected beam is attenuated and delayed in function of the reflection surface, and the distance traveled by the beam. Fig.8.2 shows the Cartesian coordinates for the distances for all the beams.

These distances can be calculated using the well known distance formulas: indicating with d_{a_h} the distance traveled by the h-th beam, then:

$$d_{a_h} = \sqrt{(d_{x,h}^{(1)})^2 + (d_{y,h}^{(1)})^2 + d_z^2} + \sqrt{(d_{x,h}^{(2)})^2 + (d_{y,h}^{(2)})^2 + d_z^2} \tag{8.3}$$

where the d_z is the altitude difference by the IR TX and IR RX. It should be noted that the LoS $a_1(t)$ has $d_{x,h}^{(2)} = d_{y,h}^{(2)} = 0$. The delay for the h-th reflected beam simply will be:

$$\tau_h = \frac{d_{a_h} - d_{a_1}}{c} \tag{8.4}$$

where c is the speed of light.

According with 8.2, it is possible to write the h-th reflected component as:

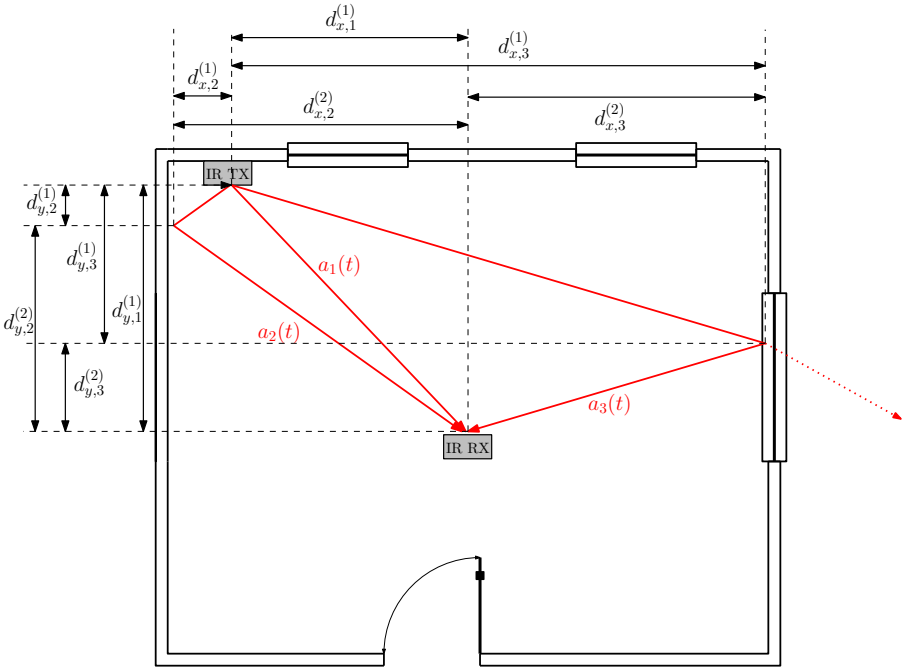

Figure 8.2: Cartesian distances for the multipath beams.

$$a_1(t) = A_1 \cos\left[2\pi f_c t + 2\pi k_{FM} \int_0^t x(u)\, du\right] \tag{8.5}$$

$$\begin{aligned} a_i(t) &= A_h \cos\left[2\pi f_c (t-\tau_h) + 2\pi k_{FM} \int_0^{t-\tau_h} x(u)\, du\right] \\ &= A_h \cos\left(2\pi f_c t - 2\pi f_c \tau_h + 2\pi k_{FM} \int_0^t x(u)\, du - \right. \\ &\qquad \left. + 2\pi k_{FM} \int_{t-\tau_h}^t x(u)\, du\right) \\ &= A_h \cos(\alpha(t) - \beta_h(t)) \end{aligned} \tag{8.6}$$

where:

$$\begin{cases} \alpha(t) = 2\pi f_c t + 2\pi k_{FM} \int_0^t x(u)\, du; \\ \\ \beta_h(t) = 2\pi f_c \tau_h + 2\pi k_{FM} \int_{t-\tau_h}^t x(u)\, du; \end{cases} \tag{8.7}$$

and the received signal at the IR RX receiver will be:

$$x_{RX}(t) = A_1 \cos(\alpha(t)) + \sum_{h=2}^{N_p} A_h \cos(\alpha(t) - \beta_h(t)) \tag{8.8}$$

where the A_h factors are the amplitude levels for each reflected beam.

Two tapped channel

Because the high directionality of the IR TX and the photodiodes, the channel could have only two taps as it is shown in [28]. In this case the received signal is simply:

$$x_{RX}(t) = A_1 \cos(\alpha(t)) + A_2 \cos(\alpha(t) - \beta_2(t)) \tag{8.9}$$

The two components $x_{RX}(t)$ are the real part of a complex expression $\bar{x}_{RX}$:

$$x_{RX}(t) = \mathrm{Re}\{\bar{x}_{RX}\} = \mathrm{Re}\left\{A_1 e^{i\alpha(t)} + A_2 e^{i(\alpha(t)-\beta_2(t))}\right\} \tag{8.10}$$

Using the LoS contribution as reference, it is possible to rotate $\bar{x}_{RX}$ of an angle opposite to $\alpha(t)$, then:

$$\bar{x}_{RX}^{(r)} = A_1 + A_2 e^{-i\beta_2(t)} \tag{8.11}$$

$$= [A_1 + A_2 \cos(\beta_2(t))] - iA_2 \sin(\beta_2(t)) \tag{8.12}$$

This complex equation can be rewritten using the absolute value - phase form, thus:

$$\bar{x}_{RX}^{(r)} = |\bar{x}_{RX}^{(r)}|\, e^{i \arg\left\{\bar{x}_{RX}^{(r)}\right\}} \tag{8.13}$$

According with Eq.8.12, the components are:

$$\bar{x}_{RX}^{(r)} \Rightarrow \begin{cases} |\bar{x}_{RX}^{(r)}| = \sqrt{A_1^2 + A_2^2 + 2A_1A_2\cos(\beta_2(t))} \\ \arg\left\{\bar{x}_{RX}^{(r)}\right\} = \arctan\left(\frac{-A_2\sin(\beta_2(t))}{A_1+A_2\cos(\beta_2(t))}\right) \\ \qquad\qquad = -\arctan\left(\frac{A_2\sin(\beta_2(t))}{A_1+A_2\cos(\beta_2(t))}\right) \end{cases}$$

Remembering the rotation imposed for simplifying the analysis, the received signal in the time domain, for a two taps channel is:

$$x_{RX}(t) = \mathrm{Re}\left\{\bar{x}_{RX}^{(r)}\, e^{i\alpha(t)}\right\} \tag{8.14}$$

$$= \sqrt{A_1^2 + A_2^2 + 2A_1A_2\cos(\beta_2(t))}\times$$
$$\times \cos\left[\alpha(t) - \arctan\left(\frac{A_2\sin(\beta_2(t))}{A_1 + A_2\cos(\beta_2(t))}\right)\right] \tag{8.15}$$

8.1.2 N Tapped channel

The derivation is the same for the previous case, where two tapped channel has been studied. In this approach, the complex expression for the received signal is:

$$\bar{x}_{RX} = A_1\, e^{i\alpha(t)} + \sum_{h=2}^{N_p} A_h\, e^{i(\alpha(t)-\beta_h(t))} \tag{8.16}$$

Using the previous notation for the rotated signal, the derivation continues with the separation of the real part and the imaginary part from the $\bar{x}_{RX}^{(r)}$ signal, thus:

$$\bar{x}_{RX}^{(r)} = \left[A_1 + \sum_{h=2}^{N_p} A_h \cos(\beta_h(t)) \right] - i \sum_{h=2}^{N_p} A_h \sin(\beta_h(t)) \tag{8.17}$$

As it is seen for the two tapped channel, the complex received signal can be rewritten in the absolute value - phase mode. The phase derivation is simple and it is:

$$\arg\left\{ \bar{x}_{RX}^{(r)} \right\} = -\arctan\left(\frac{\sum_{h=2}^{N_p} A_h \sin(\beta_h(t))}{A_1 + \sum_{h=2}^{N_p} A_h \cos(\beta_h(t))} \right) \tag{8.18}$$

For the absolute value derivation, the approach will take care to the sums of the reflected contributions. Particularly:

$$|\bar{x}_{RX}^{(r)}| = \sqrt{\underbrace{\left[A_1 + \sum_{h=2}^{N_p} A_h \cos(\beta_h(t)) \right]^2}_{C(A,\beta(t))^2} + \underbrace{\left[\sum_{h=2}^{N_p} A_h \sin(\beta_h(t)) \right]^2}_{S(A,\beta(t))^2}} \tag{8.19}$$

The cosine contributions give:

$$C(A,\beta(t))^2 = \left[A_1 + \sum_{h=2}^{N_p} A_h \cos(\beta_h(t)) \right]^2 \tag{8.20}$$

$$= \left[A_1 + \sum_{h=2}^{N_p} A_h \cos(\beta_h(t)) \right] \times \tag{8.21}$$

$$\times \left[A_1 + \sum_{l=2}^{N_p} A_l \cos(\beta_l(t)) \right]$$

$$= A_1^2 + 2A_1 \sum_{l=2}^{N_p} A_l \cos(\beta_l(t)) + \tag{8.22}$$

$$+ \sum_{h=2}^{N_p} \sum_{l=2}^{N_p} A_h A_l \cos(\beta_h(t)) \cos(\beta_l(t))$$

Similarly, the sine contributions give:

$$S(A,\beta(t))^2 = \left[\sum_{h=2}^{N_p} A_h \sin(\beta_h(t))\right]^2 \tag{8.23}$$

$$= \left[\sum_{h=2}^{N_p} A_h \sin(\beta_h(t))\right]\left[\sum_{l=2}^{N_p} A_l \sin(\beta_l(t))\right] \tag{8.24}$$

$$= \sum_{h=2}^{N_p}\sum_{l=2}^{N_p} A_h A_l \sin(\beta_h(t))\sin(\beta_l(t)) \tag{8.25}$$

The total amount for the absolute value is:

$$\begin{aligned} A_t = \Bigg[& A_1^2 + 2A_1 \sum_{l=2}^{N_p} A_l \cos(\beta_l(t)) + \\ & + \sum_{h=2}^{N_p}\sum_{l=2}^{N_p} A_h A_l \cos(\beta_h(t))\cos(\beta_l(t)) + \\ & + \sum_{h=2}^{N_p}\sum_{l=2}^{N_p} A_h A_l \sin(\beta_h(t))\sin(\beta_l(t)) \Bigg]^{\frac{1}{2}} \end{aligned} \tag{8.26}$$

$$= \sqrt{A_1^2 + 2A_1 \sum_{l=2}^{N_p} A_l \cos(\beta_l(t)) + \sum_{h=2}^{N_p}\sum_{l=2}^{N_p} A_h A_l \cos(\beta_h(t) - \beta_l(t))} \tag{8.27}$$

In the time domain, the received signal is expressed as:

$$x_{RX}(t) = A_t \cos(\alpha(t) - \arg\{\bar{x}^r_{RX}\}) \tag{8.28}$$

8.1.3 Squared transmitted wave

In the communication system presented in this thesis, the received IR optical signal is considered as a squared wave. Particularly, the analytical equation that represents the transmitted signal from the IR TX to the IR RX is a squared version of Eq.8.2. According with Eq.8.7, it is possible to write the squared FM transmitted signal as:

$$x_{TX}^{(sq)} = \frac{1}{2} + \frac{1}{2}\text{sign}\left\{\cos(\alpha(t))\right\} \tag{8.29}$$

This equation represents the transmitted signal by the IR LEDs. It should be noted that the waveform is not balanced: this because the optical signal is considered zero when the LEDs are turned off. For the received LoS signal the signal will be attenuated only by the frequency response of the channel, and the mathematical expression will be:

$$a_1^{(sq)}(t) = \frac{A_1}{2} + \frac{A_1}{2}\text{sign}\left\{\cos(\alpha(t))\right\} \tag{8.30}$$

For the reflected beams, it is easy to understand that the h-th component of the multipath interference effect will be:

$$a_h^{(sq)}(t) = \frac{A_h}{2} + \frac{A_h}{2}\text{sign}\left\{\cos(\alpha(t) - \beta_h(t))\right\} \tag{8.31}$$

The sign function squares the waveform, or, in general the function passed as argument. Taking care only about the sign function, it is useful to introduce the Fourier expansion series for the transmitted signal. This allows to manipulate trigonometrical functions instead of rectangular signal sequences. Thus:

$$\text{sign}\left\{\cos(\alpha(t))\right\} \sim \sum_{n=1}^{+\infty} \frac{4}{n\pi} \sin\left(n\frac{\pi}{2}\right) \cos(n\alpha(t)) \tag{8.32}$$

8.1.4 Two tapped channel with a transmitted squared signal

As it is shown in the previous sections, the received signal will be the sum of the LoS beam and a reflected beams. The attenuation for the h-th beam will be equal to the case seen in the previous section, and the delays will be equal to those defined in Eq.8.4. Using the Fourier expansion series for the squared

modulated signal, the two tapped interference is derived.

$$x_{RX}^{(sq)} = A_M + \sum_{n=1}^{+\infty} \frac{4}{n\pi} \sin\left(n\frac{\pi}{2}\right) \frac{A_1}{2} \cos(n\alpha(t)) + \tag{8.33}$$
$$+ \sum_{n=1}^{+\infty} \frac{4}{n\pi} \sin\left(n\frac{\pi}{2}\right) \frac{A_2}{2} \cos[n(\alpha(t) - \beta_2(t))]$$
$$= A_M + \sum_{n=1}^{+\infty} \frac{1}{n} \sin\left(n\frac{\pi}{2}\right) A_1^{'} \cos(n\alpha(t)) + \tag{8.34}$$
$$+ \sum_{n=1}^{+\infty} \frac{1}{n} \sin\left(n\frac{\pi}{2}\right) A_2^{'} \cos[n(\alpha(t) - \beta_2(t))]$$

with

$$A_h^{'} = \frac{2A_h}{\pi} \tag{8.35}$$
$$A_M = \frac{A_1}{2} + \frac{A_2}{2} \tag{8.36}$$

It should be noted that the cosine terms in Eq.8.35 are similar to the Eq.8.9. Then, focusing on the term

$$\gamma_n(t, \beta_2(t)) = A_1^{'} \cos(n\alpha(t)) + A_2^{'} \cos[n(\alpha(t) - \beta_2(t))] \tag{8.37}$$

and applying all the mathematical steps seen previously, the phase and the amplitude of the n-th harmonic component will be:

$$\gamma_n(t, \beta_2(t)) = \Gamma_n(t, \beta_2(t)) \cos(n\alpha(t) + \theta_{\beta_2}(n, t)) \tag{8.38}$$

where

$$\begin{cases} \Gamma_n(t, \beta_2(t)) = \sqrt{(A_1^{'})^2 + (A_2^{'})^2 + 2(A_1^{'}A_2^{'}) \cos(n\beta_2(t))} \\ \\ \theta_{\beta_2}(n, t) = -\arctan\left(\frac{A_2^{'} \sin(n\beta_2(t))}{A_1^{'} + A_2^{'} \cos(n\beta_2(t))}\right) \end{cases} \tag{8.39}$$

The received signal will be:

$$x_{RX}^{(sq)} = A_M + \sum_{n=1}^{+\infty} \frac{1}{n} \sin\left(n\frac{\pi}{2}\right) \gamma_n(t, \beta_2(t)) \tag{8.40}$$

8.1.5 N tapped channel with a transmitted squared signal

The approach will mix the results obtained with the general case and the Fourier expansion for the squared signal. This allows to write the general form for the multipath interference. Assuming the general form of $\gamma_n(t, \beta_i(t))$:

$$\gamma_n(t, \bar{\beta}) = \Gamma_n(t, \bar{\beta}(t)) \cos(n\alpha(t) + \theta_{\bar{\beta}}(n, t)) \tag{8.41}$$

where

$$\begin{cases} \Gamma_n(t, \bar{\beta}(t)) = \Big[(A_1^{'})^2 + 2A_1^{'} \sum_{l=2}^{N_p} A_l^{'} \cos(n\beta_l(t)) + \\ \qquad\qquad + \sum_{h=2}^{N_p} \sum_{l=2}^{N_p} A_h^{'} A_l^{'} \cos(n\beta_h(t) - n\beta_l(t))\Big]^{\frac{1}{2}} \\ \theta_{\bar{\beta}}(n, t) = -\arctan\left(\frac{\sum_{h=2}^{N_p} A_h^{'} \sin(n\beta_h(t))}{A_1^{'} + \sum_{h=2}^{N_p} A_h^{'} \cos(n\beta_h(t))}\right) \\ \bar{\beta}(t) = [\beta_2(t) \dots \beta_{N_p}(t)] \end{cases} \tag{8.42}$$

The general multipath interference at the receiver, with a transmitted squared wave is:

$$x_{RX}^{(sq)}(t) = A_M + \sum_{n=1}^{+\infty} \frac{1}{n} \sin\left(n\frac{\pi}{2}\right) \gamma_n(t, \bar{\beta}) \tag{8.43}$$

8.2 Multipath simulations

In order to give an idea of the multipath contribution using a squared FM signal, it is useful to write a Matlab Script that simulates an entire transmission system presented in the previous chapters. No noise is added, then only the multipath effect has been simulated. In this simulation a two tap channel

is studied, and the BER is shown. The simulation takes care of a FM wave transmitted from a certain point, modifying the attenuation of the second received ray in a known set of values. Moreover, also the distance of the scatter changes in the script. This cause a delay variation of the second ray. Fig. 8.3 shows the simulation of the transmission system. For each distance (and, consequently, each delay), and for each reflected amplitude, the number of wrong received bits is calculated, an then the BER is calculated.

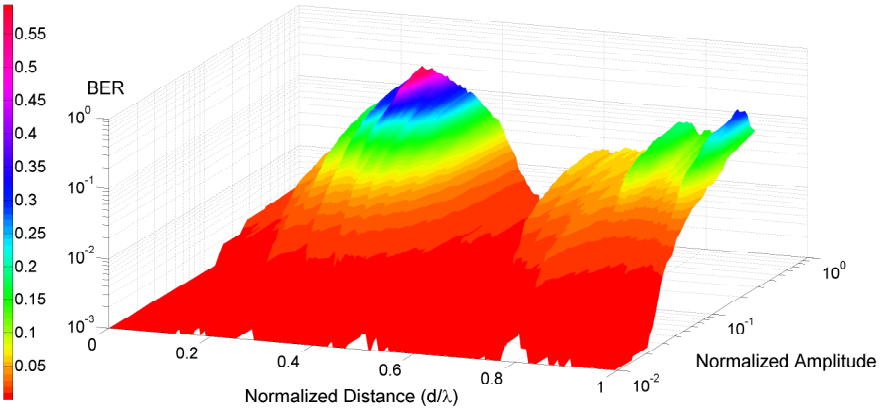

Figure 8.3: Simulated BER for a certain scatterer distance and a certain value of reflected light amplitude value.

The distance is expressed in a normalized value, particularly is related to the wavelength of the FM carrier. It is clear to understand that a value of delay that about 0.35 times the wavelength λ, creates an high amount of errors. The phase φ_{ref} of the reflected beam, with a scatter located at the distance of $d_{sc} = 0.35\lambda$, with respect to the direct received beam will be:

$$\varphi_{ref} = 2\pi\frac{d_{sc}}{\lambda} = 0.7\pi \approx 2.2\text{rad} \tag{8.44}$$

For the navigation architecture, (hypothesizing the propagation in the

empty space), the wavelength of the carrier frequency is given by:

$$\lambda_{x_{TX}} = \frac{c_0}{f_c} = 1.2 \cdot 10^3\, m \tag{8.45}$$

the received signal will be corrupted if the scatter is placed near the 0.35λ. Fig.8.4 shows the simulated environment. In this case, the space two dimensional, but nothing changes in the three dimensional space. As it is explained

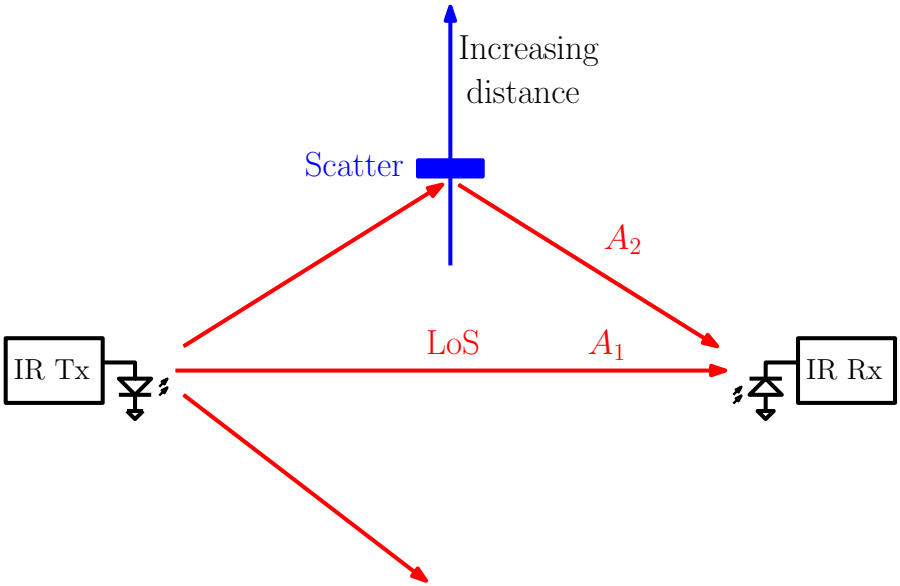

Figure 8.4: Simulated environment.

before in this chapter, the simulations are executed varying the scatter distance and the amplitude of the reflected beam A_2. Because the wavelength is many times bigger than the typical indoor environments, it is clear that the FM demodulation algorithm is totally useful for the project.

Chapter 9

Implementation of the entire system

In this chapter, the entire implementation of the EasyMob IR system is presented and commented. As it is explained before, the entire prototype has been developed over a FPGA board, using ISE Xilinx software for the VHDL compilation and synthesis. The receiver board is equipped with a supply battery that assures the power needed for the FPGA board and all the peripherals. The optical Front End and the audio amplifier are implemented with discrete components on a stripboard. In the following, the principle of operation of the receiver is explored, with the description of the phases done by the algorithm implemented.

9.1 Principle of operation of the receiver

The user approaches to the IR transmitter. The indicator bar on the receiver gives the strength of the received signal to the user. When the

- The modulator sends the ID symbol selected with the `Encoder` entity. This ID symbol is composed by a combination of tones stored into a N LUTs, according with the scheme in Fig.6.3.

    - The user presses the "GO" button, and the system is ready to decode the transmitted ID;

  - The acquisition will not begin until the amplitude of the received signal remains under the maximal value;
  - When the amplitude is at the maximum level AND the "GO" button has been pressed, the maximum value of the demodulated signal is reached;
  - When the maximum value of the demodulated signal is reached, a *shot* of 800 samples is processed (the length of a complete period of the minimum frequency of A-MTM constellation) ;
  - In order to mitigate the noise, a set of 32 shots is captured. The M decoded bits are bitwise averaged;
  - When the 32 shots are finished, the averaged decoded bit word is shown and ready to be processed;

- With the button "Listen", the navigation vocal information (stored as audio samples with a sample frequency of 8 kHz, and 12 bit depth) is sent to the DAC, amplified with a TBA820M small power audio amplifier, and played for the user.

- A new ID decoding process is set up by the button "GO".

The red edged board is the FPGA board where the synthesized VHDL project is stored. The yellow edged block is the voltage regulator, that is used for the conversion of the voltage from 12 V (supplied by the battery) to 5 V. The green edged block is the audio amplifier. The DAC board attached to the amplifier Printed Circuit Board (PCB) is used to convert the audio samples into an audible messages. The cyan edged block is the optical front - end, with the ADC board used for convert into a digital domain the IR signal. The purple edged block is the LED bar used to show the level of the received signal. In Fig.9.2, the command buttons are shown: the orange edged button is used for the "GO" impulse, and the dark blue edged one is the "Listen" button. The eight green LEDs, edged with a blue line, indicate the recognized ID.

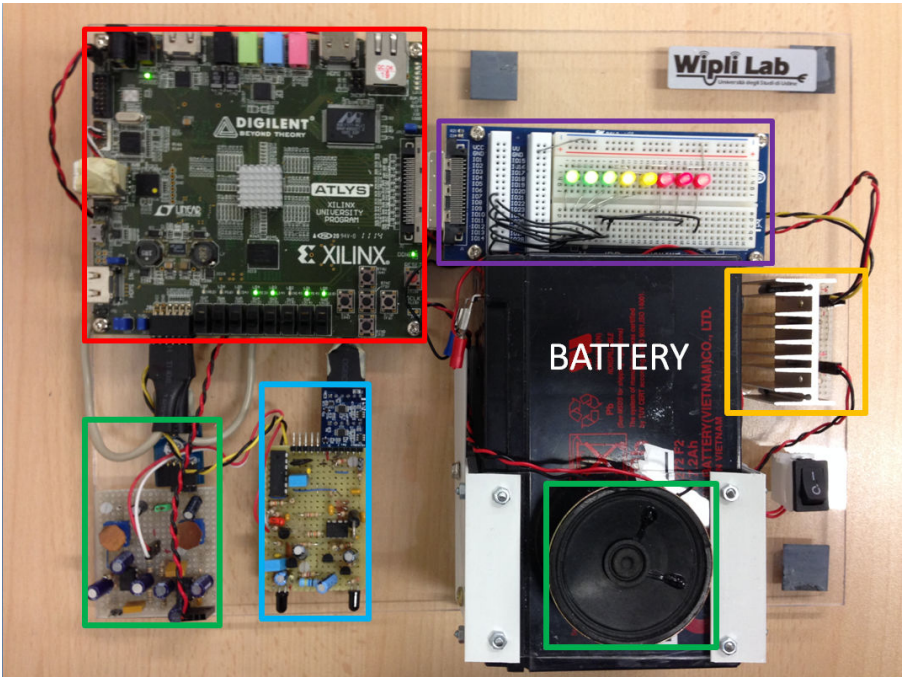

Figure 9.1: Overview of the receiver: the FPGA platform with all the implemented peripherals

9.2 The entire system

In Fig.9.3, the entire prototype of the IR communication system is presented. In the left side of the picture it is possible to see the transmitter, with the power supply and the transmission Front End. It is composed by three BDX53C Darlington BJTs, that assure a maximum current level equal to 8 Ampere. The IR illuminator is composed simply by nine IR LEDs, and here, only one channel is connected. In the right side, the receiver has decoded the sent ID, since the signal strength is at its maximum value.

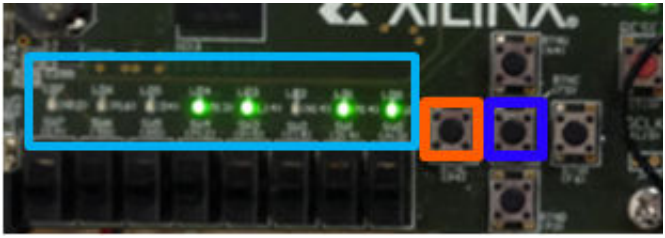

Figure 9.2: Command buttons on the board

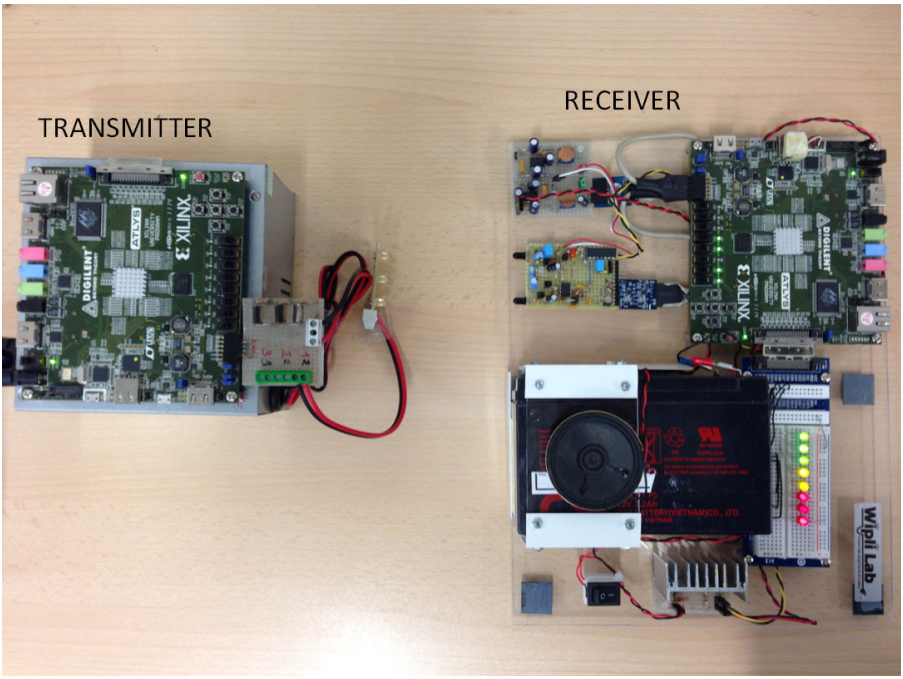

Figure 9.3: The entire prototype of the IR communication system

Chapter 10

Conclusions

In this thesis, a complete architecture, useful to navigate a user in an indoor environment has been discussed, studied and developed. The presented architecture bases its functionality on the InfraRed (IR) communication system: for this reason a study on the most important components used in the optical communication systems is presented. Particularly, since the IR Light Emitting Diode (LED)s and the photodiodes play an important role in an IR link, an overview of the physical phenomena and the electric characteristics has been done. This is useful when the development of both the transmitter Front End and the receiver Front End is required. Moreover, the most popular modulation schemes used in InfraRed (IR) communications are described and commented.

The IR navigation architecture developed in this thesis has stemmed out from a first reverse engineering step where an existing IR analog solution suited to transmit only voice signals has been analyzed. A number of tests has been carried out to characterize the existing analog solution, the modulation used (FM) and its main parameters. With the information retrieved from the reverse engineering step, a new architecture has been developed. The proposed new digital solution is motivated by the goal of increasing the flexibility and to be able to realize a bidirectional data transmission link exploiting an Frequency Modulation (FM) modulated carrier. This allows keeping the compatibility

with the existing analog FM solution when voice signals are transmitted, but at the same time it enables the transmission of digital data. In the framework of developing a navigation system, various architectures that include the IR system have been discussed. In particular, emphasis has been given to a hybrid solutions where the IR link is used to locate and identify the user, while a Radio Frequency (RF) BlueTooth (BT) link is used to deliver navigation information from a central unit to the user.

The thesis discusses all aspects related to the hardware realization of such a system. An optimized realization on a Field Programmable Gate Array (FPGA) board has been developed and it is herein described.

The impairments that can affect the performance of the IR digital link have been studied. The effects of multipath propagation to the received signal has been derived analytically, even for a square wave transmission. Some numerical results are also reported. Moreover, the impact of the thermal noise at the receiver is simulated, and the architecture optimization has been done taking care of the simulation results.

It has been found that the IR digital link is suitable to locate an user in an easy way, exploiting the high directivity of the optical electronic components. In fact, due to the possibility to tune the IR beams, it is easy to illuminate a specific restricted area. This allows to retrieve the user position in an easily and inexpensive way. Moreover, the reflections induced by the walls are avoidable by setting the optical power at its optimal value for the specified area. This minimizes the effects of the reflections generated by the walls located in front of the illuminator, that cannot be erased digitally. Simulation results show that the realized demodulation algorithm is robust to the multipath reflections: in fact the BER increases dramatically when the reflected beam has a phase that differs from the direct beam phase of about 0.7π. Consequently, the distance traveled by the reflected beam must be approximately 0.35λ: this value is much larger than the propagation distance in a typical indoor environment. The thermal noise at the receiver has been characterized, and the threshold at the decision element in the Decoder has been chosen for a BER maximum value equal to 0.025.

The entire base band system has been developed on a digital board equipped with a FPGA. With the approach followed in this thesis, the FM demodulator and the decoder at the receiver require a low number of digital resources (e.g., DSP Slices and gates on the FPGA). For example, the correlator bank used to determine which Audio Multi Tone Modulation (A-MTM) symbols are contained into the received signal, is computed using the Pulse Width Modulation (PWM) modulation to approximate the M cosine signals. This allows to use simple AND gates instead of multipliers. Furthermore, the demodulator uses a digital architecture suitable to demodulate both squared wave and sine wave: this allows to avoid the implementation of a very selective passband filter onto the FPGA in order to extract the first harmonic of the squared signal.

On the other hand, the implementation of the digital FM modulator has been optimized with respect to the available electronic peripherals (e.g., Digital to Analog Converter (DAC), Analog to Digital Converter (ADC)) and to the working parameters (e.g., the sampling frequencies and the voltage supplied). Since the overall complexity is low, both the transmitter and the receiver have been implemented in a single FPGA boars allowing to realize bidirectional link, which may allow to realize other navigation architectures than the one considered which uses a combination of IR and radio systems.

The BS and the MS are equipped also with analog parts: in this thesis a complete overview of the receiver Front End is given, focusing on the hardware implementation of the optical amplifier. The resulting circuitry is easy to develop, and totally reconfigurable in terms of bandwidth. In fact, a simple LC passband filter is used to tune the receiver in the Carson's band used by the transmitter, and a cascode amplifier is used to achieve the optimal gain and input resistance for the current generated by the photodiode. The receiver Front End also implements a feedback block that prevents the background luminosity, improving the performance of the digital blocks. The entire Front End is cheap and easy to implement; moreover the output voltage can be interfaced with the next digital blocks, and in particular the maximum voltage of the output signal can be tuned for the dynamic range of the ADC. This

allows to be able to retrieve the Received Signal Strength (RSS), which is useful for the decoding algorithm. For the transmitter, a simple Darlington Bipolar Junction Transistor (BJT) is used as a current amplifier for driving the IR LEDs that compose the illuminators.

As it is explained in the introduction, this architecture uses the high directivity of the optical devices: using this strength, it is possible to have a relative high accuracy about the postiono of the user. In fact, assuming to drive an illuminator with a low current, then a low IR light power will be radiated over a specific area: the higher levels of RSS are achievable near the IR illuminator. This allows to understand the position of the user implicitly, with a small range of tolerance.

The real field experimentation of the system has also been done. In fact the entire navigation system has been installed at the CRO hospital in Aviano (Italy), in the framework of the EasyMob project (introduced in this thesis). The validation of it has shown that the IR navigation system is a good and easy to use tool for the navigation of people in the considered scenario.

The main future activity will be focused on the bidirectional link over IR, with a decreasing of the power consumption at the receiver device: in fact the BT link will be unnecessary, due to the fact that the transmitter will deliver the navigation data to the user via IR link.

Bibliography

[1] Max Plank, M. Masius, "The Theory of Heat Radiation", 1914.

[2] J.R. Biard et al. "Semiconductor Radiant Diode", Dec. 20, 1966, http://www.freepatentsonline.com/3293513.pdf.

[3] D. Zhang, F. Xia, Z. Yang, L. Yao, W. Zhao, "Localization Technologies for Indoor Human Tracking", *Future Information Technology (FutureTech), 2010 5th International Conference on*, pp.1-6, 21-23 May 2010.

[4] D. Inserra, A. M. Tonello, N. Moret, "Positioning Based on 2-D Angle of Arrival Estimation," P*roc. of IEEE VTC 2011 Spring*, Budapest, Hungary, pp.1-5, May 15-18, 2011.

[5] C. Falsi, D. Dardari, L. Mucchi, M. Z.Win, "Time of Arrival Estimation for UWB Localizers in Realistic Environments", EURASIP Journal on Applied Signal Processing, 2006, Article ID 32082, 13 pages.

[6] Hui Liu, H. Darabi, P. Banerjee, Jing Liu, "Survey of Wireless Indoor Positioning Techniques and Systems," IEEE Trans. Systems, Man, and Cybernetics, Part C: Applications and Reviews, Vol.37, No.6, October 2007, pp. 1067 - 1080

[7] R. Want, A. Hopper, V. Falcao, J, Gibbons, "The Active Badge Location System" *ACM Transactions on Information Systems* Volume 10 Issue 1, Jan. 1992, Pages 91-102.

[8] P. Bahl and V. Padmanabhan, "RADAR: an in-building RF-based user location and tracking system". *Proceedings of the Nineteenth Annual Joint Conference of the IEEE Computer and Communications Societies*, Vol. 2, 2000.

[9] Heredia, B.; Ocaa, M.; Bergasa, L.M.; Sotelo, M.A.; Revenga, P.; Flores, R.; Barea, R.; Lopez, E., "People Location System based on WiFi Signal Measure," *Intelligent Signal Processing, 2007. WISP 2007. IEEE International Symposium on* ,pp.1-6, 3-5 Oct. 2007.

[10] Schubert, E.F., "Light-Emitting Diodes", 2002, Boston University.

[11] EasyMob project website, http://www.easymob.eu.

[12] T. Strothotte, H. Petrie, V. Johnson, and L. Reichart, "MoBIC: User needs and preliminary design for a mobility aid for blind and elderly travellers", in *Proc. 2nd Tide Congr., The European Context for Assistive Technol.*, I. Placeencia Porrero and R. Puig del la Bellacase, Eds. Amsterdam, The Netherlands: IOS Press, 1995, pp. 348 - 351.

[13] P. Blenkhorn and D. G. Evans, "A System for Enabling Blind People to Identify Landmarks: The Sound Buoy", *IEEE Transactions on Rehabilitation Engineering*, Vol. 5, No. 3, Sep. 1997.

[14] J. Brabyn, W. Crandall, and W. Gerry, "Talking signs: A remote signage solution for the blind, visually impaired and reading disabled", in *Proc. 15th Annu. Int. Conf., IEEE Engineering in Medicine and Biology Society*, 1993, pp. 1309 - 1310.

[15] Yanying Gu, Anthony Lo, Ignas Niemegeers, "A Survey of Indoor Positioning Systems for Wireless Personal Networks", *IEEE Communications Surveys & Tutorials*, vol. 11, no. 1, 2009, Pages:13 - 32.

[16] M. De Piante, D. Inserra, A. M. Tonello, "People Navigation System in Confined Spaces," *Proc. of IEEE AESS European Conference on Satellite Telecommunications* 2012, Rome, September 2012.

[17] J. M. Kahn, J. R. Barry, "Wireless Infrared Communications", *Proceedings of the IEEE* , vol.85, no.2, pp.265,298, Feb 1997

[18] Z. Ghassemlooy, A. R. Hayes, N. L. Seed, E. D. Kaluarachchi, "Digital Pulse Interval Modulation for Optical Communications", *IEEE Communications Magazine*, pp. 95-99, Dec. 1998.

[19] http://www.fairchildsemi.com/ds/LM/LM555.pdf

[20] D. Zhang, F. Xia, Z. Yang, L. Yao, W. Zhao, "Localization Technologies for Indoor Human Tracking", *Future Information Technology (FutureTech), 2010 5th International Conference on*, vol., no., pp.1-6, 21-23, May 2010, doi: 10.1109/FUTURETECH.2010.5482731.

[21] M. De Piante, A. M. Tonello, "Digital Implementation for a Indoor Positioning System using Infrared Optical Link", *to be submitted*

[22] Rice, M., Padilla M., Nelson B. "On FM Demodulators in Software Defined Radios Using FPGA's" *Military Communications Conference 2009. IEEE.* Oct. 2009.

[23] Hemmert K.S., Underwood K.D., "Floating-Point Divider Design for FPGAs", *Very Large Scale Integration (VLSI) Systems, IEEE Transactions on*, vol.15, no.1, pp.115-118, Jan. 2007.

[24] Proakis J., "Digital Communications", McGraw-Hill, 2000.

[25] Holtz, J., "Pulsewidth modulation-a survey", *Power Electronics Specialists Conference*, 1992. PESC '92 Record., 23rd Annual IEEE , vol., no., pp.11-18 vol.1, 29 Jun-3 Jul 1992.

[26] Khoman Phang; Johns, D.A., "A CMOS optical preamplifier for wireless infrared communications", Circuits and Systems II: Analog and Digital

Signal Processing, IEEE Transactions on , vol.46, no.7, pp.852,859, Jul 1999

[27] Adel S. Sedra, Kenneth Carless Smith, "Microelectronic Circuits 6th edition", Oxford University Press, Incorporated, 2010.

[28] J.M. Kahn, W.J. Krause, J.B. Carruthers, "Experimental characterization of non-directed indoor infrared channels" *Communications, IEEE Transactions on* , vol.43, no.234, pp.1613,1623, Feb/Mar/Apr 1995

[29] L. Zeger, P. Chen, H. Kobayashi, "Effects of Multipath Interference on an FM Data Subcarrier" *Proc. of the 1997 IEEE Pacific Rim Conference on Communications, Computers and Signal Processing (PACRIM '97)*, pp 40-44, Victoria, B.C., Canada, August 20 - 22, 1997.

[30] L. Zeger, P. Chen, H. Kobayashi, "Analysis and Simulation of Multipath Interference of FM Subcarrier Digital Signals" *Computers and Communications, 1998. ISCC '98. Proceedings. Third IEEE Symposium on* , vol., no., pp.35-41, 30 Jun-2 Jul 1998.